

N64-27398-N64-27402

Code-1

Cat.-21

Nasa Cr-53381

U. S. Department of Commerce
Weather Bureau
National Severe Storms Project

FINAL REPORT ON
National Aeronautics and Space Administration
PROJECT NO.R-55
August 1963

~~HANDLING OF PRELIMINARY DATA~~

OTS PRICE

XEROX	\$	<u> ph </u>
MICROFILM	\$	<u> </u>

U. S. DEPARTMENT OF COMMERCE
Luther H. Hodges, Secretary
WEATHER BUREAU
F. W. Reichelderfer, Chief

NATIONAL SEVERE STORMS PROJECT

G. F. Van Thullenar, Director

Final Report On

NATIONAL AERONAUTICS AND SPACE ADMINISTRATION

Project No. R-55

J. T. Lee



August 1963

U. S. DEPARTMENT OF COMMERCE
Luther H. Hodges, Secretary
WEATHER BUREAU
F. W. Reichelderfer, Chief

NATIONAL SEVERE STORMS PROJECT

G. F. Van Thullenar, Director

Final Report On
NATIONAL AERONAUTICS AND SPACE ADMINISTRATION
Project No. R-55

J. T. Lee

August 1963

Final Report on
NATIONAL AERONAUTICS AND SPACE ADMINISTRATION

Project No. R-55

J. T. Lee

In accordance with the agreement in the subject purchase order, a final report is hereby submitted.

The purchase order provided for partial support for the National Severe Storms Project (NSSP) including

Area 1. Acquisition and analysis of turbulence data

Area 2. Comparisons of storm project data with satellite data, and

Area 3. Studies of the effect of meteorological phenomena on supersonic aircraft design and operation.

Under these conditions the following division of the funds was approved by NASA:

Item A. Preliminary processing of aircraft flight data including computer rental.

Item B. Modification of DC-6 aircraft for Drone control.

Item C. Rental of facilities for Research Flight Facility (RFF) aircraft during staging operations at Oklahoma City.

Item D. Direct supporting costs.

Item E. Research on data already collected and preparation of reports.

Item A (above)

Reference is made to NSSP Report No. 14, "Field Operations of the National Severe Storms Project in Spring 1962," for a detailed description of the aircraft and other types of observations made during the operational season.

In the operation of aircraft, the B-26 flew on 26 days. These flights have been machine processed and time histories of these data machine plotted. IBM 1620 computer time was rented from the U. S. Army Corps of Engineers and machine-plotted curves were provided by McDonnell Automation Center of St. Louis, Mo., under contractual agreement with the Weather Bureau. While the machine plots are not in completed form (time hacks have to be entered manually), an example is attached with the corresponding post-navigated flight path.

A preliminary analysis of these data has been started. Machine plotting of time histories of the DC-6's and B-57 data is also being accomplished. When completed, the material will be incorporated in the study of the dynamics and wind structures around thunderstorms. Coincident with some of these times, aircraft penetrations were being made to study turbulence distributions in clouds.

Item B (above)

The modification of a DC-6 aircraft for drone control was made and a number of test flights were accomplished. The feasibility of the use of drone aircraft for meteorological sampling was "conditionally" proved. However, during the trial period, no opportunity presented itself for actual penetration of clouds by the drone aircraft. Therefore, the utilization of drone aircraft as an instrument platform to probe areas expected to be too turbulent for manned aircraft still needs to be tested. A report, "Research Use of Instrumental Drones in Cloud Physics and Meteorology," by R.E. Ruskin (NRL Report 5923, June 1963) gives the full details and an evaluation of this effort, and is included as a part of this report.

Items C and D (above)

The RFF aircraft consisting of two DC-6's, one B-57 and one B-26 were based at Will Rogers Field at Oklahoma City from around April 20 to June 8. Approximately 60 flights were made by these aircraft gathering data in severe local storm environments. These flight altitude data include:

1. Aircraft position as determined by Doppler radar
2. Temperature
3. Humidity
4. Wind speed and direction
5. Pressure altitude
6. Radar altitude

7. Horizontal and vertical cross sections of thunderstorms as seen by airborne radar
8. Time lapse cloud photography
9. Dropsonde measurements of the temperature and humidity of the layer of air beneath the aircraft.

Item E (above)

Research under this grouping was aimed at yielding as much of an answer as possible under the limitations of staff and time to the subjects mentioned in Areas 1, 2 and 3 above. Since most of these have been incorporated into the NSSP preprint reports a complete list of the publications to date is included. These preprints should be considered as constituting a portion of this final report. Preprints Nos. 8 through 16 are of particular interest. Copies of these have already been sent to NASA. Report No. 19, now in preparation, is a study of the high liquid water content measured in a cloud at a penetration altitude near 30,000 ft. A copy of this report will be forwarded to NASA as soon as it is published.

Turbulence data for twenty-two T-33 flights have been analyzed and compared to the path of the aircraft through the thunderstorm. The report on this work is included in the attached paper, "Thunderstorm Turbulence Measurements by Aircraft and Concurrent Radar Echo Evaluations," which, although prepared for the FAA, contains such materials also considered to be of value to NASA. In addition, twenty-four thunderstorm penetrations by

the F-100 used as a turbulence probe with the T-33 have had the turbulence data broken down into derived gust velocities. Preparation of time histories of this parameter and the study of the relationship to the T-33 and radar data is a continuing research project.

The attached report "On Vectoring Aircraft Through Thunderstorms," also prepared for the FAA but containing material significant to NASA, is a summary of the problems encountered in thunderstorm penetrations and the meteorological aspects thereof.

As a part of the investigation into the liquid water content found in clouds at levels above 35,000 ft. and the extent to which thunderstorms can rise above the height of the surrounding tropopause, a number of U-2 flights have been analyzed according to cloud formations. Due to 30 nautical miles or larger errors in the Doppler navigation system, the postnavigation has been very complicated and the resultant work very slow. However, included here is one example of a thunderstorm cloud (see cloud photograph) which appears unique in several ways.

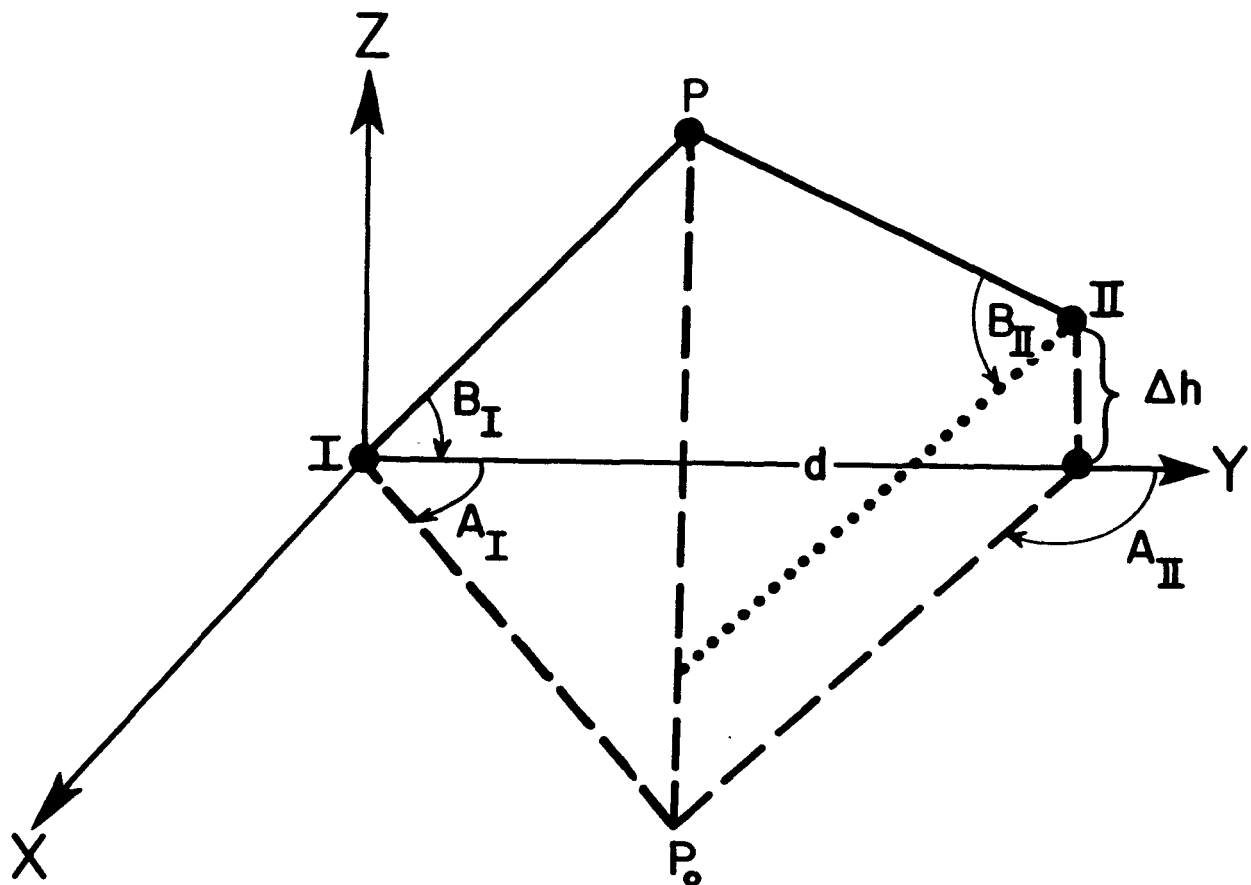
1. The almost complete depletion of sunlight on the right-hand side of the cloud even at the extreme top where the horizontal distance is about 3,000 ft. This, plus the texture of the cloud, suggests the presence of relatively high liquid water content.

2. Note that this cloud has an apparent base of near 30,000 ft. and the top, as computed by two different triangulation measurements, is near 55,000 ft. How numerous clouds of this type are and the number which rise above 50,000 ft. have not been ascertained.

Below are listed some heights of thunderstorm cloud tops as obtained from U-2 data. A few of the pilot's comments on turbulence are included as points to be considered in the operation of supersonic aircraft in the vicinity of thunderstorms.

May 24, 1962	Tops 53,000 - 54,000 ft. T-33 and F-100 penetrated this storm (see report "Thunderstorm Turbulence Measurements by Aircraft and Concurrent Radar Echo Evaluations," pages 45-47, for derived gust velocities experienced by the T-33).
May 25, 1962	Tops 55,000 to 58,000 ft., gradually building to 65,000 ft. Pilot experienced moderate-severe turbulence and vertical currents above top of cloud.
May 28, 1962	Tops 50,000 to 55,000 ft. common.
June 5, 1962	Tops averaged 57,000 ft., maximum tops 62,000 ft. Pilot reported severe turbulence at 56,000 ft., 3 nautical miles northwest of storm. Airspeed increased as if aircraft were in an updraft, but rate of climb decreased as in a downdraft.

In order to provide an additional method of obtaining cloud top heights, rate of growth, and relationship of the visible cloud to the cloud as seen on radar, a pair of phototheodolites was installed at Norman, Oklahoma. The enclosed aerial photograph shows the locations of the two instruments. Also included is a photograph of one of the phototheodolites. The two units are separated by a distance of 6764.72 ft. Since the degree of accuracy of the instrument itself is 0.1 mil (0.056 deg.) the main source of error is in atmospheric refraction, orientation, base line accuracy, etc. The total error is probably less than 0.5 mils and in tests by the U. S. Army the accuracy was normally better than 0.3 mils under operating conditions. A synchronous timing circuit was employed to take simultaneous photographs for triangulation. Using the following diagram



where I = position of phototheodolite No. 1

II = position of phototheodolite No. 2

d = length of base line

Δh = difference in height of No. 1 and No. 2 installations

P = point of cloud in space

then assuming a flat earth and a right-handed coordinate system as shown,
the Cartesian coordinate of point P in space is given by

$$X = \frac{d}{\cot A_I - \cot A_{II}}$$

$$Y = X \cot A_I$$

$$Z = X \tan B_I \csc A_I = X \tan B_{II} \csc A_{II} + \Delta h$$

Cloud tops growth determined by this method has an accuracy of better than ± 4 meters sec^{-1} . However, due to lack of suitable clouds, no useable data was obtained during the 1963 operational season.

Investigations into possible causes of clear air turbulence at jet altitudes so far have led into the possibility of the use of the vertical shear of the winds and the vertical motion at flight levels as forecast parameters. The included unpublished papers, "Vertical Velocity as Expressed by the Horizontal Equation of Motion," and "A Dynamic-Kinematic Method for Computing Vertical Motion," are admittedly only a start on what still is a very perplexing problem.

In preparation for preprints are,

"Free-Water Content Measurement and High-Speed Droplet Photography
During Penetration of Great Plains Thunderstorms," by G.P. Roys.

"Preliminary Result of Analysis of the Cumulonimbus Cloud of April 21, 1961,"
by T. Fujita.

"An Aircraft Investigation of the cT - mT Boundary and Its Role in the
Development of Organized Convective Activity," by L. D. Sanders, and

"Seasonal Tornado Frequencies," by N. E. Prosser.

These preprints should be considered as supplements to this report and will be
forwarded in the appropriate quantities when received from the printer.

Attachments:

- I. List of NSSP Reports Nos. 1 through 16
- II. B-26 time history and flight path
- III. Report, "Thunderstorm Turbulence Measurements by
Aircraft and Concurrent Radar Echo Evaluations"
- IV. Report, "On Vectoring Aircraft Through Thunderstorms"
- V. U-2 photograph of cumulonimbus
- VI.a Aerial photo of location of phototheodolites
b. Photo of phototheodolite
- VII. Paper, "Vertical Velocity as Expressed by the Horizontal
Equation of Motion"
- VIII. Paper, "A Dynamic-Kinematic Method for Computing
Vertical Motion"

ATTACHMENT I

LIST OF NSSP REPORTS NOS. 1 THROUGH 16

List of NSSP Preprints Nos. 1 through 16

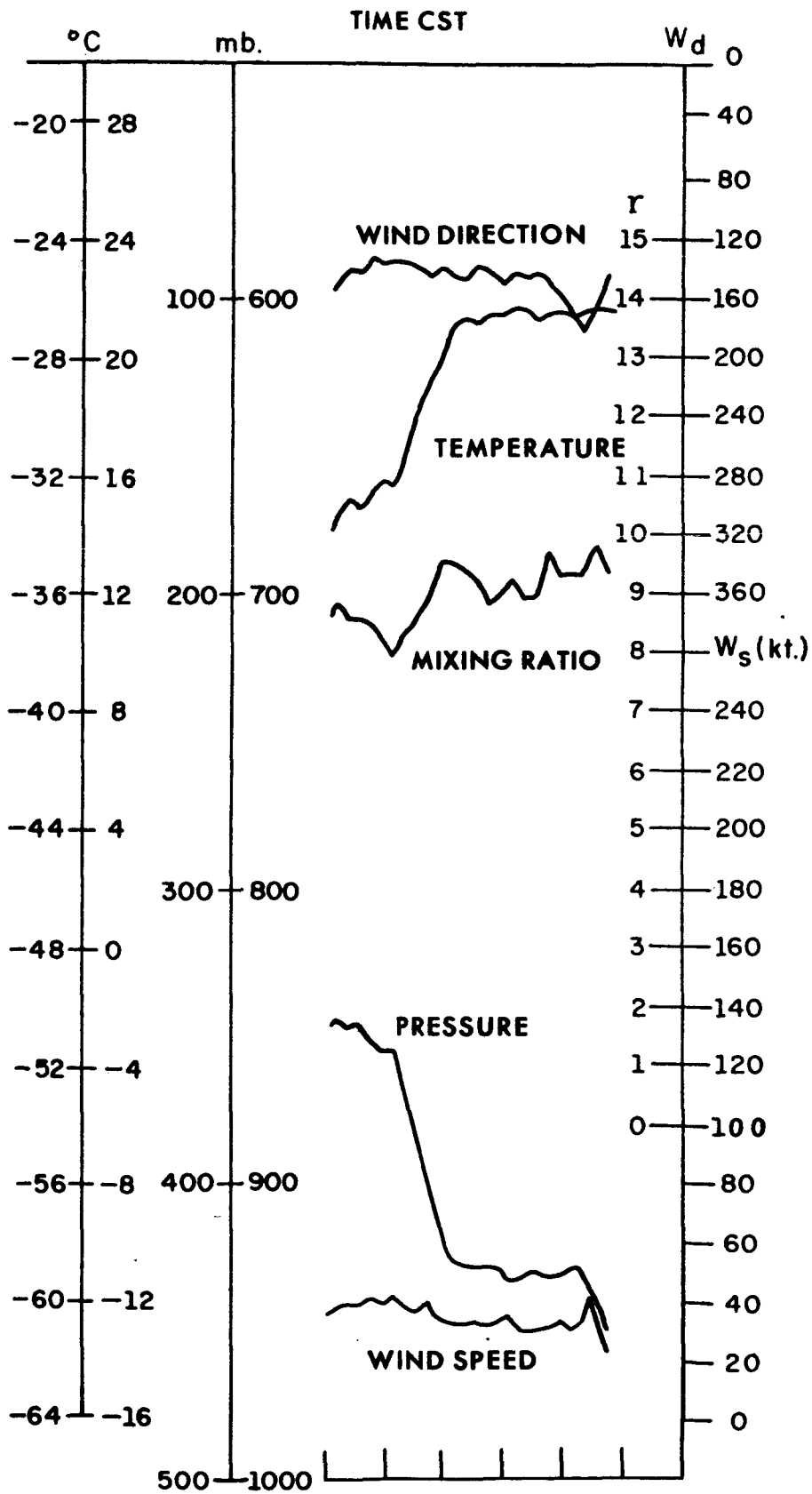
- No. 1 "National Severe Storms Project Objectives and Basic Design,"
Staff, NSSP, March 1961.
- No. 2 "The Development of Aircraft Investigations of Squall Lines from
1956-1960," B. B. Goddard, February 1962.
- No. 3 "Instability Lines and Their Environments as Shown by Aircraft
Soundings and Quasi-Horizontal Traverses," D. T. Williams, February 1962.
- No. 4 "On the Mechanics of the Tornado," J. R. Fulks, February 1962.
- No. 5 "A Summary of Field Operations and Data Collection by the National
Severe Storms Project in Spring 1961," J. T. Lee, March 1962.
- No. 6 "Index to the NSSP Surface Network," T. Fujita, April 1962.
- No. 7 "The Vertical Structure of Three Dry Lines as Revealed by Aircraft
Traverses," E. L. McGuire, April 1962.
- No. 8 "Radar Observations of a Tornado Thunderstorm in Vertical Section,"
Ralph J. Donaldson, Jr., April 1962.
- No. 9 "Dynamics of Severe Convective Storms," Chester W. Newton, July 1962.
- No. 10 "Some Measured Characteristics of Severe Storm Turbulence,
Roy Steiner and Richard H. Rhyne, July 1962.
- No. 11 "A Study of the Kinematic Properties of Certain Small-Scale Systems,"
D. T. Williams, October 1962.
- No. 12 "Analysis of the Severe Weather Factor in Automatic Control of Air
Route Traffic," W. Boynton Beckwith, December 1962.
- No. 13 "500-Kc./Sec. Sferics Studies in Severe Storms," Douglas A. Kohl
and John E. Miller, April 1963.
- No. 14 "Field Operations of the National Severe Storms Project in Spring 1962,"
L. D. Sanders, May 1963.
- No. 15 "Penetrations of Thunderstorms by an Aircraft Flying at Supersonic Speeds,"
G.P. Roys.
"Radar Photographs and Gust Loads in Three Storms of 1961 Rough Rider,"
Paul W. J. Schumacher, May 1963.

No. 16 "Analysis of Selected Aircraft Data from NSSP Operations, 1962,"
T. Fujita, May 1963.

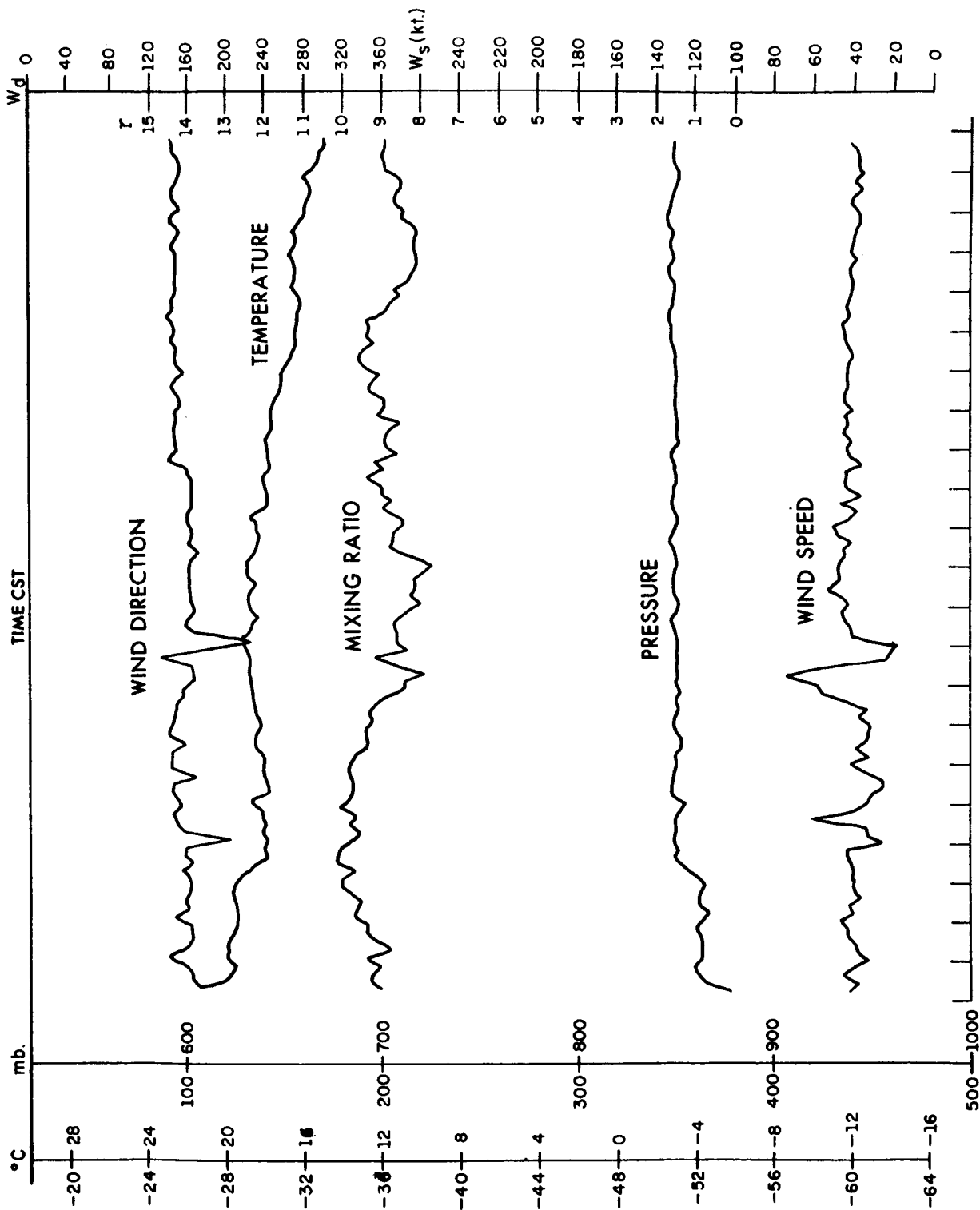
ATTACHMENT II

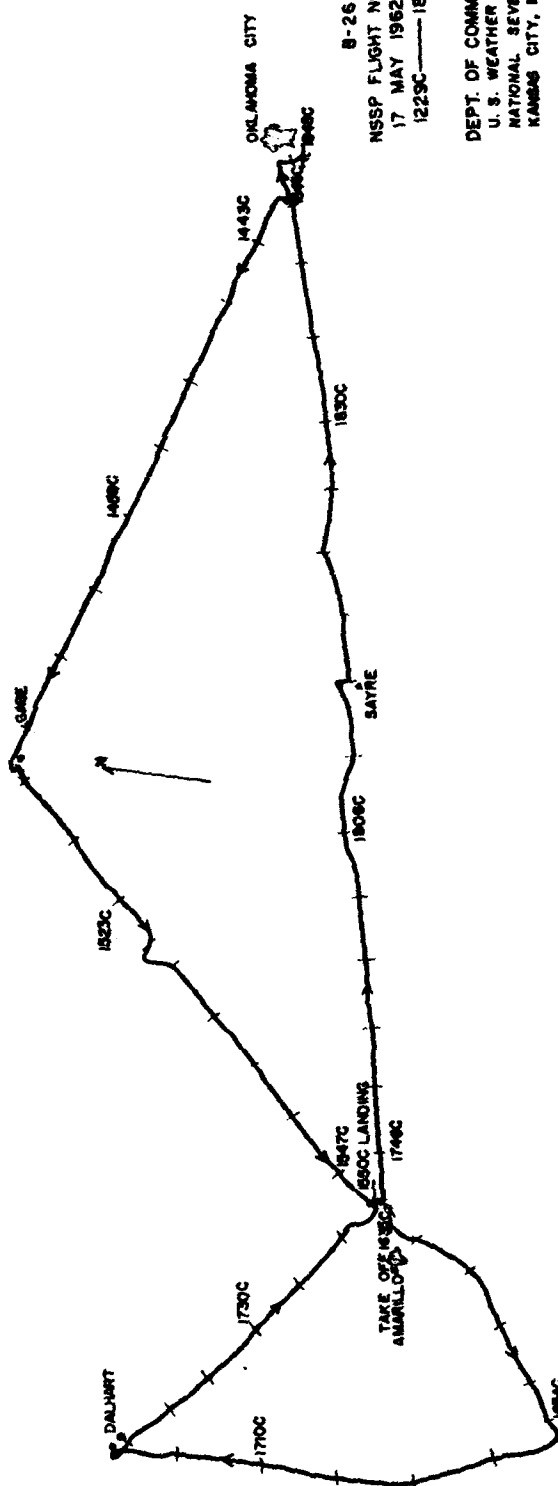
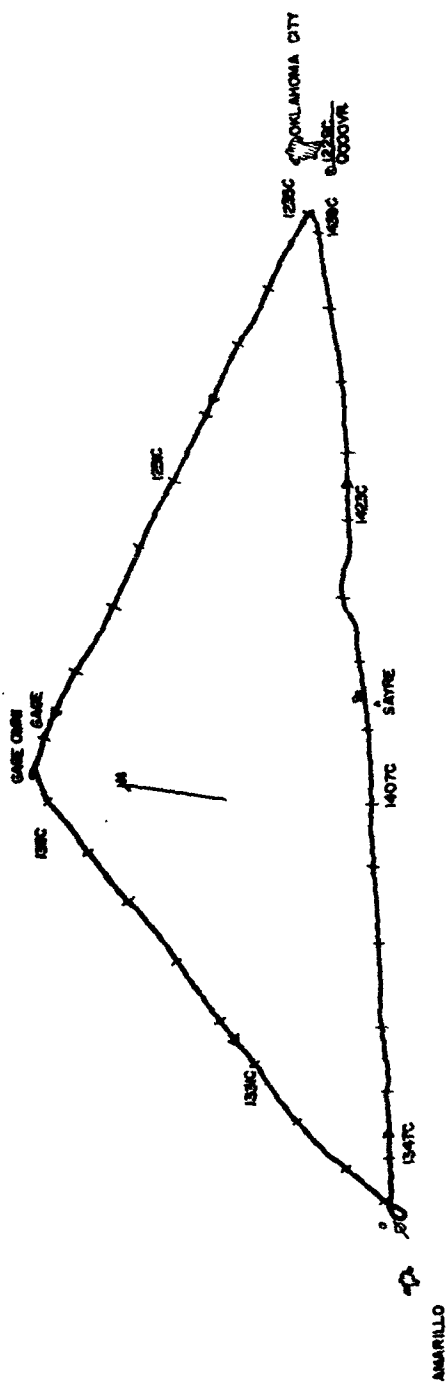
EXAMPLE OF AIRCRAFT POSTNAVIGATION AND TIME-HISTORY OF RECORDED METEOROLOGICAL PARAMETERS

NSSP FLIGHT PROFILE



NSSP FLIGHT PROFILE





8-26
INSSP FLIGHT NO. 25-62
17 MAY 1962
1229C-----1848C

DEPT. OF COMMERCE
U. S. WEATHER BUREAU
NATIONAL SEVERE STORMS PROJECT
KANSAS CITY, MISSOURI

FLIGHT SCHEDULE
OKC--GAGE--AMA--SAYRE--OKC
GAGE--AMA LAND & REFUEL
TEXICO--DALHART--AMA--SAYRE--OKC



N64-27399

Cat-21

ATTACHMENT III

"THUNDERSTORM TURBULENCE MEASUREMENTS BY AIRCRAFT
AND CONCURRENT RADAR ECHO EVALUATIONS"

J. T. Lee

ABSTRACT

Atmospheric turbulence in thunderstorms has always created a problem in aircraft operations. In order to define the most critical areas so that suitable avoidance procedures may be developed, a study was made of a number of controlled aircraft penetrations of thunderstorms. The relationship between thunderstorm growth, radar measurements and atmospheric turbulence was investigated. As background material, a brief resume of turbulence, turbulence measurements and radar reflectivity concepts is given. Case studies, along with data from previous reports, are used to show that there appears to be no direct correlation between radar echo intensity or gradient of successive reflectivity values and turbulence. Rather, there appears to exist a positive correlation between turbulence and rate of change in radar reflectivity. The most likely position of the critical area is also discussed. Altitude changes occurring during thunderstorm penetrations are also given to indicate the amount of air space required by an aircraft.

THUNDERSTORM TURBULENCE MEASUREMENTS BY AIRCRAFT AND CONCURRENT RADAR ECHO EVALUATIONS

1. INTRODUCTION

Sutton [1] defines turbulence as "a state of fluid flow in which the instantaneous velocities exhibit irregular and apparently random fluctuations..." With respect to a thunderstorm, turbulence is usually thought of as a sequence of irregular vertical or horizontal motions of the air within the storm area. This motion can be divided for convenience into two classes - drafts and gusts, although it is recognized that no sharp division exists. The Thunderstorm Project Report of 1949 [2] defined these as: "Draft - a sustained, nonhorizontal, current or stream of air in a thunderstorm. Drafts are continuous over regions as large as a thunderstorm cell, and vertical components are greater than approximately 3 ft. sec.⁻¹." "Gust - an irregular, local, transitory variation in a velocity field. These irregular variations are usually considered to be a number of small eddies superimposed on the general air flow. They may be found both inside and outside the main drafts."

The Meteorological Glossary [3] defines gusts related to aircraft turbulence as "a sharp change in wind speed relative to the aircraft . . . resulting in increased structural stress upon the aircraft." Thus, turbulence caused by gusts within a thunderstorm can be considered as resulting from shear zones associated with the thunderstorm drafts.

The Thunderstorm Project [2] in 1946-47 working at altitudes below 26,000 ft. m.s.l. found that the most frequent gust size was approximately 150 ft. in diameter although ranges from 25 ft. to 800 ft. were measured.

2. AIRCRAFT

In the investigations of the National Severe Storms Project during the period 1960-1962 under the code name "Rough Rider", aircraft penetrations of thunderstorms were made predominantly from above 25,000 ft. to 40,000 ft. Some of the aircraft used are shown in figure 1. These thunderstorm penetrations were controlled penetrations of selected storms by the specially-instrumented jet aircraft. The controlling was done by a Federal Aviation Agency controller, the storms selected by the National Severe Storms Project personnel and the aircraft operated by the Aeronautical Systems Division of the United States Air Force. The aircraft were equipped with a recording accelerometer mounted at the plane's center of gravity. Accelerations normal to the axis of the aircraft (ΔN) were recorded in analogue form. These records were then read at 0.1-second intervals in the data reduction process. This interval was found to be sufficiently short to define most of the turbulence experienced. In addition, airspeed, pressure altitude, aircraft weight, aircraft altitude and other special information were recorded.

The main portion of this report will be restricted to data collected by a T-33 aircraft flying at an average true air speed

of 360 knots or 608 ft. sec.⁻¹.

3. RADAR

Concurrent with the aircraft observations, reflectivity measurements were made with a calibrated WSR-57 10 cm. weather radar. The location of the aircraft was monitored by use of an IFF transponder in the aircraft and an MPX-7 radar on the ground, the MPX-7 antenna being synchronized with the WSR-57 radar. The resulting radar data consists of 35 mm. photographs (fig. 2) taken at 15- to 17-second intervals - one for each revolution of the antenna - showing the radar echo configuration of the storm at the penetration altitude and the IFF position of the aircraft. A profile of the intensity of the storm was acquired by systematic attenuation of the radar return during a series of antenna scans. This technique provided a quantitative measurement of echo intensity or "Z" values for comparison with the vertical acceleration measured by the aircraft.

Basically, the equation used in radar computations for the ratio of the average power returned (\bar{P}_r) from a cloud section to the power transmitted (P_t) is given by Battan [4] as

$$\frac{\bar{P}_r}{P_t} = \frac{\pi^5}{72} \left(\frac{\theta \varphi h A_p^2}{\lambda^6} \right) \frac{|K^2|}{r^2} \sum_{vol} D^6 \quad \text{where}$$

\bar{P}_r = average power returned (energy received at the antenna)

P_t = power transmitted

θ = horizontal width of radar beam

φ = vertical width of radar beam

h = pulse length

A_p = apertural area of the paraboloidal reflector of the antenna

λ = wave length of radiation

$K = \frac{m^2 - 1}{m^2 + 2}$ where "m" is the complex index of refraction

r = range of target

D = diameter of droplets

As can be seen in the above equation, all factors except K , r , and D are fixed by the physical properties of the radar. For water droplets $|K^2|$ has been found to have a value near 0.93 for 10 cm. radar [5] and will be considered as 0.93 in this report. This leaves the range (r) and the number and size of the drops in the radar beam as the only variables which will change the numerical value of the ratio, or, in practice, the "brightness" of the echo. The term $\sum_{vol} D^6$ in the preceding equation is called the reflectivity factor and is designated by the symbol Z and has the unit of $\text{mm.}^6 \text{ m.}^{-3}$. Thus, the equation can be written for a particular radar as

$$\frac{P_r}{P_t} = C \frac{Z}{r^2} \text{ where } C \text{ is a constant equal to}$$

$$\frac{\pi^5}{72} \left(\frac{\theta \varphi h A_p^2}{\lambda^6} \right) |K^2|.$$

In the following report the radar echo intensities are given in terms of the reflectivity "Z" normalized for range. This then yields a quantitative measurement of echo intensity which can be used in comparing one case to another. It has been assumed in this report that the entire radar beam is intercepted by the cloud.

The radar data were extracted from the film recordings by making composite tracings of the intensity contours and IFF track at two-minute intervals as shown in fig. 3. For the 1962 data, the area enclosed by each Z level contour was planimetered in order to determine the horizontal cross-sectional area of that particular echo intensity. Time cross sections of these data were then constructed to provide horizontal growth profiles of the thunderstorm. It is assumed that if an area of particular intensity is increasing in size then the storm is increasing in intensity. If the area is decreasing, then the storm is decreasing. Gradient values were determined along the aircraft track and were measured along a normal to the isopleths of echo intensity.

4. TURBULENCE

A. Discussion

Prior to 1954 a gust-load formula was developed and utilized by the National Aeronautics and Space Administration in the evaluation and interpretation of gust and gust-load data experienced during flights through turbulent air. This formula reduced

the data to an "effective" gust velocity (U_e) [6]. This served to relate the peak accelerations due to gusts to be expected on a given aircraft to the peak accelerations measured by another aircraft. After 1954 a revised gust-load formula was developed by Pratt and Walker [7]. The basic assumptions are:

1. The airplane is a rigid body,
2. The airplane forward speed is constant,
3. The airplane is in steady level flight prior to entry into the gust,
4. The airplane can rise but cannot pitch,
5. The lift increments of the fuselage and horizontal tail surfaces are negligible in comparison with the wing lift increment,
6. The gust velocity is uniform across the wing span and is parallel to the vertical axis of the airplane at any instant.

Disregarding forces associated with steady level flight a summation of vertical or normal forces on the airplane in a gust, the following equation was developed:

$$\begin{aligned}
 M \frac{d^2 z}{dt^2} + \frac{\rho}{2} V^2 \text{Sm} \int_0^t \frac{1}{2\pi} C_{L_\alpha} (t - t_1) \frac{d^2 z}{dt_1^2} \frac{1}{V} dt_1 \\
 = \frac{\rho}{2} V^2 \text{Sm} \frac{U}{V} \int_0^t \frac{1}{2\pi} C_{L_g} (t - t_1) \frac{d\left[\frac{u(t_1)}{U}\right]}{dt_1} dt_1 + \\
 \frac{\rho}{2} V^2 \text{Sm} \frac{U}{V} \frac{u(0)}{U} \frac{1}{2\pi} C_{L_g} (t)
 \end{aligned}$$

where C_{L_g} = transient lift response to penetration of sharp-edge gust

C_{L_α} = transient lift response to unit-jump change in angle

of attack

m = wing lift-curve slope, per radian

M = airplane mass, slugs

S = wing area, sq. ft.

t = time, sec.

t_1 = dummy variable in superposition integral, sec.

U = gust velocity (maximum value), fps

u = gust velocity at any penetration distance, fps

V = airspeed, fps

z = airplane vertical displacement (positive upward), ft.

ρ = air density, slugs/cu. ft.

The first term on the left-hand side is the inertia reaction and the second term is the damping force due to the aircraft vertical velocity. On the right-hand side, both terms are forces due to gusts having zero velocity at the beginning of penetration and the second term is the force due to a gust having an initial velocity other than zero at the beginning of penetration.

Pratt and Walker solved the above equation using certain relationships and assuming a $(1 - \cos)$ gust shape (fig. 4c) with the gust reaching maximum value in 12.5 chord lengths. This yielded a new term called "derived" gust velocity U_{de} and is given by

$$U_{de} = \frac{2 a_n W}{m \rho_0 S V_e K_g} \quad \text{where}$$

a_n = normal acceleration

W = aircraft weight

m = wing lift-curve slope

ρ_o = air density at sea level

S = wing area

V_e = equivalent air speed

K_g = gust factor (revised alleviation factor)

The "effective" gust velocity U_e formerly used is related to the derived gust velocity U_{de} as follows:

$U_{de} = U_e \frac{K}{K_g}$ where K is the alleviation factor used in computing the "effective gust" and the other terms are the same as previously defined. The factor $\frac{K}{K_g}$ averages about 1.8 and this value has been used in this report to compare data gathered in thunderstorm penetrations before 1954 with the present project data.

The values of the derived gust velocities (U_{de}) form a better means of transferring the acceleration measurements on one aircraft to another. The basic measurements used in this method are the peak accelerations at the center of gravity of the airplane.

For delineating various degrees of turbulence the following definitions [8] and corresponding U_{de} values have been agreed upon and are given in Table 1.

In the following studies the U_{de} values are presented in several forms, (1) time histories, (2) frequency distribution per flight, and (3) average number of gusts per unit distance (fig. 4).

Table 1. Turbulence definitions and corresponding derived gust velocities.

TURBU- LENCE	DEFINITION	U_{de}
Light	A turbulent condition during which occupants may be required to use seat belts, but objects in the airplane remain at rest.	Less than 20 fps
Moderate	A turbulent condition in which occupants require seat belts and occasionally are thrown against the belt. Unsecured objects in the aircraft move about.	20-35 fps
Severe	A turbulent condition in which the aircraft momentarily may be out of control. Occupants are thrown violently against the belt and back into the seat. Objects not secured in the aircraft are tossed about.	35-50 fps
Extreme	A rarely encountered turbulent condition in which the aircraft is violently tossed about, and is practically impossible to control. May cause structural damage.	50 fps and above

If a continuous time history of the true vertical velocity (w_g) is desired the following equation must be evaluated:

$$w_g = V\alpha_v - V\dot{\theta} + w_a + \ell\ddot{\theta}$$

where w_g = vertical velocity of the air

w_a = airplane vertical velocity

V = true airspeed

α_v = vane indicated angle of attack

θ = pitch angle

ℓ = distance between the accelerometer and the angle-of-attack vanes

$\dot{\theta}$ = pitch velocity

All of the quantities are measured directly by the penetration aircraft except w_a which can be determined from an integration of the accelerometer measurements.

A comparison between the derived gust velocity (U_{de}), vertical component of true gust velocity (w_g) and lateral component of true gust velocity (v_g) is shown for a particular case in figure 5 and is stated by Steiner [9].

The derived gust velocity and true gust velocity scales on the plot are of the same magnitude and units but are really not comparable. The w_g and v_g time histories represent the true air flow, the U_{de} time history represents a resulting load level on an aircraft. Each arrow at the top of the figure is located at the instant along the time history at which the aircraft reached a maximum acceleration and the length of the arrow represents the magnitude of the computed derived gust velocity. It can be seen

that each derived gust velocity appears to correlate with, or result from, a sharp change in the vertical velocity of the air flow. The broader or longer wave length changes in the air flow, although most times several times greater than U_{de} , do not give rise to very large aircraft accelerations. Thus U_{de} represents the turbulence but does not give a measure of the draft velocities.

Due to instrumental difficulties in 1962 accurate evaluation of the vertical gust velocity (w_g) has not been completed, and therefore only the derived gust velocity (U_{de}) will be used.

When thinking of turbulence it must also be borne in mind that several factors enter into a pilot's determination of the classification of turbulence and that the official definitions and U_{de} values may not always be in agreement with comments of pilots as to the degree of turbulence.

During a preliminary evaluation of the 1961 data [10] the records taken during the penetrations indicated high roll and pitch rates, and if the pilot were not expecting such disturbances the aircraft could quickly end up in extreme attitudes. The pilot was given the opportunity to engage in both physical and mental preparation and thus successful thunderstorm penetrations were accomplished. This was as true for the subsonic penetrations as it was for those conducted at supersonic speeds. From this experience and records, the Air Force Aeronautical Systems Division developed the following list of factors which influence pilots' reports on turbulence:

(a) Meteorological

1. Presence or absence of large gust velocities
2. Frequency of occurrence of all gusts

(b) Personal

1. Mental attitude-preparation for encounter
2. Prior training
3. Prior experience in turbulence
4. Prior experience in the type of aircraft

(c) Operational

1. Type and airspeed of aircraft
2. Time spent in turbulence.

This is illustrated in figure 6, using data from the 1961 flights. In this figure the envelopes surrounding the pilot reports of turbulence in the "moderate" and "severe" categories are superimposed upon the frequency and derived gust velocity recorded at the time of the pilot's comment. It can be seen that at high frequencies (1 or more per n. mi.) and up to U_{de} value of 25 ft. sec.⁻¹, the two envelopes are roughly equivalent. The pilot's evaluation of intensity of turbulence in this region must therefore be considered very subjective. Above U_{de} values of 25 ft. sec.⁻¹, this ambiguity tends to disappear.

Earlier work in the Thunderstorm Project [2] also showed this. The intensity of the turbulence reported was almost entirely determined by the gusts encountered and not by the altitude displacement experienced by the aircraft. Their data indicated that if the frequency of gusts greater than U_{de} value

of 27 ft. sec.⁻¹ was more than 8 per 3,000 ft. (5 sec. of T-33 time) the turbulence was called "heavy". However, in the following discussion only in a few cases will the pilot comments be used. Normally the defined class limits of the derived gust velocity will be used in the characterization of the turbulence encountered.

B. New data

In the computations of the derived gust velocities the following assumptions have been made in addition to those made for the basic equation:

(a) The weight of the aircraft remains constant during a specific run or pass.

(b) Variations of ± 500 ft. from a particular altitude can be neglected; variations of more than ± 500 ft. are recognized in the computations in factors involving air density.

(c) Airspeed can be used at 10-knot intervals without introducing more than a 0.5% error.

These above assumptions have been found to produce at a maximum less than a 5% error which is within the limits of the instrumental accuracy.

Specific examples of the turbulence measurements are shown in figures 7 - 13 for May 23, 1962, and figures 14 - 16 for May 24, 1962. These show,

(a) Series of tracings of the radar scope echo of the penetration cloud with several reflectivity levels indicated. True North is toward the top of the page. The radar beam is

centered at the level of penetration;

(b) The path of the aircraft through the cloud as indicated by the IFF;

(c) A time history of derived gust velocities for the most intense portions of the flight. A negative value means a downward gust and a positive value an upward gust;

(d) A time history of the area enclosed by various reflectivity levels. It is assumed that a growth in area reflects an increasing storm intensity and that a decreasing area size suggests a decreasing storm activity;

(e) A frequency distribution of the derived gust velocities for the complete run.

Figure 7 is the depiction of the first run on May 23. The synoptic situation was dominated at 0600 CST by a deep low pressure center in the vicinity of St. Cloud, Minnesota. From this low pressure center a cold front curved eastward into Wisconsin, thence southward into Illinois and then southwestward through central Missouri to a point just north of Fort Smith, Arkansas. From this point to north of McAlester, Oklahoma, south of Oklahoma City to Wichita Falls, Texas, the front was gradually losing its forward speed and by 1200 CST it had become stationary through the Oklahoma region. Surface dewpoints which had been in the low 60°F. at 0600 CST were now 67°F. - 69°F. The front remained quasi-stationary the rest of the day in Oklahoma, with the dewpoints reaching 70°F. and temperatures near 90°F. by 1800 CST. The 0600 CST 850 mb. chart indicated a tongue of high

moisture content extending from Del Rio, Texas, to west of Fort Worth to the vicinity of Fort Smith, Arkansas. By 1800 CST the moist tongue had shifted nearer to Oklahoma City, Oklahoma, before curving northeastward.

Near the intersection of this moist tongue and the surface quasi-stationary front a number of cumulus clouds formed, some of which developed into moderate thunderstorms. The jet stream was over the area and was centered near an altitude of 41,000 ft. Winds in the jet stream were from 250 - 270 degrees at 100 knots.

The storm cell penetrated was originally 154 degrees and 50 n. mi. from Oklahoma City. During the course of the penetrations the cell moved north-northeastward along the quasi-stationary front until at the end of the penetrations the cell was almost due east of Oklahoma City at about 40 miles. The top of the cloud was measured by the T-33 as 40,500 ft. m.s.l. at 1647 CST. Run #1 made by the T-33 at a pressure altitude near 15,000 ft. m.s.l. was from west to east. The so-called hard core of this storm was just beginning to grow and covered a very small area (fig. 7c) and the reflectivity had a relatively low value. The penetration was characterized by a sharp downdraft just after entering the cloud, then light to moderate turbulence, with the moderate turbulence ($U_{de} = 20 \text{ ft. sec.}^{-1}$ or more) being shown mainly by negative derived gust velocities (fig. 7b and d). Precipitation was classified as heavy by the pilot. In figure 7a the area enclosed by Z_2 appears to be the limit of the cloud at the penetration altitude, the Z_1 area is mainly the cloud overhang

reported by the pilot as being just above him. The U_{de} time history is only an excerpt from the total run and is used in this to show the most important portion of the flight. The same convention is followed in succeeding figures. In general, the portions of flight preceding and following the shown section are characterized by light turbulence.

Run #2 was also at 15,000 ft. just under the overhang. This was an east to west pass and cut very near the center of the cell which showed a reflectivity (Z) value of $9.3 \times 10^3 \text{ mm}^6 \text{ m}^{-3}$. This run was made when both the Z_3 and Z_4 areas were at a momentary maximum (fig. 8c). As can be seen by comparing the frequency distribution for runs #1 and #2 the turbulence experienced was greater for run #2. The pilot's comments during run #1 were for light to moderate turbulence and for run #2, moderate to heavy turbulence with "heavy" precipitation.

Run #3 (fig. 9) represents an altitude change to 23,000 ft. and occurred when the first cell was decreasing in intensity (fig. 9c). Light to moderate turbulence was again experienced with a frequency distribution more nearly equal to run #1. It should be noted that the turbulence experienced was at least as great as in run #1 even though the altitude was increased, the Z_3 had decreased and the path of the aircraft was at least 2 miles southeast of the core.

Run #4 (fig. 10), made at the same altitude as run #3, occurs as the area enclosed by Z_3 is increasing again, and we can assume

the storm is increasing. The aircraft this time comes closer to the hard core although still skirting the southeastern edge by a few miles. The contour for Z_3 at 1612 CST was not available but one can see in fig. 10a the reactivation of the thunderstorm cell. The time history of U_{de} , the frequency distribution and the pilot's comments are all in agreement that this was the most turbulent one so far. It is interesting to note in the time history the grouping of the U_{de} values of 20 ft. sec.^{-1} or more at 0.5 miles, 1.5 miles, and just before 2.5 n. mi. Insufficiently accurate time synchronization prohibits a positive placement of these areas but as near as can be ascertained the turbulent maximum near 2.5 n. mi. on the U_{de} time history occurs as the aircraft passes close to the small Z_3 cell in the northeastern section; the one at 1.5 n. mi. occurs as the aircraft passes 1.5 miles east of the main core; and the one at 0.5 n. mi. is associated with the other small Z_3 core areas just a half mile southeast of the track.

Run #5 (fig. 11) was made at an altitude of 29,000 ft. m.s.l. and at a time when the Z_3 as well as Z_4 reflectivity limits were not reached - at a time when the storm could be said to be "resting". The radar area shown is actually larger than the cloud where the pilot penetrated because a portion of the lower cloud intercepts the beam. Turbulence at this altitude and with reflectivity values below 2.3×10^3 still reached U_{de} values of 20 ft. sec.^{-1} or more several times - sufficient for the pilot to occasionally classify the turbulence as "moderate".

Run #6 at 29,000 ft. m.s.l. (fig. 12) coincided with an increase in storm activity. It should be pointed out that it is very apparent that a single storm system does undergo a pulsation in intensity with the time intervals varying from 5 to 10 minutes and that this pulsation does correlate with the varying degrees of turbulence at the same altitude which may be experienced by aircraft separated by a corresponding time interval. When comparing the U_{de} time histories for runs #5 and #6 and the U_{de} frequency distributions, the definite increase in the occurrence of greater turbulence is readily evident. If we compare run #6 which passes 0.5 miles east of the Z_3 level at 29,000 ft. and run #1 in which the aircraft penetrated or approached very close to the Z_4 level at 15,000 ft. we find the derived gust velocities larger although still holding very nearly a Gaussian distribution with a mean of zero. This tends to substantiate the hypotheses stated in the Thunderstorm Project [2] that the gust velocities can be expected to increase with height at least to within 5,000 ft. of the top of the visible cloud.

Figure 13 is of run #7. The aircraft has descended 9,000 ft. to a pressure altitude of 20,000 ft. m.s.l. The aircraft path cuts the center of the Z_3 reflectivity area just at the time the area is momentarily decreasing. Most of the turbulence experienced is below $U_{de} = 20$ ft. sec.⁻¹ with a few "strong bumps" as can be seen in the U_{de} time history section. The pilot experienced a little hail but very little precipitation.

Unfortunately, data for the succeeding three passes which occurred as the storm was again building rapidly are not available due to the records jamming. It will have to suffice to say that the pilot's comments indicated the turbulence increased and hail did extensive damage to the aircraft. The pilot's summary of the penetrations for this day stated that the flights followed a general pattern of a sharp "jolt" upon cloud entry, then rather light turbulence until approaching the vicinity of the core of the storm at which time the turbulence showed a marked increase. This storm, as evidenced by the relatively low reflectivity values can at most be classified as moderate. While altitude changes occurred during the penetrations, the maximum experienced was on run #9 in which the aircraft gained 2000 ft. even though the pilot held at 10° to 15° nose-down attitude.

The next day, May 24, the quasi-stationary front which had existed through southeastern Oklahoma on the 23rd moved by 1200 CST north of the Kansas-Oklahoma border leaving the area south of it covered by hot, humid air with surface dewpoints around 65°F. The surface temperatures were near 90°F. over a large area and surface winds were southerly 10 to 15 knots. There was a weak "dry line" west of Gage, Oklahoma, to west of Childress, Texas.

At 0600 CST, 850 mb. a dewpoint temperature ridge of 13°C. extended from Del Rio, Texas to Altus, Oklahoma, then to a point just west of Oklahoma City. Winds at this level were south in the southern portion, shifting to southwest in the northern portion at 20 knots. By 1800 CST or about 1-1/2 hours after

the penetrations were made, the ridge had shifted slowly eastward and was centered on a line from Laredo, Texas, to just west of Fort Worth, Texas, to west of Oklahoma City. The winds were southerly but had increased to 30 knots. A temperature ridge at 850 mb. extended north-south through the Texas and Oklahoma Panhandle region.

The upper jet stream still persisted from El Paso, Texas, to Altus, Oklahoma, to Little Rock, Arkansas, but had decreased from 100 knots on the 23rd to near 80 knots. Under these conditions a few cells developed in the early afternoon, 255° and 125 n. mi. from Oklahoma City. These cells formed a short squall line later in the afternoon, with a strong meso-low development. The aircraft penetrations were made between 1545 and 1630 CST prior to the development of tornadoes and baseball-size hail conditions reported in the Hobart-Altus-Fort Sill area after 1758 CST.

Figures 14 - 16 show the 2nd, 3rd, and 4th penetrations. Run #1 is not shown because complete radar data were not available. Note that the mileage scale for the echo size is considerably different than that used for the May 23 data. This is due to the fact that the storm system covered a much larger area on the 24th making it impractical to use the same mileage scale. The mileage scales on the U_{de} time histories are based on the average true airspeed for each traverse as was done for the 23rd. Since the distance involved in the U_{de} time histories is also greater than that on the 23rd the distance scale is more compact, which does result, unfortunately, in an appearance of shorter time

variations in the derived gust velocities. This is in part true as the turbulence experienced on the 24th was more pronounced than on the 23rd. The cloud being penetrated had a top between 53,000 and 55,000 ft. m.s.l. or an average of 14,000 ft. higher than the cloud on the 23rd. The radar reflectivity values outlined are also on order of magnitude greater than on the 23rd.

Run #1, which is not shown, experienced very little moderate turbulence, mostly very light, with precipitation ranging from light to moderate. Static was experienced on all flights this day and at times air-to-ground contact had to be carried on by use of a relay aircraft.

Run #2 (fig. 14) began at 25,000 ft. and grazed the northeastern edge of the $Z_3 = 1.5 \times 10^4 \text{ mm.}^6/\text{m.}^3$ contour. The area enclosed by this contour shows relatively little change during the penetration. Moderate turbulence was experienced by the pilot almost immediately upon entry on the northwest side of the cell with one derived gust velocity of $-38 \text{ ft. sec.}^{-1}$ (severe turbulence) occurring over the decreasing cell to the northwest of the main core. Derived gust velocities greater than 20 ft. sec.^{-1} are found almost to the vicinity of the hard core - precipitation was light to moderate. Just before reaching the area delineated by Z_3 the pilot began to enter a strong updraft. Rain increased in intensity but the turbulence decreased. In fact, the pilot's comment was "Turbulence has been quite smooth throughout this strong precipitation area." This is one illustration where relatively high radar reflectivity values, while no doubt

indicating large liquid water concentrations, does not in itself indicate the degree of turbulence. What is of at least equal importance is whether a steady-state condition has been reached, in which case the turbulence apparently is light. This will be illustrated in another case later.

Run #3 (fig. 15) was made 15 minutes later and 5,000 ft. higher in altitude (30,000 ft.). At this time the Z_3 contour encloses a slightly larger area than for run #2 and two very small cores having a radar reflectivity value of at least 5.8×10^4 mm.⁶/m.³ begin to appear. This run, however, skirts more than 4 miles north of the center and so cannot be a true measure of the intensity closer in. The frequency distribution (fig. 15d) does show a broader spectrum of turbulence even though most of it is in the light category. Here, as in run #2, the derived gust velocities exceed 20 ft. sec.⁻¹ only in the negative values even though strong updrafts were encountered.

Run #4 most nearly approaches a penetration of the core of the thunderstorm. The areas enclosed by the Z_3 and Z_4 (figs. 16a and c) are already showing a rather rapid decrease in size. The pilot began to experience moderate turbulence 50 sec. after entry. As the pilot passed through the center of the cell severe turbulence was recorded, mixed with areas of light to moderate turbulence. This flight, as shown by the frequency distribution of the derived gust velocity (fig. 16d), was the most turbulent of the day. Of interest, not shown in the figure but derived from the pilot's comments, is that while sometimes the severe

turbulence occurred along with heavy precipitation, at other times the precipitation was only light. The reverse was also true, that is, that some heavy precipitation areas produced severe turbulence while other areas of heavy precipitation yielded a smooth flight. Strong updrafts and large hail were encountered during this traverse, bearing out that the nearer one approaches a changing reflectivity value of 10^4 to 10^5 mm.⁶/m.³ the more probable damaging hail will be encountered.

The above cases indicate the variability found within thunderstorms. As a composite, figure 17 shows the frequency distribution of 5451 derived gust velocities computed for the T-33 flights made on May 20, 23, 24, 31 and June 5, 1962. These flights covered over 360 n. mi. of in-thunderstorm cloud runs. The distribution is Gaussian with a computed mean of -0.39 ft. sec.⁻¹ and a standard deviation of 8.10 ft. sec.⁻¹. That a definite difference does exist between runs can be seen by comparing figures 18a and 18b. Run #4 of the 24th of May has a mean of -1.3 ft. sec.⁻¹ and a standard deviation of 10.5 ft. sec.⁻¹. Run #1 of June 5 is definitely a much smoother flight with a mean also of -1.3 ft. sec.⁻¹ but a standard deviation of only 5.6 ft. sec.⁻¹. Of great significance is the fact that the negative values predominate such that even though the aircraft may experience an increase in pressure altitude due to the larger drafts, the greatest or more frequent turbulence is negative or downward. Figure 19 is a graph showing the number of times values of derived gust velocities may be expected per 10 n. mi. of thunderstorm flying. A unit of

10 n. mi. was chosen as this is close to the diameter of the average-sized thunderstorm. Since the 1962 flights penetrated clouds which in nearly all cases yielded lower radar reflectivity values than the clouds penetrated in 1960 or 1961 the figures given above must be considered very conservative.

This is illustrated in the case of May 5, 1961 shown in figures 20 and 21 from a paper by Schumacher [11]. The turbulence in this storm was called severe by the pilot and U_{de} values exceeded 35 ft. sec.⁻¹. This storm was located on an axis of moisture running from Texas into central Oklahoma. The cloud was about 100 n. mi. southwest of Oklahoma City and had started as a single cell, grew, then began dissipating while a new cell grew at the southwest end. This new cell was the one penetrated. Selected radar echo contours for the storm are shown in figures 20a and b. The contour sequence for figure 20a was started at 1227:30 and completed at 1228:30 CST. The aircraft was near the center of the cloud at 1233 CST or 4.5 min. after figure 20a was completed. Figure 20b is the contour cycling sequence beginning at 1236 and ending at 1238 CST (2 minutes being required for an 8-step cycle, however, only selected contours are shown). Thus, the penetration occurred 3 minutes prior to the start of figure 20b. The innermost intensity reflectivity factor (Z), range normalized, increased from $6 \times 10^3 \text{ mm.}^3/\text{m.}^3$ to $10^5 \text{ mm.}^6/\text{m.}^3$. The increase in gradient between contours also attests to the increasing intensity, and from this it is judged that the center of the core probably had a reflectivity factor of near $10^6 \text{ mm.}^6/\text{m.}^3$.

The derived gust velocity distribution for this penetration is shown in figure 21 as the number of gusts per nautical mile of flight. Multiplying the values on the vertical scale by 10 makes it easier to compare this figure with figure 19 and it is immediately apparent severe turbulence was experienced four times as often and moderate turbulence nearly ten times greater than the average of the 1962 storms. That this penetration was made at 40,000 ft. m.s.l. with the cloud top near 45,000 ft. further illustrates a point previously stated that there is an indication that turbulence increases with height in a thunderstorm rapidly changing in intensity.

Another case of interest is shown in figure 22. This penetration on May 20, 1962, is of interest not only for the high free water content recorded at 29,000 ft. but also because the aircraft penetrated the center of the core at the time of the radar maximum reflectivity of at least 1.93×10^4 . Noticeable is that the areas enclosed by Z_2 , Z_3 , and Z_4 show little change. Thus, though the pilot reports "hitting a wall of water" during this penetration, only light turbulence was experienced.

As far as can be ascertained from the 1962 data, no correlation can be found between turbulence and radar reflectivity gradients - part of this failure may be due to inadequate time synchronizations and to the limitations of the radar to delineate the reflectivity profile in sufficient detail due to beam width. This point needs further investigation.

Table 2 is a tabulation of the area of maximum turbulence for each penetration as determined from the time histories. The western half of the main storm in 90 per cent of the cases contained the area of maximum turbulence. This is similar to data collected in 1960 but as yet not published.

Table 3 is a tabulation of the distance between the western edge of the visible cloud and the place at which the derived gust velocity equaled or exceeded 20 ft. sec⁻¹. Figure 23 shows the most rapid change in derived gust velocities with time. The most rapid change occurred during the first penetration on May 20. The rate of change in the derived gust velocity was 142 ft. per sec.³ or in this particular case of going from a -0.5 g to a +0.73 g in 0.2 sec. which is equivalent to a change of 6.15 g per sec. The greatest time interval between large U_{de} values which could be considered significant occurred during run #3 on the 5th of June when a change from a $U_{de} = +28$ ft. sec.⁻¹ to a $U_{de} = -38$ ft. sec.⁻¹ occurred in 1.6 sec. or a rate of change in derived gust velocities of 41 ft. per sec.³. These rapid changes are no doubt partly responsible for the pilot sometimes giving turbulence estimations one class higher than recorded by instruments. Figures 24 and 25 [12] illustrate the difference in the degree of turbulence experienced during thunderstorm penetrations made in different geographical areas of the United States. Project Hi Cu was conducted in Arizona while NSSP Rough Rider operations were in Oklahoma. Reflectivity values for the clouds penetrated are not available, and therefore no definite statement

Table 2. Section of T-33 flight path exhibiting the relative maximum and minimum recorded turbulence per penetration.

DATE	RUN	MAXIMUM TURBULENCE	MINIMUM TURBULENCE	CODE NO.
May 20	1	Southwest	Northeast	1
	2	Southwest	Northeast	2
May 23	1	West	East	3
	2	West	East	4
	3	Center	Southwest	5
	4	West	East	6
	5	West	East	7
	6	Center	East	8
	7	Center	East	9
May 24	1	West	East	10
	2	West	East	11
	3	West	East	12
	4	MDT SVR TURBC ENTIRE FLIGHT		13
May 31	1	North-northwest	South-southeast	14
	2	North-northwest	South-southeast	15
June 5	1	West	East	16
	2	Center	East	17
	3	West	East	18
	5	West	East	19
	6	West	East	20
	7	West	East	21
	8	Center	Ends	22

Table 3. Distance from western edge of visible cloud to first recorded value of moderate turbulence (U_{de} equal to or exceeding 20 ft. sec.⁻¹) for 1962 T-33 penetrations.

Date	Run Number	Altitude (ft. MSL)	Distance (n. mi.) from west edge of cloud to U_{de} value 20 ft./sec. or more
May 20	1	27,000	1.93
	2	28,000	2.19
May 23	1	17,000	3.15
	2	15,000	.32
	3	28,000	3.54
	4	23,000	.93
	5	29,000	5.80
	6	30,000	4.09
	7	22,000	3.05
May 24	1	25,000	1.86
	2	25,000	3.43
	3	30,000	7.62
	4	31,000	4.93
May 31	1	29,000	2.40
	2	29,000	1.40
June 5	1	30,000	5.00
	2	30,000	6.55
	3	30,000	3.80
	5	29,000	2.18
	6	27,000	5.01
	7	27,000	1.40
	8	27,000	1.96

can be made as to the reason for occurrence of larger derived gust velocities and higher normal acceleration in the Oklahoma area. However, synoptic data indicate that dynamic and thermodynamic features were stronger in the Oklahoma area and in all probability were a more deciding factor than geographical features.

5. DRAFTS

While in a study on turbulence, the size and magnitude of drafts are not as important as other factors in pilot and passenger reactions this may not be true in air traffic control where the altitude displacement which can occur can be of extreme importance. Table 4 lists some of the more significant altitude changes as reported by the pilot and experienced by the penetration aircraft. The fact that a gain in altitude (updraft) was most often encountered can possibly be explained by the fact that the penetrations were normally made above 20,000 ft. m.s.l. Vertical (true) gust velocities of $208 \text{ ft. sec.}^{-1}$ [9] have been encountered.

6. SUMMARY

The flights made by NSSP Rough Rider operations in 1960-1962 have yielded many pieces of information. However, since the analyses of all the data are not either available or completed, some of the following statements must be considered provisional. Turbulence and turbulence measurements and radar correlations are difficult. With this in mind the following points are made:

1. Thunderstorm turbulence compared to radar echo intensity does not bear a direct correlation. There appears to be a

Table 4. Significant involuntary altitude changes experienced during NSSP thunderstorm penetrations 1960-1962.

DATE	RUN	AIRCRAFT	PENETRATION ALTITUDE	ALTITUDE CHANGE	REMARKS
May 8, 1962	3	F-100	31,000 ft.	+1500 ft.	
May 20, 1962	1	T-33	27,000 ft.	+1800 ft.	
	4	T-33	22,000 ft.	+1900 ft.	
	5	T-33	22,000 ft.	+2200 ft.	
May 23, 1962	5	T-33	20,000 ft.	+1350 ft.	
	9	T-33	20,000 ft.	+2000 ft.	10-15° nose down attitude.
May 24, 1962	4	F-100	30,000 ft.	+1800 ft.	
May 5, 1962	7	T-33	27,000 ft.	+2900 ft.	Power back and nose down.
April 24, 1961	1	F-106	35,000 ft.	+1600 ft.	
May 5, 1961	1	F-106	40,000 ft.	+3500 ft.	
May 21, 1961	2	F-106	25,000 ft.	+2000 ft.	
June 2, 1961	3	F-106	15,000 ft.	+5000 ft.	Encountered severe turbulence also. Nose of aircraft in a pitched down attitude.
June 3, 1961	1	F-106	30,000 ft.	+2500 ft.	
May 4, 1960	1	F-102	40,000 ft.	-3000 ft.	
	1	T-33	40,000 ft.	-3000 ft.min ⁻¹	about 6° nose-up pitch.
May 17, 1960	4	F-106	40,000 ft.	+2000 ft.	
	2	F-102	40,000 ft.	-8000 ft.	
May 19, 1960	5	F-106	40,000 ft.	-5000 ft.	Average loss of 2500 ft.on runs 1-4.
May 24, 1960	3	T-33	40,000 ft.	+2000 ft.	
May 24, 1960	4	T-33	40,000 ft.	-3000 ft.	

critical radar reflectivity value of $10^3 \text{ mm}^6/\text{m}^3$ when derived gust velocities can exceed 20 ft. sec.^{-1} . When the radar reflectivity exceeds $10^5 \text{ mm}^6/\text{m}^3$ severe to extreme turbulence can be expected. In some cases, however, and this is important, if a steady state has been reached the turbulence experienced tends to be in the light category. On the other hand, if there is a rapid increase or decrease in the core at reflectivity values above $10^3 \text{ mm}^6/\text{m}^3$ moderate to severe turbulence is encountered. These fluctuations or pulsations in thunderstorm intensity may have a period of less than 12 minutes. Therefore, in attempting to predict for control purposes the turbulence which might be encountered by an aircraft flying through a thunderstorm area the critical reflectivity intensity and the rate at which the area enclosed by this intensity is changing must be recognized.

2. There does not appear to be a direct correlation between gradients of successive radar reflectivity values per se and turbulence.

3. The preponderance of evidence indicates that the center and western portions of thunderstorm complexes as seen at a zero attenuation level (i.e., lowest Z value) contain the most severe turbulence. A new cell growing in the eastern portion of the thunderstorm complex can produce severe turbulence but the number of cases of this type so far encountered is less than 10%. Data are insufficient to assess the hypotheses that the turbulence in the southwest quadrant is more severe than the northwest quadrant of the storm. It is to be stressed that what has been said of the occurrence of turbulence does not apply to the occurrence of hail,

data for which is not now currently available.

4. Pilots can expect to encounter moderate turbulence 3.3 n. mi. on the average after entering the western edge of the visible cloud portion of a thunderstorm. Thus for an aircraft flying at a true airspeed of 400 knots the pilot could expect to encounter a derived gust velocity of 20 ft. sec.^{-1} or greater within 30 sec. after entering the visible portion of the cloud if his path is toward the center of the system.

5. Vertical accelerations tended to be biased toward negative values.

6. Rapid changes in vertical accelerations from U_{de} values of $-11.8 \text{ ft. sec.}^{-1}$ to $+17.8 \text{ ft. sec.}^{-1}$ in 0.2 sec. of T-33 flight time or approximately 120 ft. have been experienced. A change from U_{de} values of $-34.4 \text{ ft. sec.}^{-1}$ to $+46.8 \text{ ft. sec.}^{-1}$ in 0.7 sec. was recorded and cannot be considered unusual.

7. Altitude variations of as much as 5,000 ft. can occur even with the nose of the aircraft pitched down during a traverse of a thunderstorm cell. These changes have occurred at altitude above 15,000 ft. up to and including 40,000 ft.

8. Vertical true gust velocities of $+208 \text{ ft. sec.}^{-1}$ and -124 ft. sec. have been experienced.

9. If the pilot is not prepared for the turbulence the roll and pitch rates may be sufficient for him to lose control of the aircraft. An example of what has been encountered is illustrated by run #3 on May 19, 1960 when the F-102 flying at 35,000 ft. experienced an extreme roll rate that carried the aircraft to a 45° bank with full aileron against it.

7. ACKNOWLEDGEMENTS

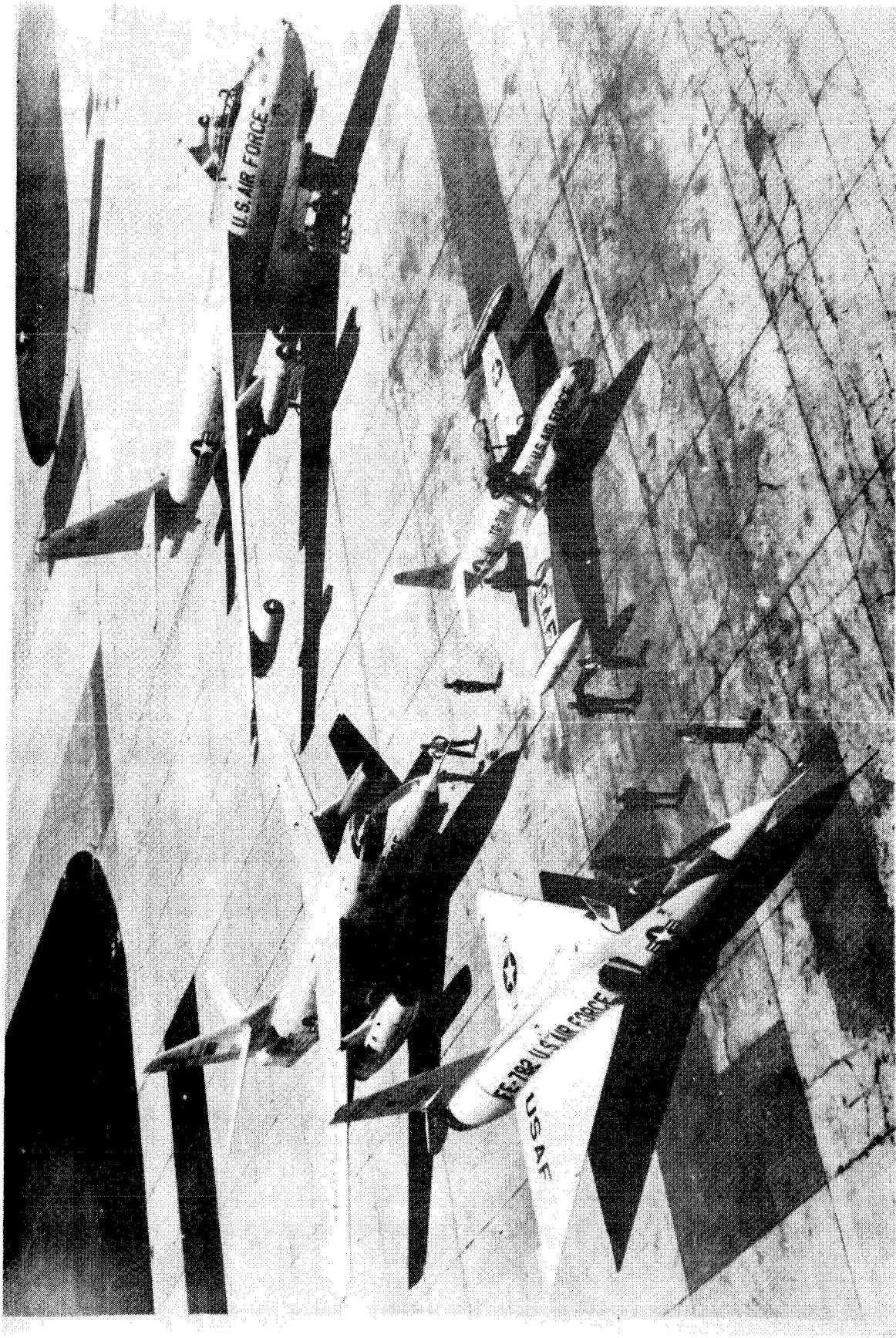
The author wishes to express his appreciation to Mr. Kenneth E. Wilk for furnishing the radar data, to Dr. Chester W. Newton for his helpful suggestions and to the others who helped in compiling the data and drawings.

REFERENCES

1. Sutton, O. G. Atmospheric Turbulence 1955, London, Methuen, 2nd ed, p. 9.
2. U.S. Weather Bureau, The Thunderstorm, Washington, D.C., 1949, pp. 39-46.
3. Meteorological Glossary, American Meteorological Society, Boston, 1959, p. 266.
4. Battan, L.J., Radar Meteorology, The University of Chicago Press, 1960, p 29.
5. Gunn, K. L. S., and T. W. R. East, "The Microwave Properties of Precipitation Particles," Quarterly Journal of the Royal Meteorology Society, 1954, pp. 522-545.
6. Anonymous: "Airplane Airworthiness - Transport Categories," Part 4b of Civil Air Regulations, Civil Aeronautics Board, U.S. Department of Commerce, Washington, D.C., July 20, 1950.
7. Pratt, K. G. and W. G. Walker, "A Revised Gust-Load Formula and a Re-Evaluation of V-G Data taken on Civil Transport Airplanes from 1933 to 1950," National Advisory Committee for Aeronautics Report 1206, 1954, pp. 1-4.
8. U.S. Weather Bureau, Weather Bureau Manual, Washington, D.C., 1957, Section III-B-2011.
9. Steiner, R. and R. H. Rhyne, "Some Measured Characteristics of Severe Storm Turbulence," National Severe Storms Project Report No. 10, July 1962, pp. 3-8.
10. Roys, G. P., "Operation of an F-106A in Thunderstorms at Supersonic and High Subsonic Airspeeds," Aeronautical Systems Division Technical Note 61-97, October 1961.

11. Schumacher, P. W. J., "Radar Photographs and Gust Loads in Three Storms of 1961 Rough Rider," National Severe Storms Project Report No. 15, 1962.
12. Roys, G. P., "Thunderstorm Penetrations by F-106A Aircraft at High Speed and High Altitude," Wright Air Development Division Technical Note 60-274, December 1960.

Figure 1.- Some of the aircraft used in Project "Roughrider"



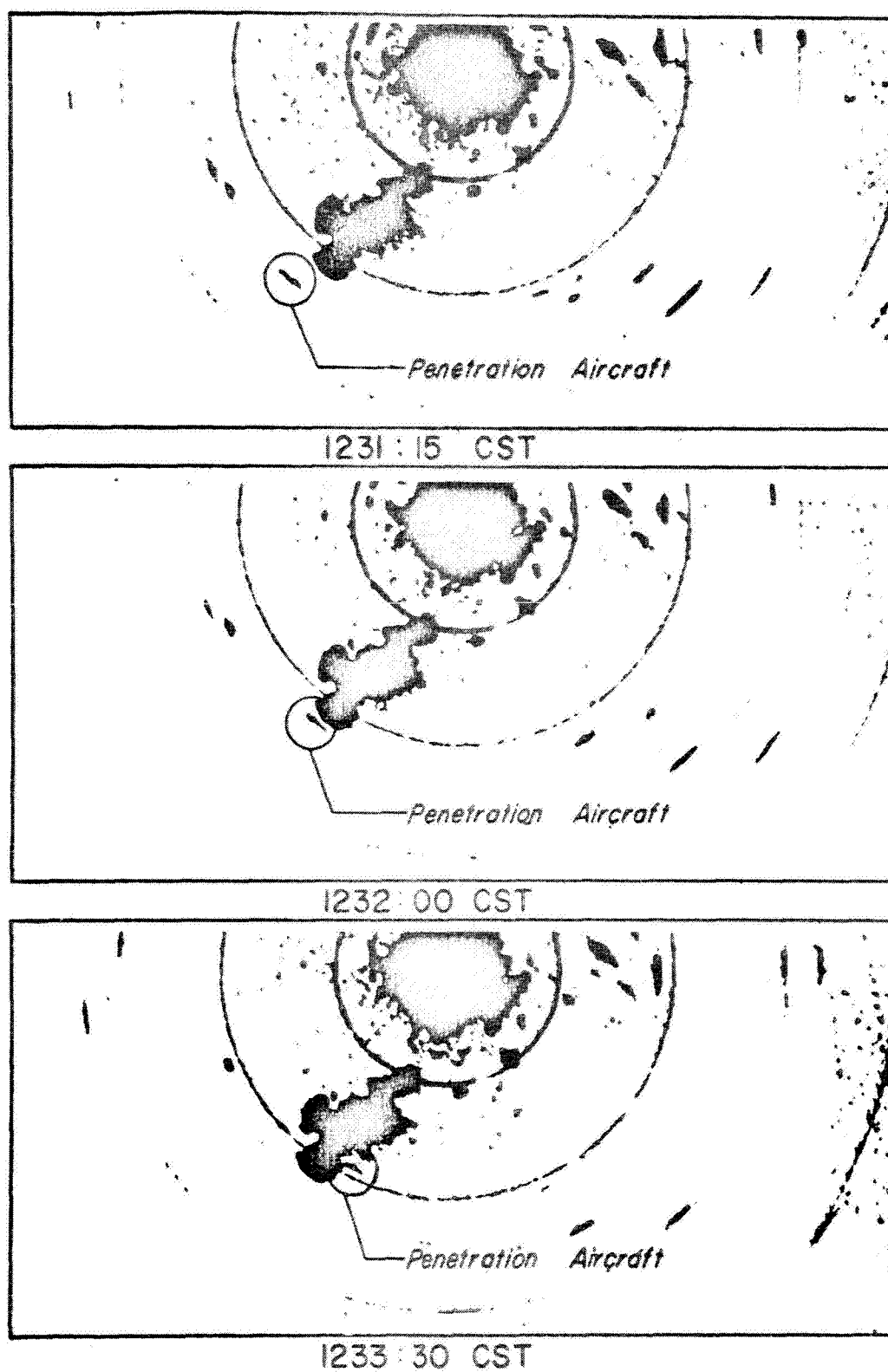


Figure 2.- Series of photographs of a portion of the Oklahoma City WSR-57 scope illustrating the penetration by the F-106 of an echo 100 miles southwest of Oklahoma City, May 5, 1961.

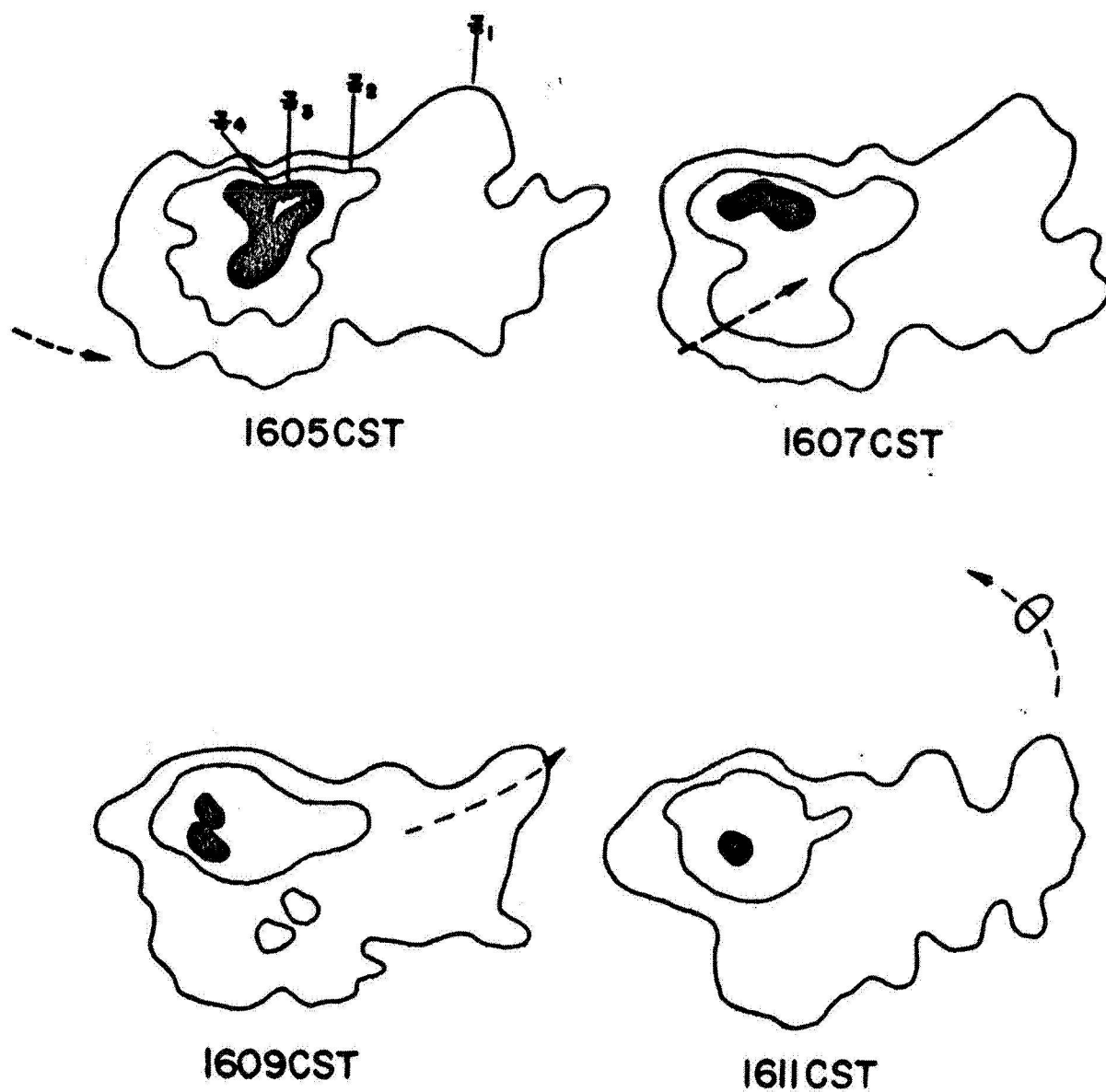


Figure 3.- Example of composite radar tracings made at two-minute intervals on May 23, 1962 illustrating the depiction of the outer edge of selected reflectivity (Z) values.

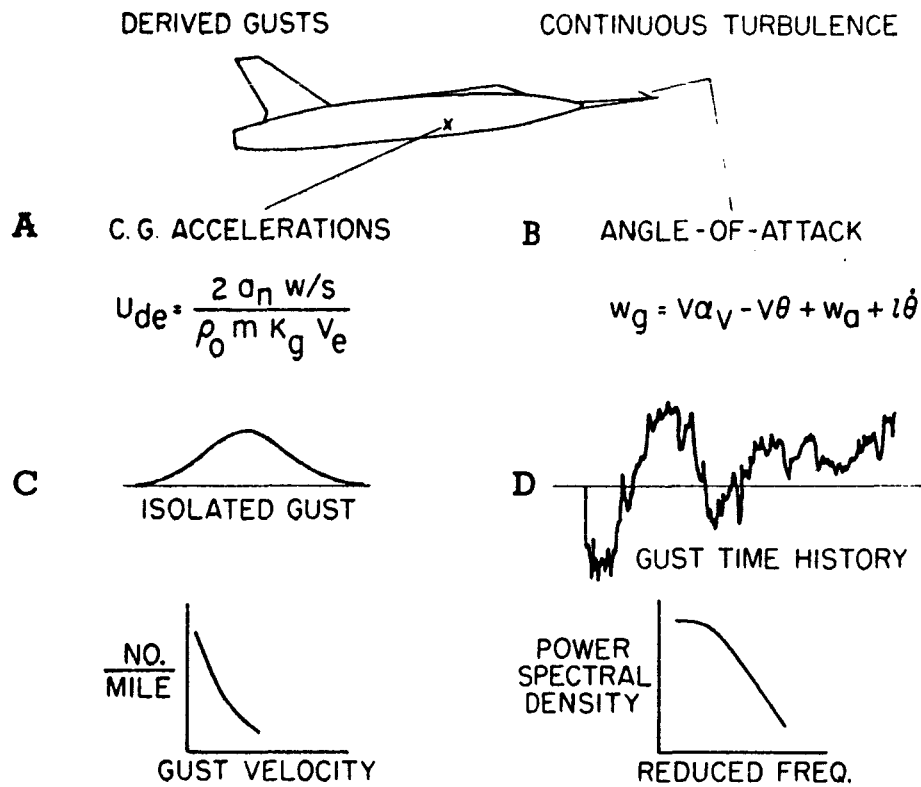


Figure 4.- Methods for measuring and describing atmospheric turbulence (after Steiner [9]).

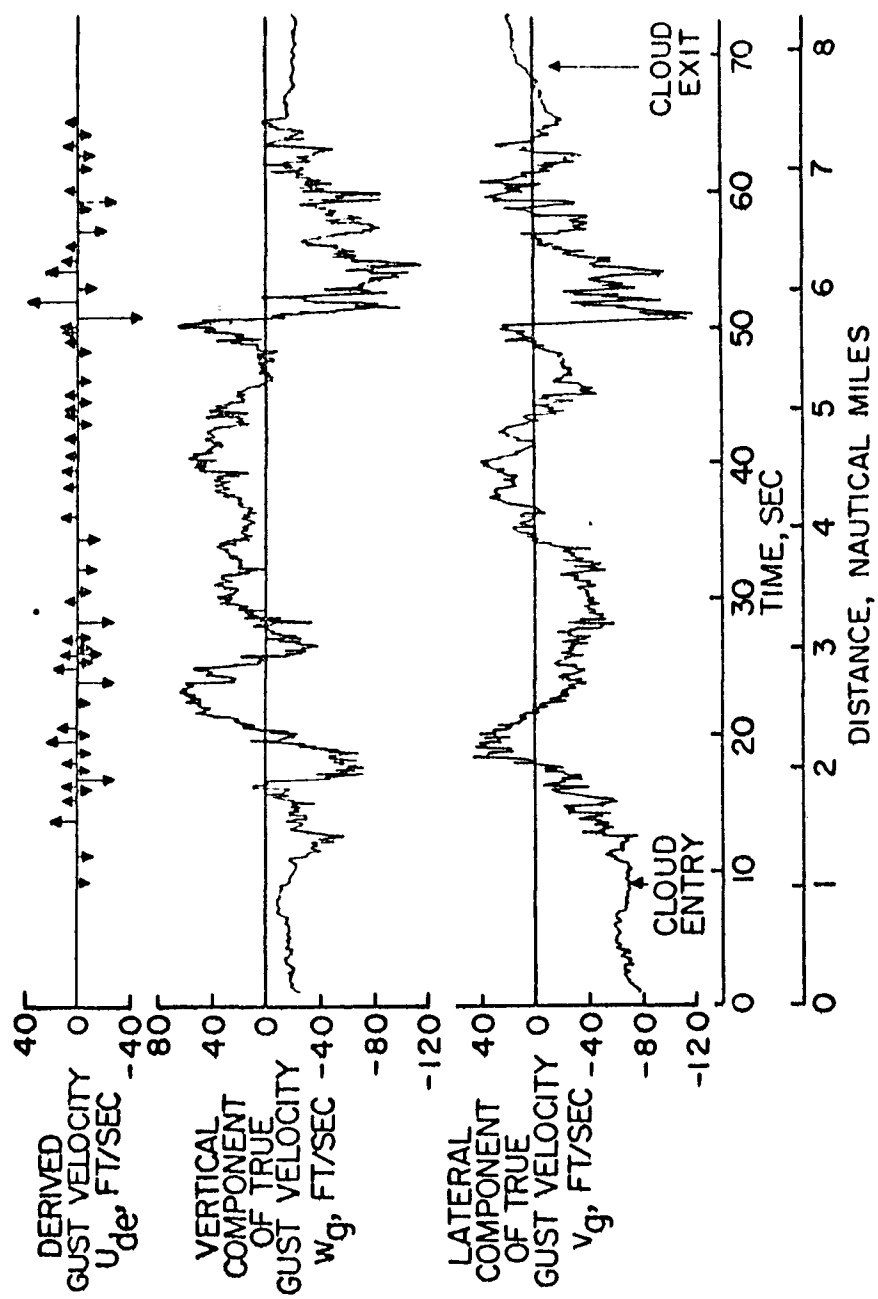


Figure 5.- Derived gust velocities and time histories of vertical and lateral gust components, transonic aircraft at 39,000 ft., May 17, 1960 (after Steiner [9]).

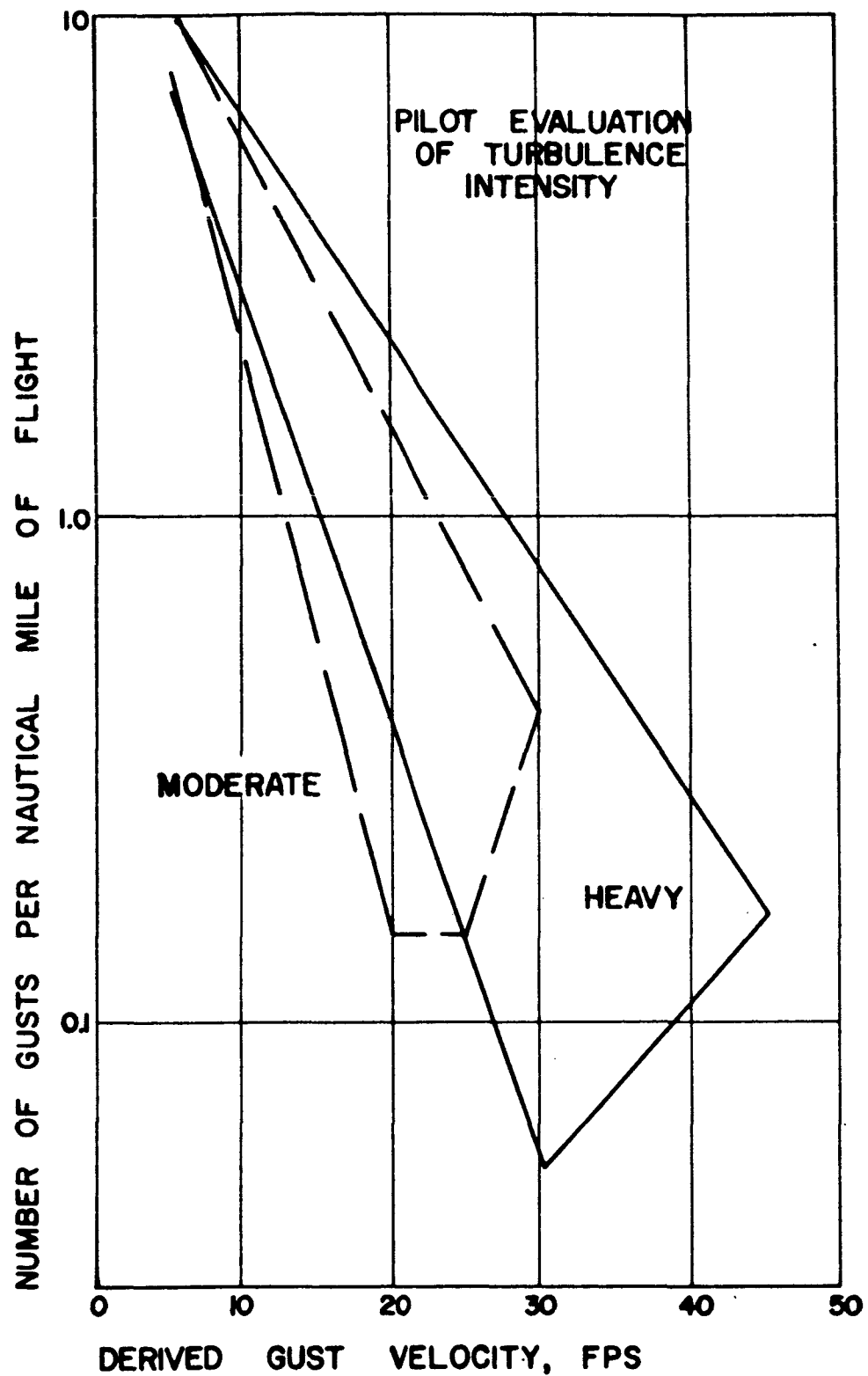


Figure 6.- Summary of the pilot's evaluation of turbulence and the computed frequency and magnitude of the derived gust velocities based on 1961 operations (after Roys [10]).

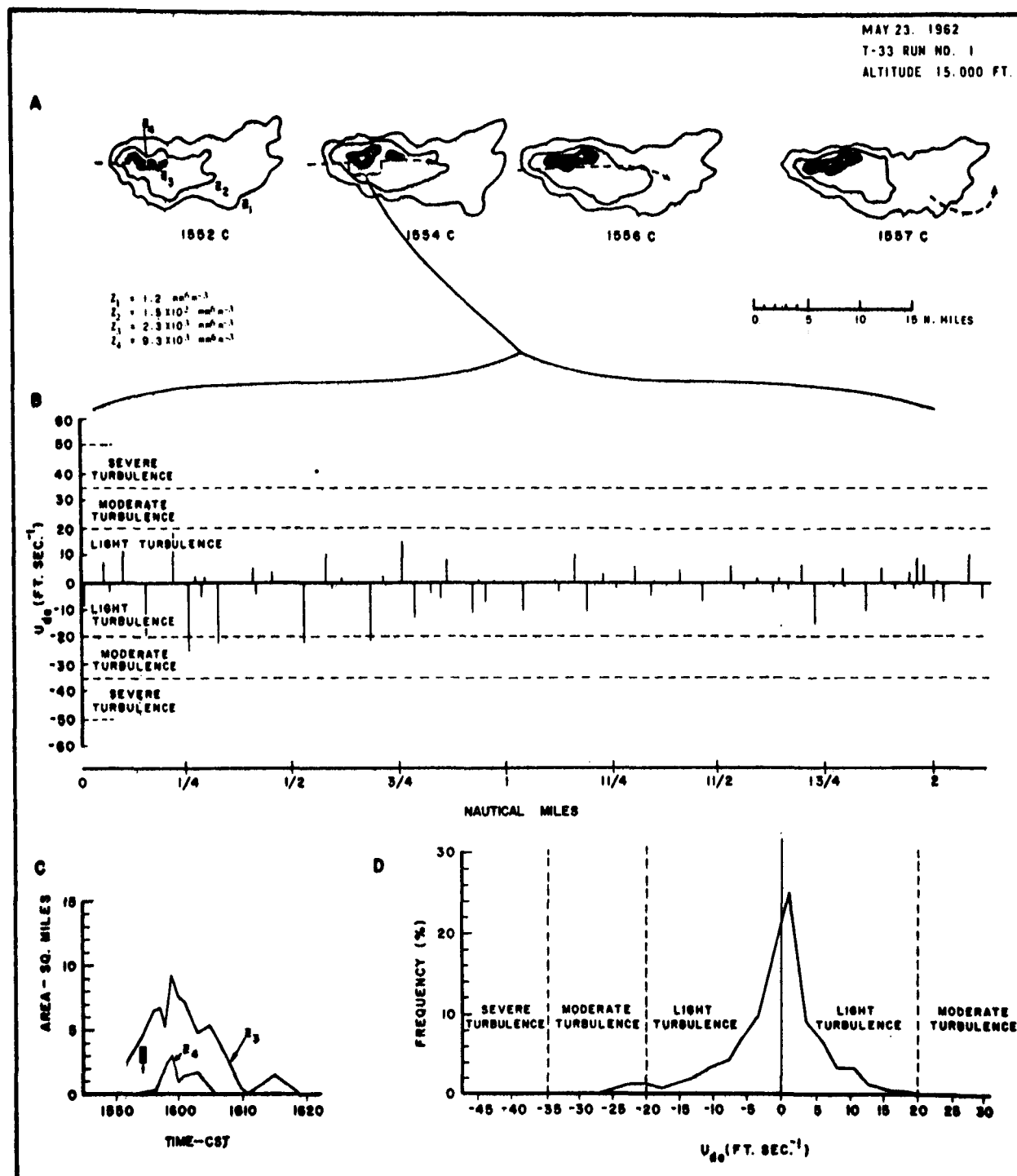


Figure 7.- Run #1 on May 23, 1962 made by the T-33. (A) The path of the aircraft and the radar presentation of the cloud being penetrated. North is toward top of page. (B) A selected portion of the derived gust velocity time history corresponding mainly to areas of maximum turbulence. Western portion is to left. (C) Time history of the size of the area enclosed by selected radar reflection values. Crosshatched area indicates approximate time of penetration. (D) Frequency distribution of derived gust velocities for the entire penetration.

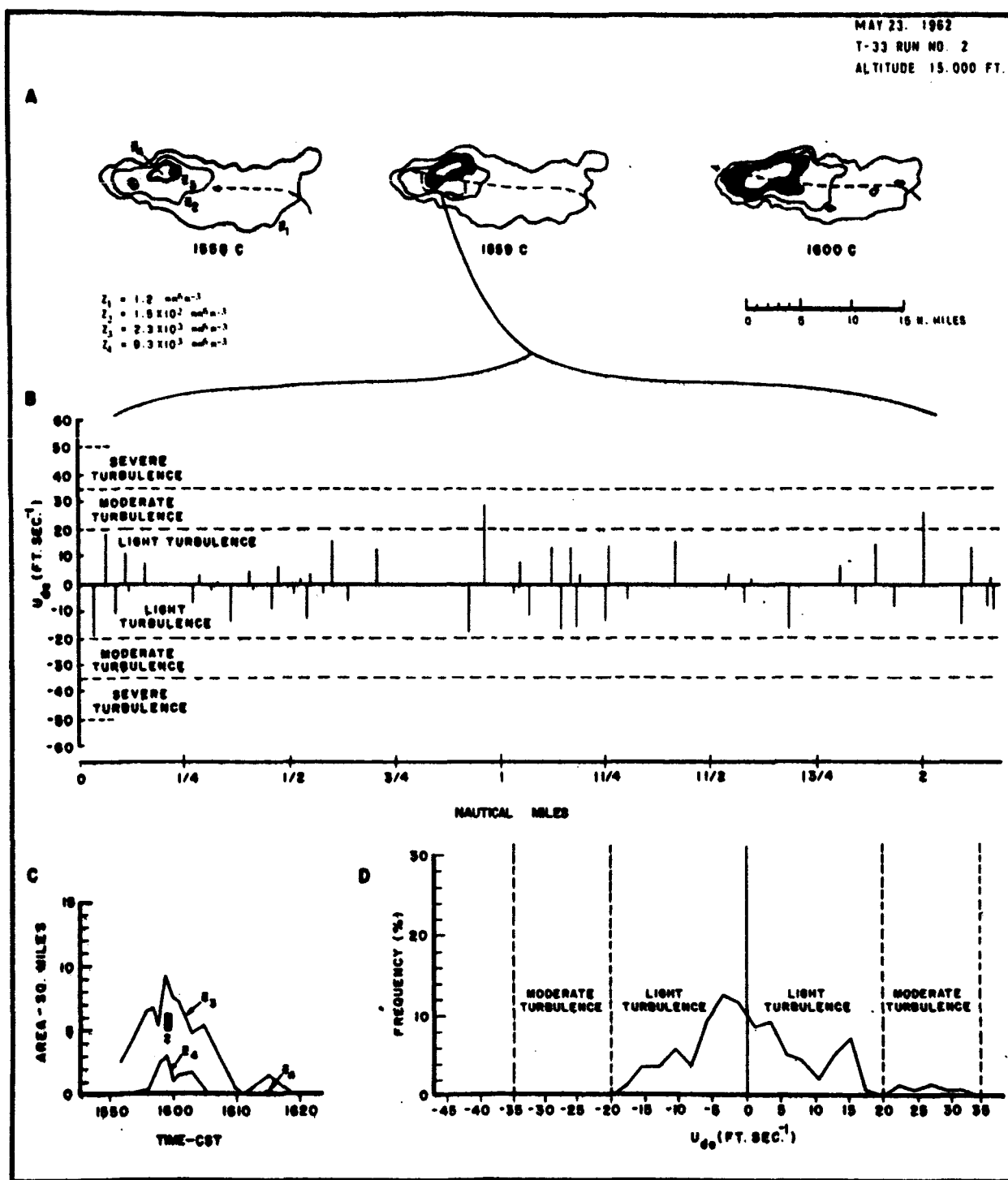


Figure 8.- Run #2 on May 23, 1962 made by the T-33. Sections A, B, C, and D are for the same parameters as indicated for figure 7.

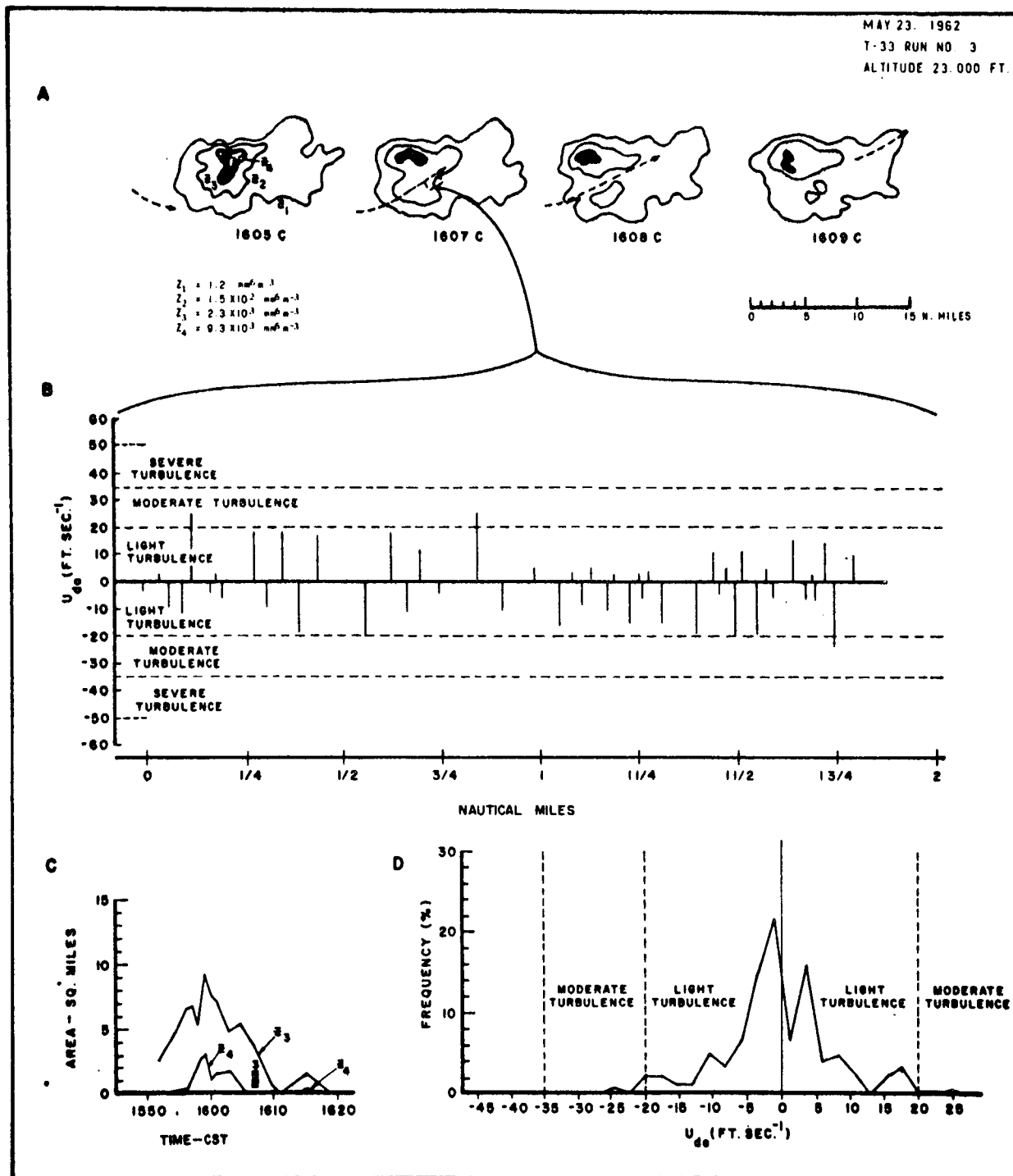


Figure 9. - Run #3 on May 23, 1962 made by the T-33. Sections A, B, C, and D are for the same parameters as indicated for figure 7.

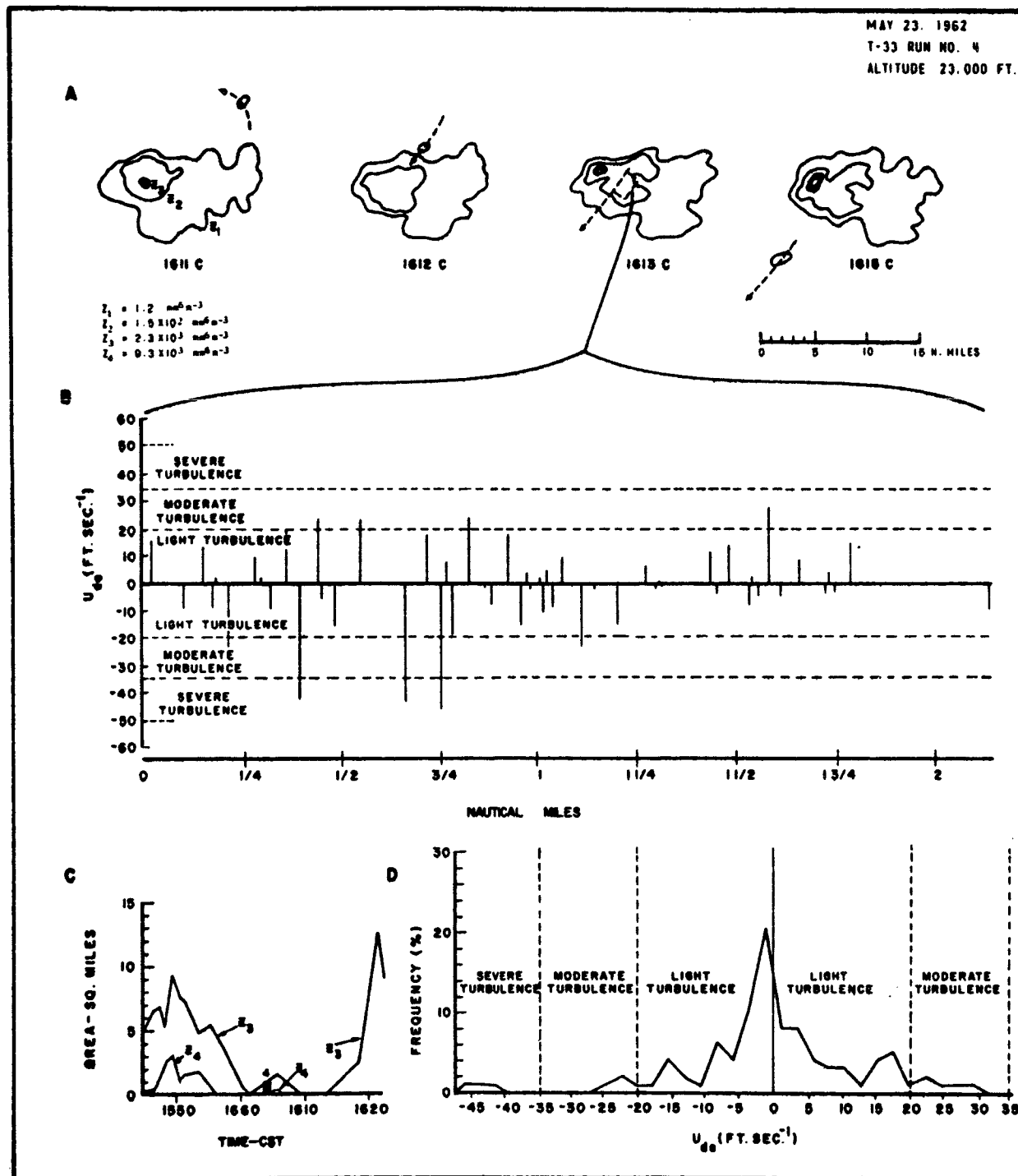


Figure 10. Run #4 on May 23, 1962 made by the T-33. Sections A, B, C, and D are for the same parameters as indicated for figure 7.

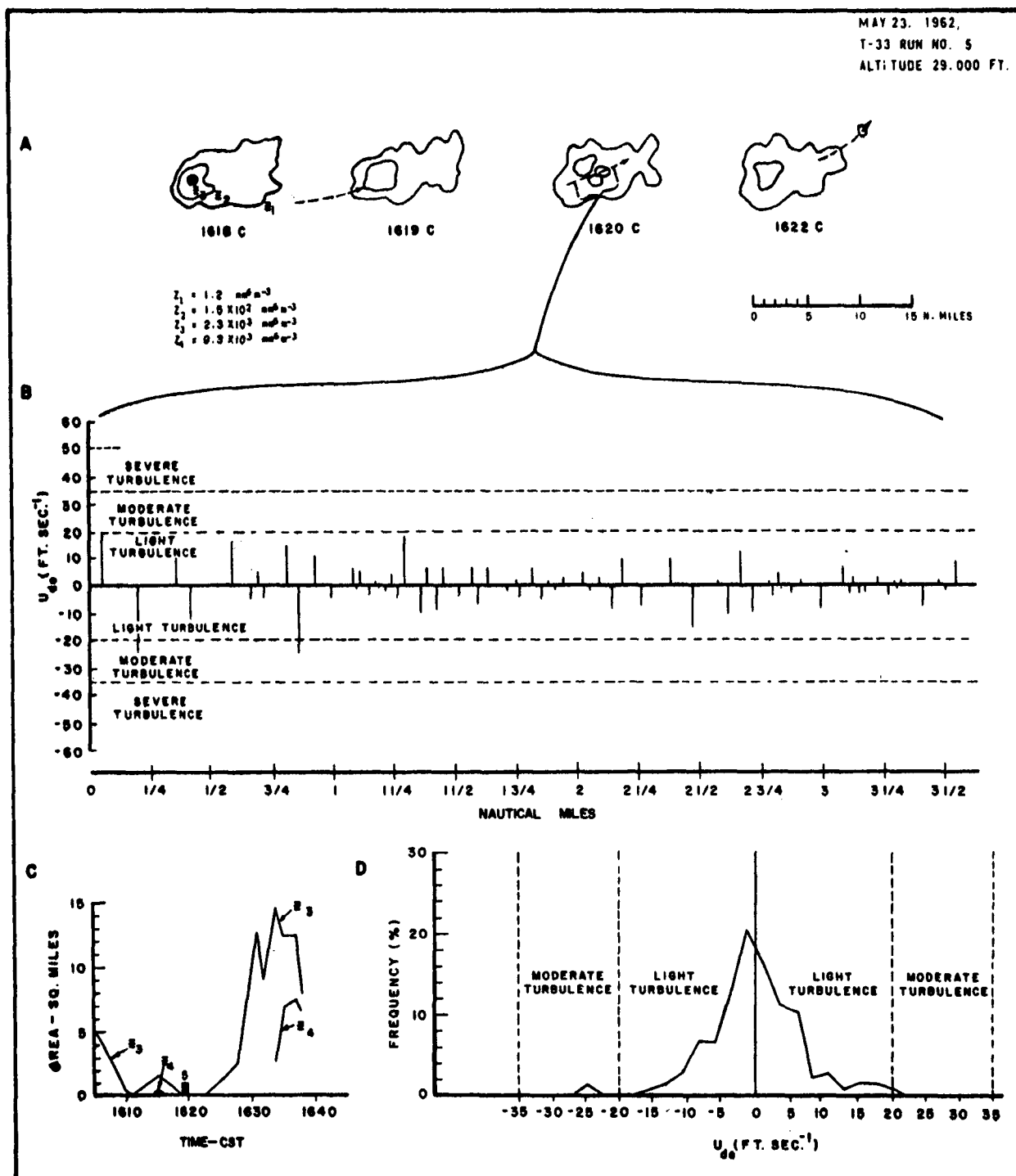


Figure 11.- Run #5 on May 23, 1962 made by the T-33. Sections A, B, C, and D are for the same parameters as indicated for figure 7.

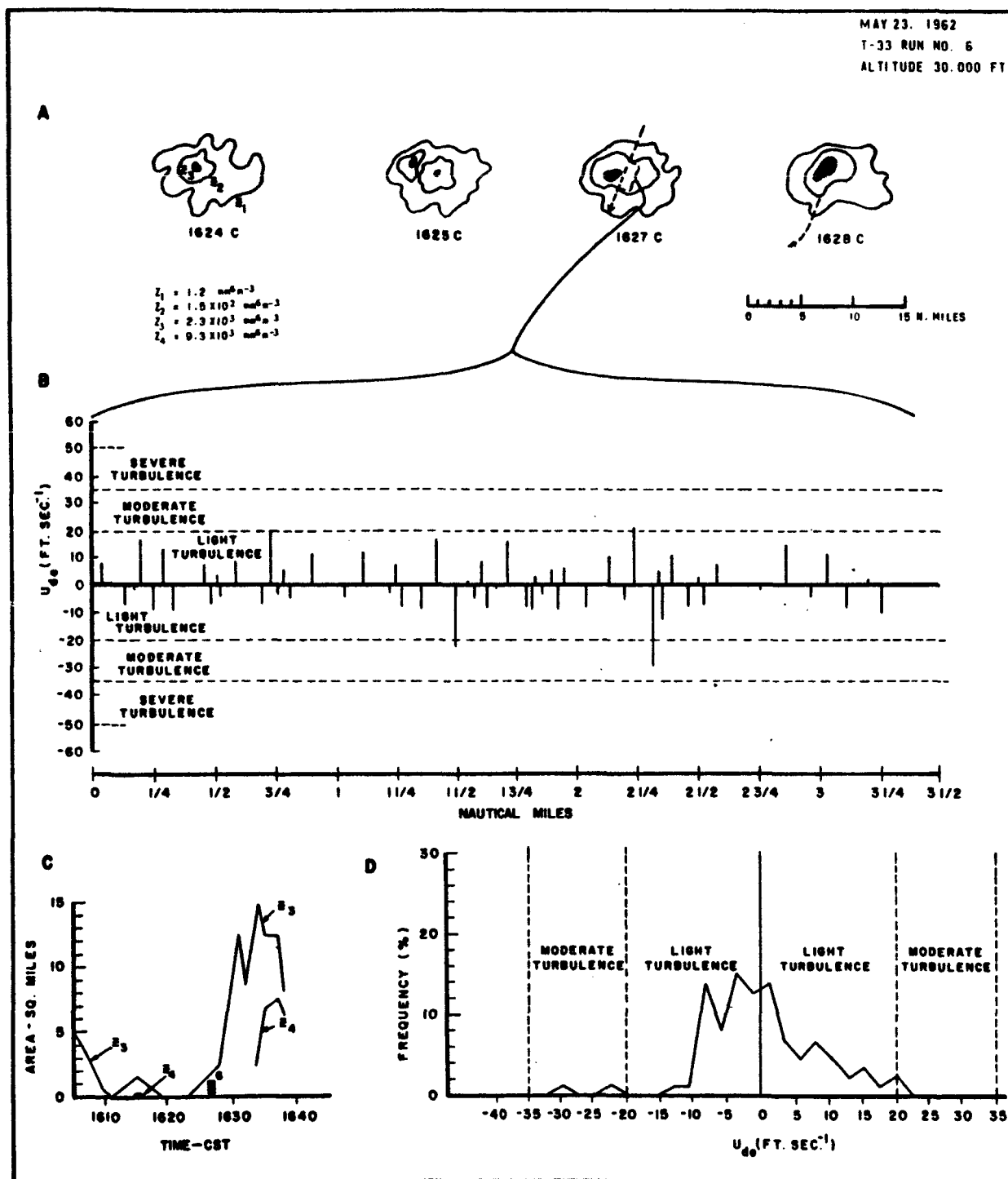


Figure 12.- Run #6 on May 23, 1962 made by the T-33. Sections A, B, C, and D are for the same parameters as indicated for figure 7.

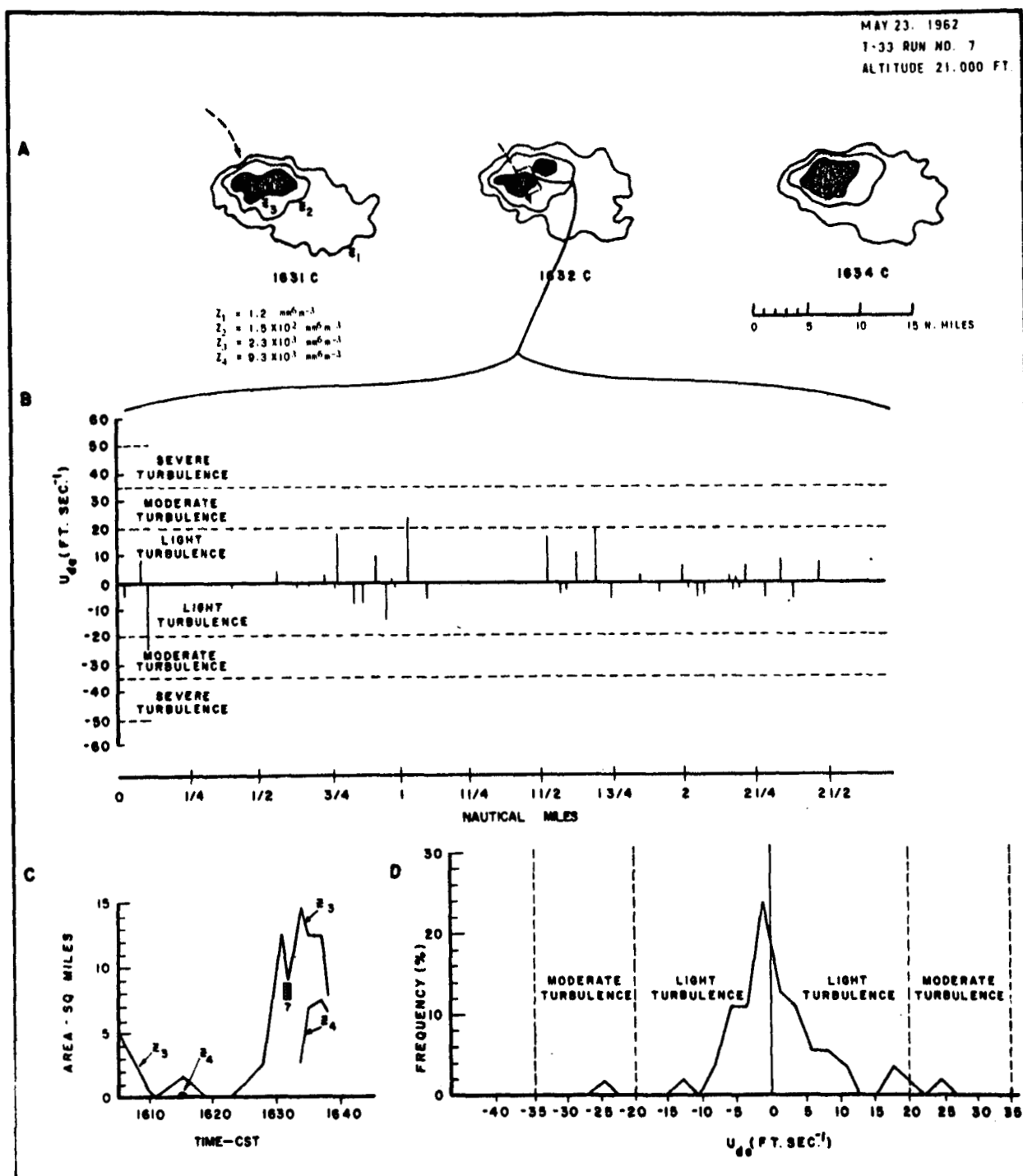


Figure 13.- Run #7 on May 23, 1962 made by the T-33. Sections A, B, C, and D are for the same parameters as indicated for figure 7.

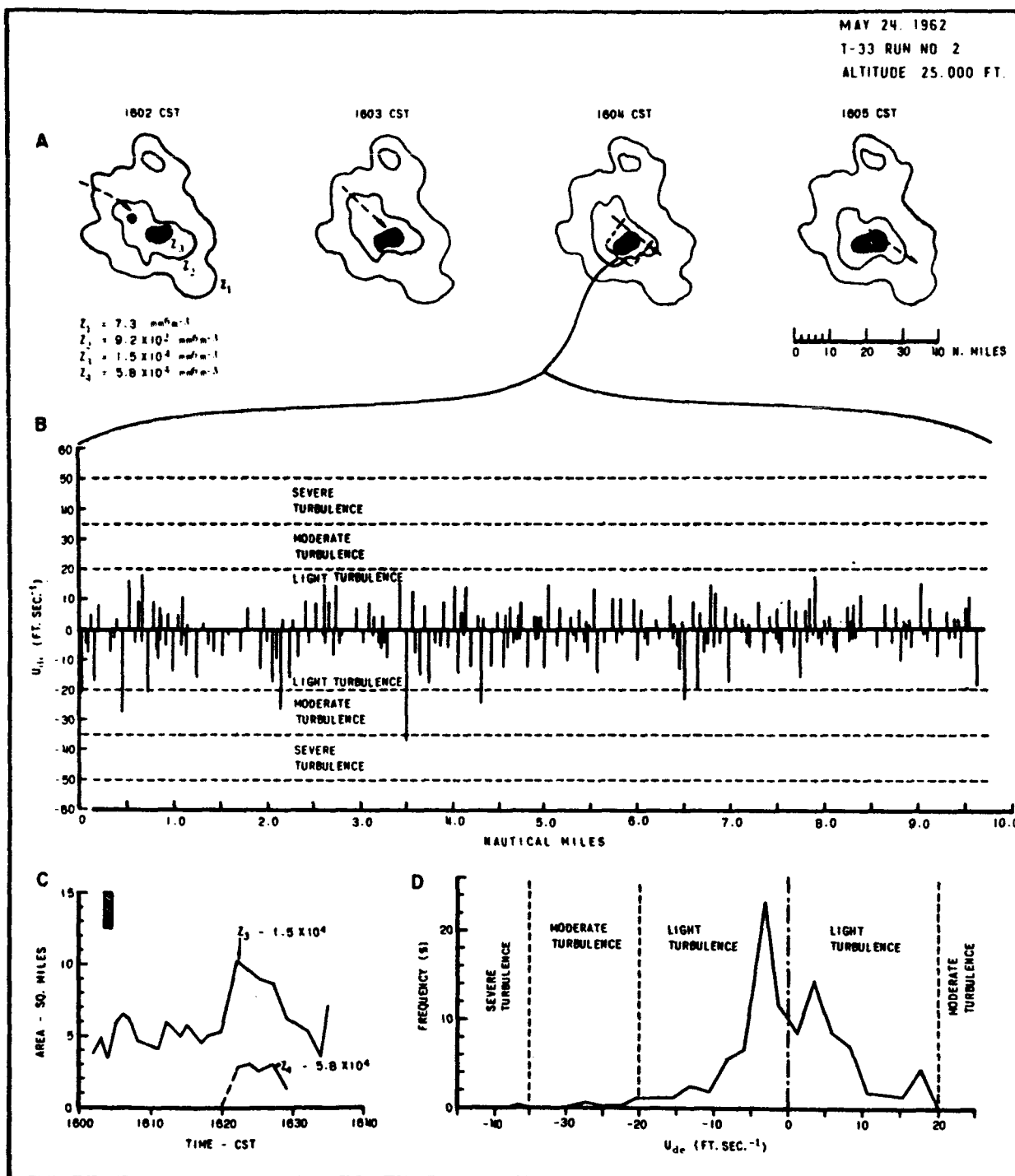


Figure 14.- Run #2 on May 24, 1962 made by the T-33. Sections A, B, C, and D are for the same parameters as indicated for figure 7.

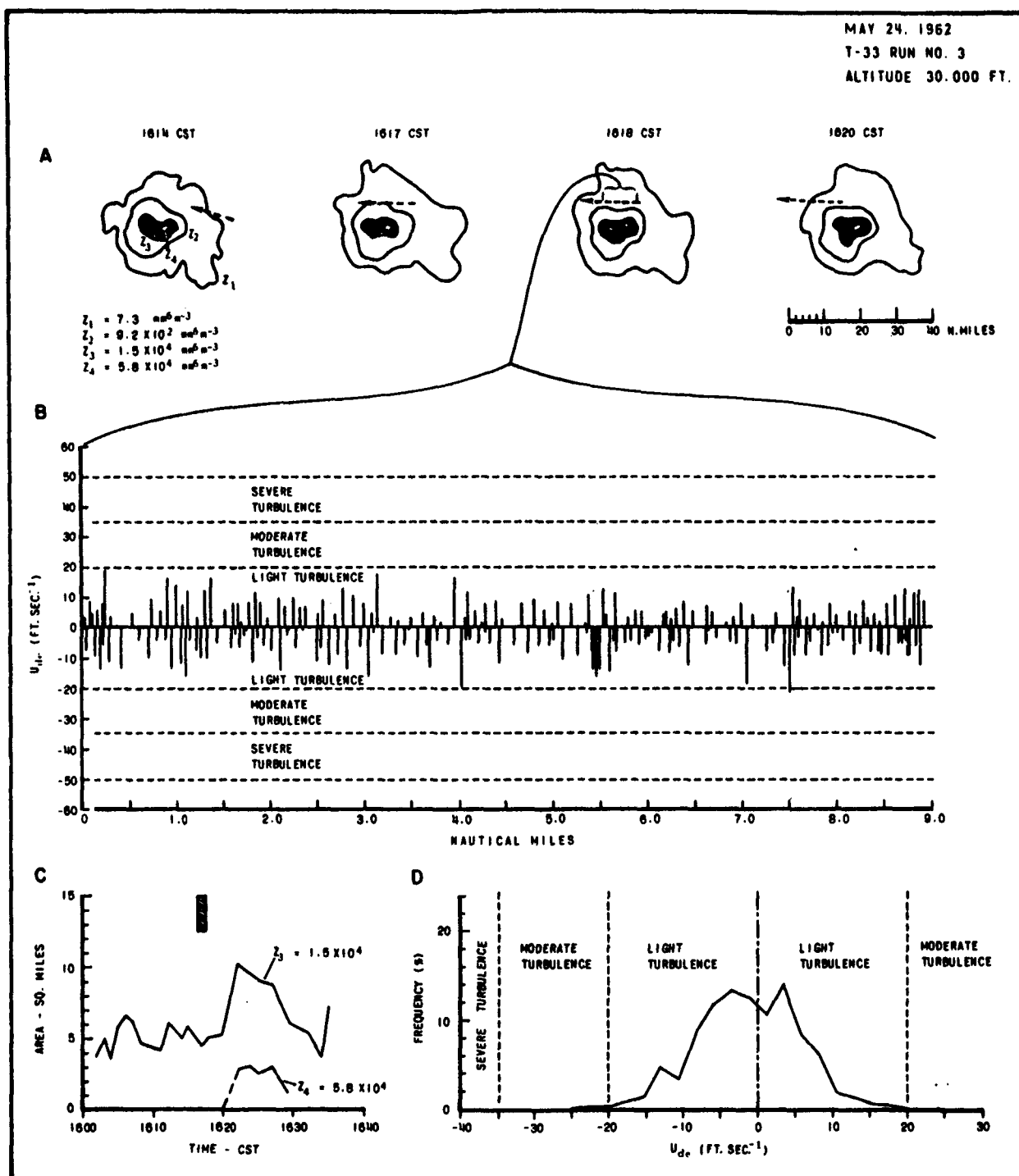


Figure 15.- Run #3 on May 24, 1962 made by the T-33. Sections A, B, C, and D are for the same parameters as indicated for figure 7.

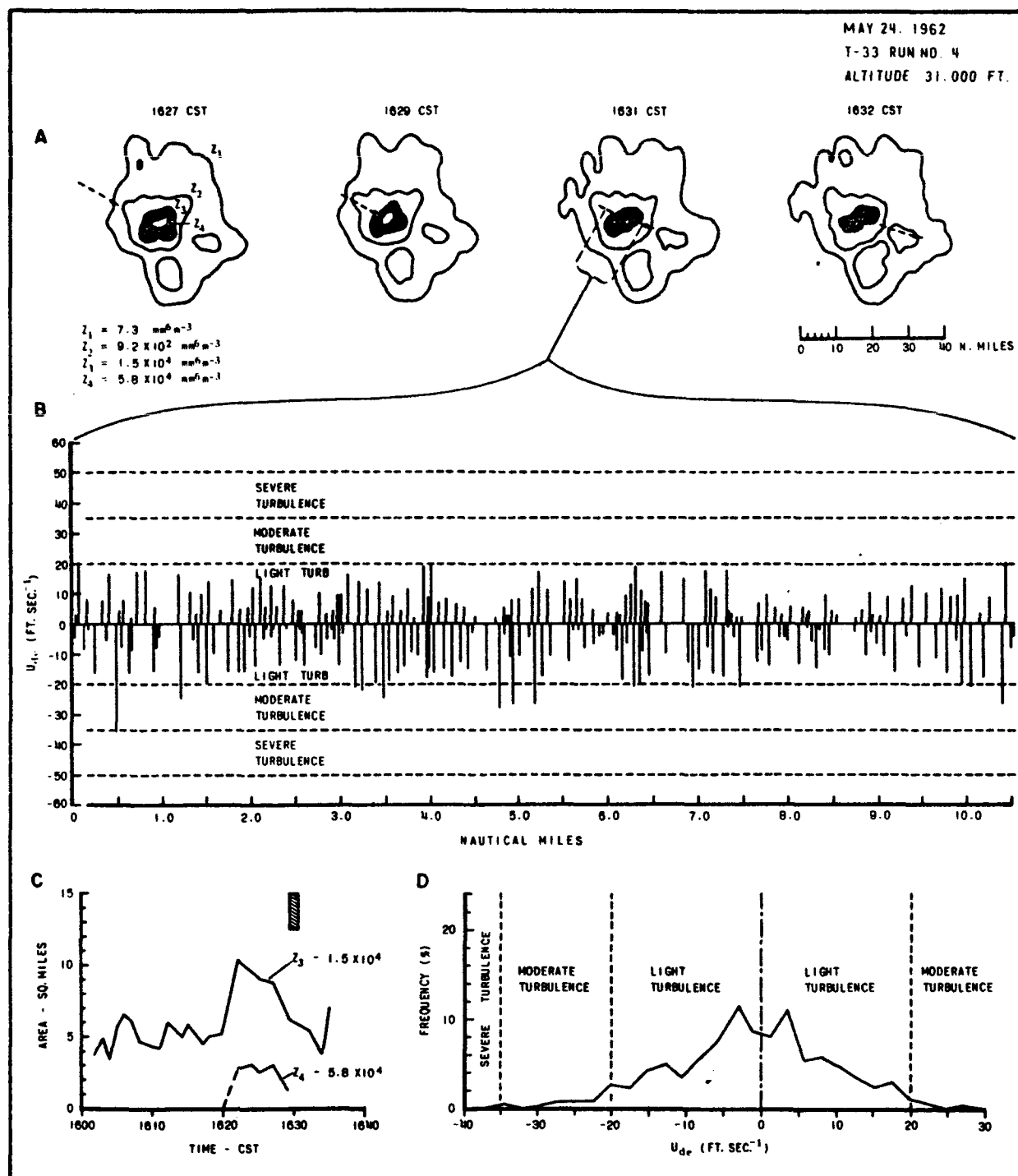


Figure 16.- Run #4 on May 24, 1962 made by the T-33. Sections A, B, C, and D are for the same parameters as indicated for figure 7.

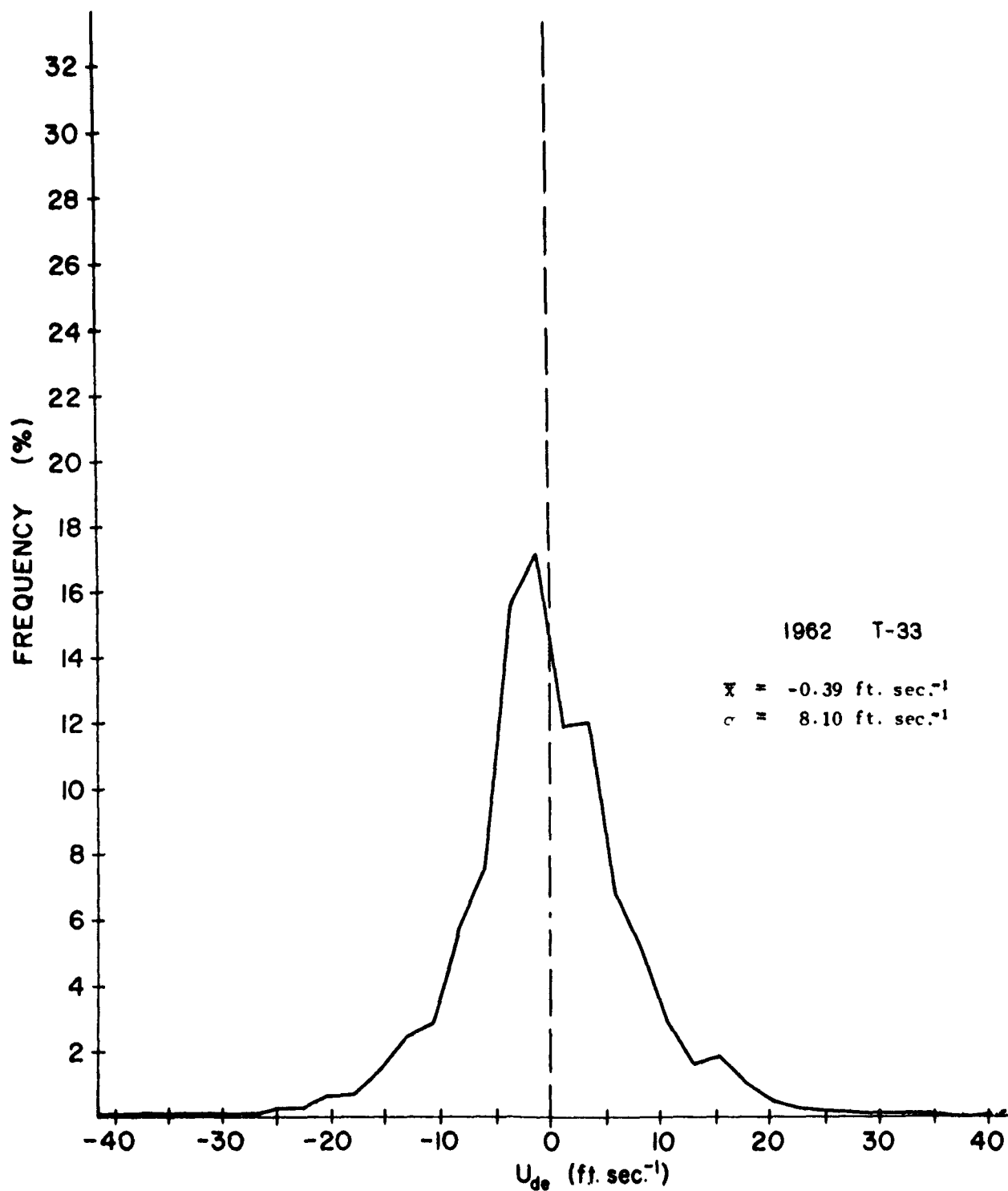


Figure 17.- Frequency distribution of derived gust velocities recorded during 1962 T-33 thunderstorm penetrations. The mean and the standard deviation values are tabulated.

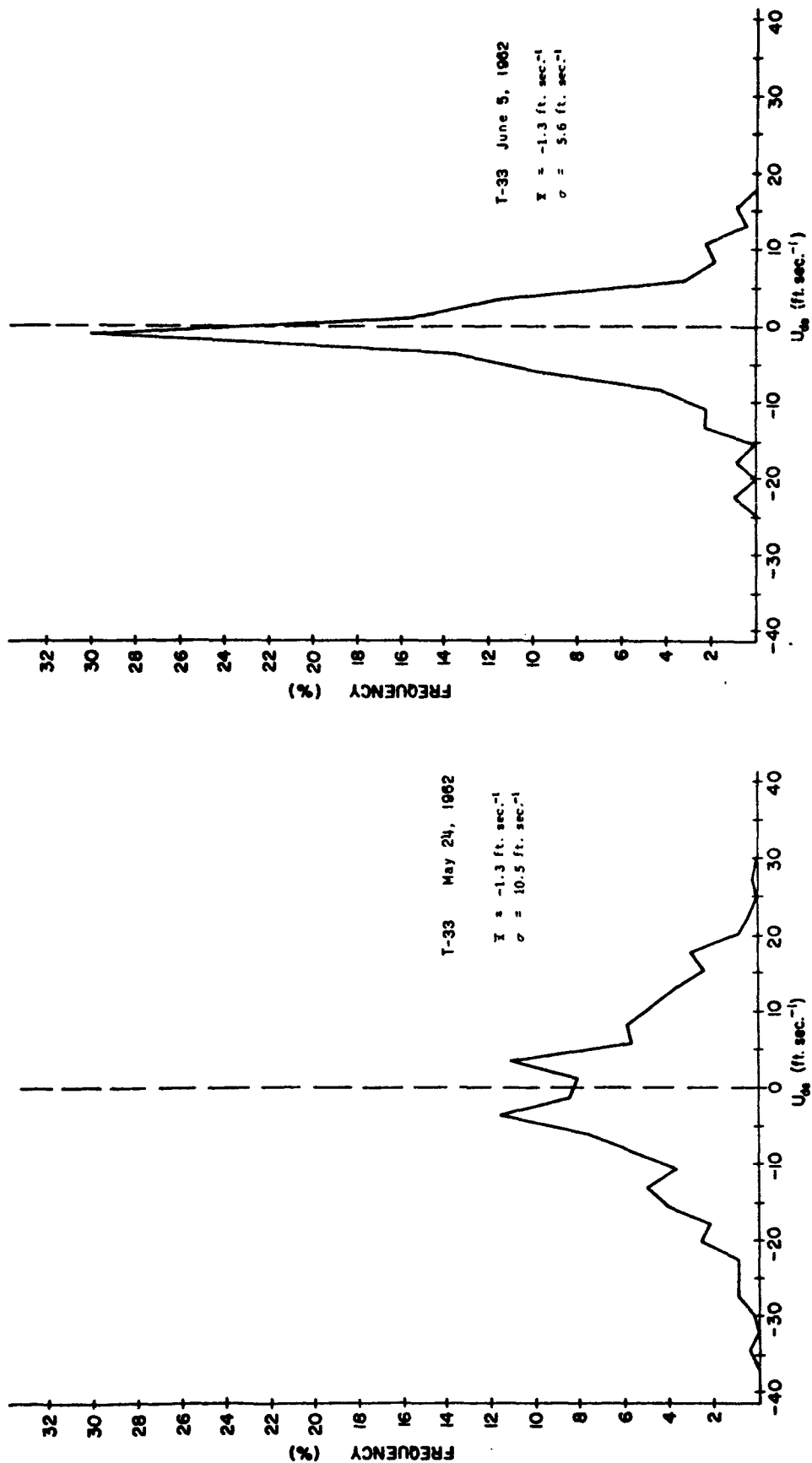


Figure 18.- (A) Frequency distribution of derived gust velocities for run 4 on May 27, 1962 with the mean and the standard deviation tabulated values. (B) Frequency distribution of derived gust velocities for run 1 of June 5, 1962 with the mean and the standard deviation values tabulated.

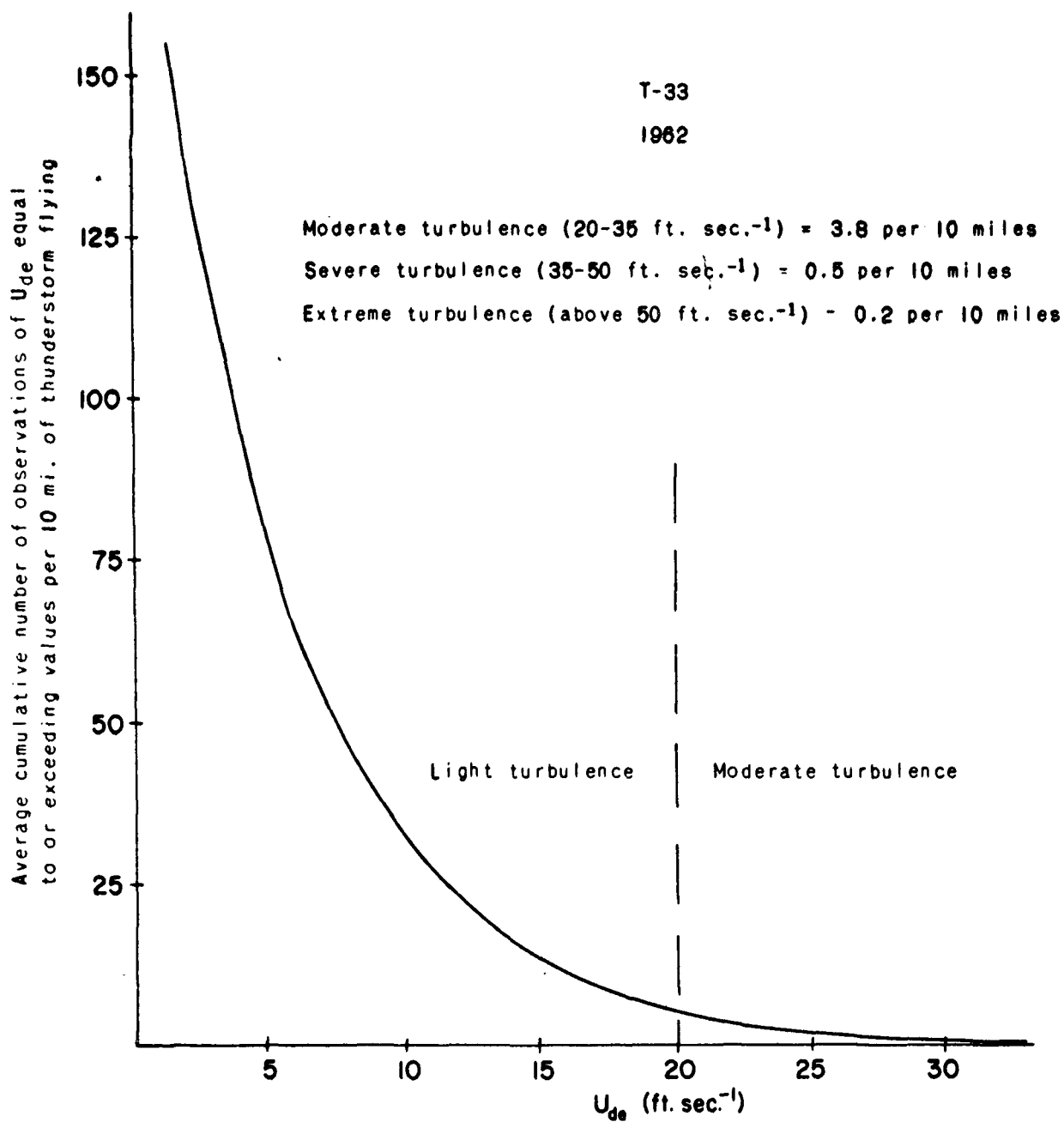


Figure 19.- Average number of times derived gust velocities equaled or exceeded per 10 n. mi. of flight in thunderstorms during 1962.

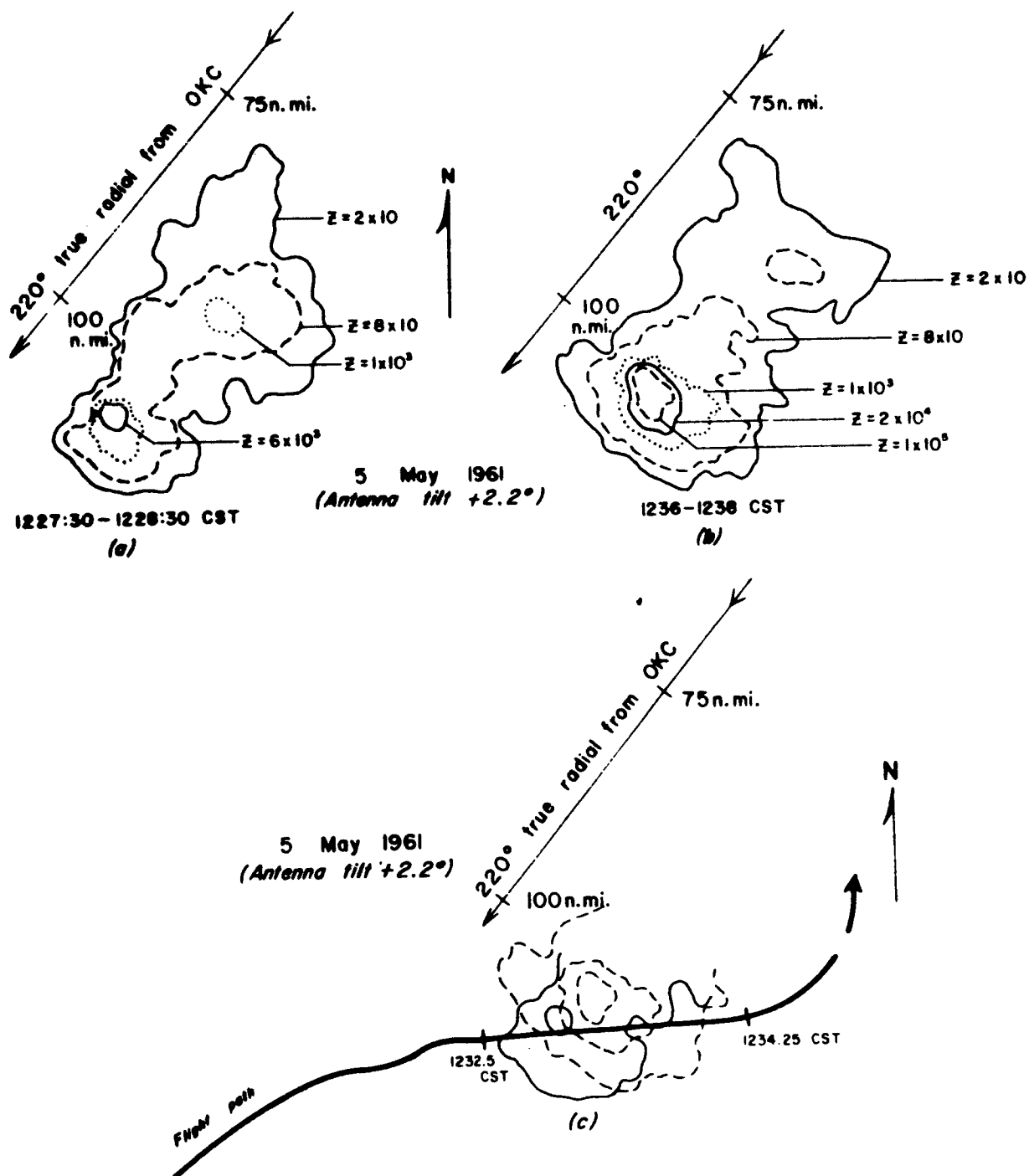


Figure 20.- (A) Reflectivity contours of storm May 5, 1961 complex prior to penetration. (B) Reflectivity contours of storm complex after penetration. (C) Path of aircraft through storm and storm movement. Solid echo contours correspond to those in (A) dashed echo contours to (B) thereby showing movement of storm between periods of contouring sequences.

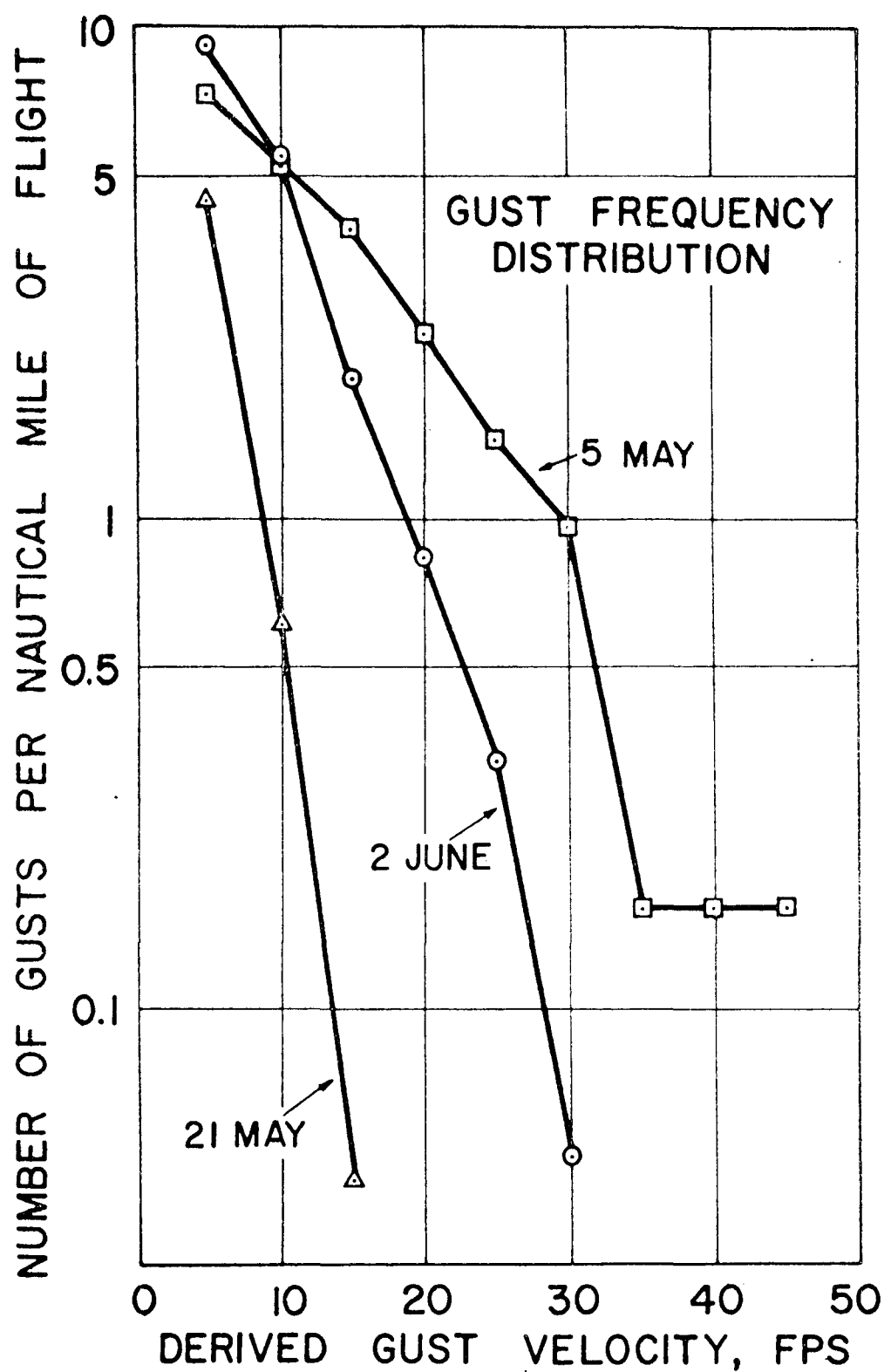


Figure 21.- Cumulative frequency distribution of derived gust velocity for three penetration flights in 1961. May 5 can be catalogued as an example of a characteristic distribution of "heavy" turbulence; June 2 moderate turbulence, and May 21 light turbulence (after Schumacher [15]).

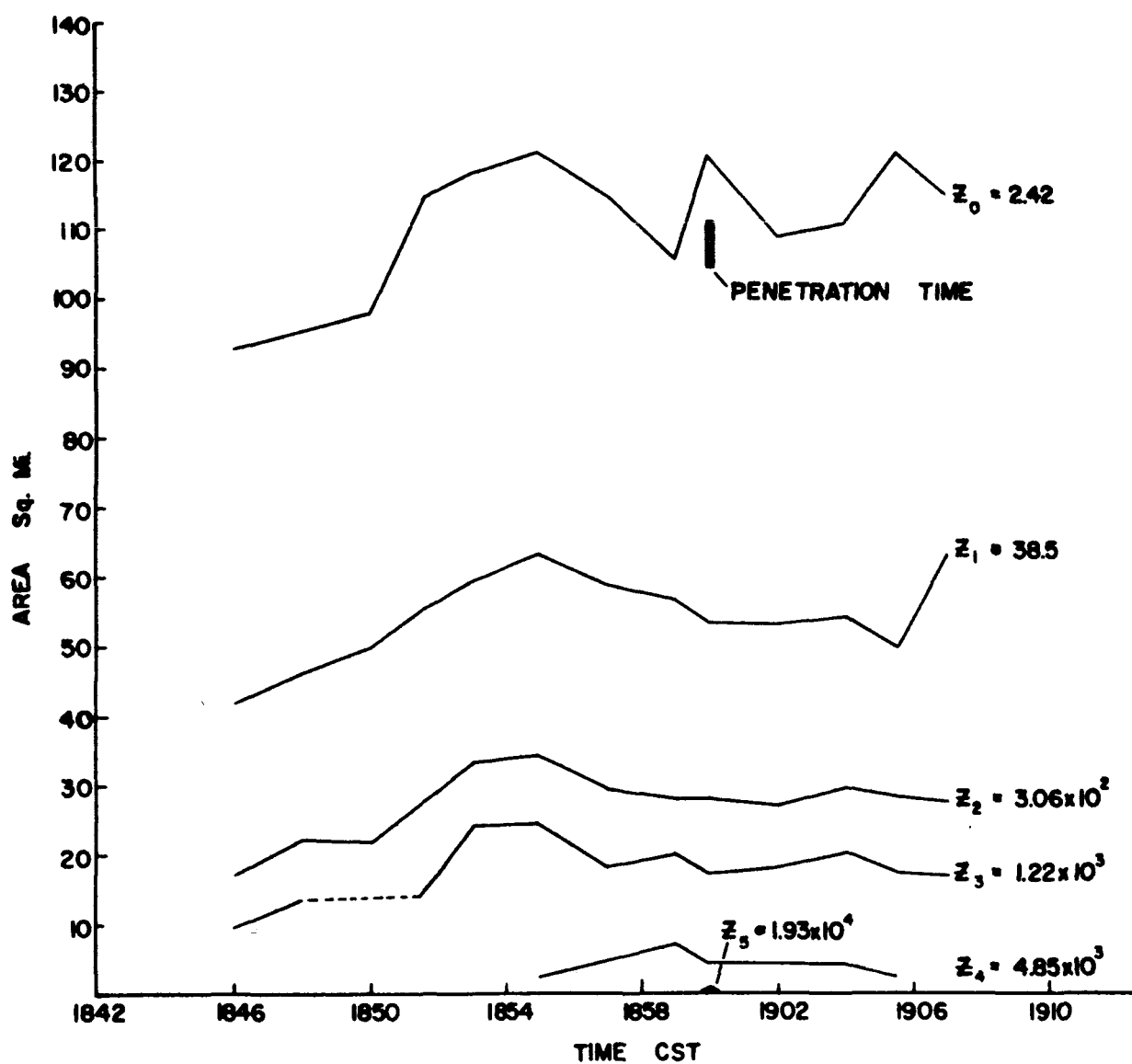


Figure 22.- Time history of areas included within specific radar reflectivity values for May 20, 1962. Crosshatched area indicates approximate time of aircraft penetration.

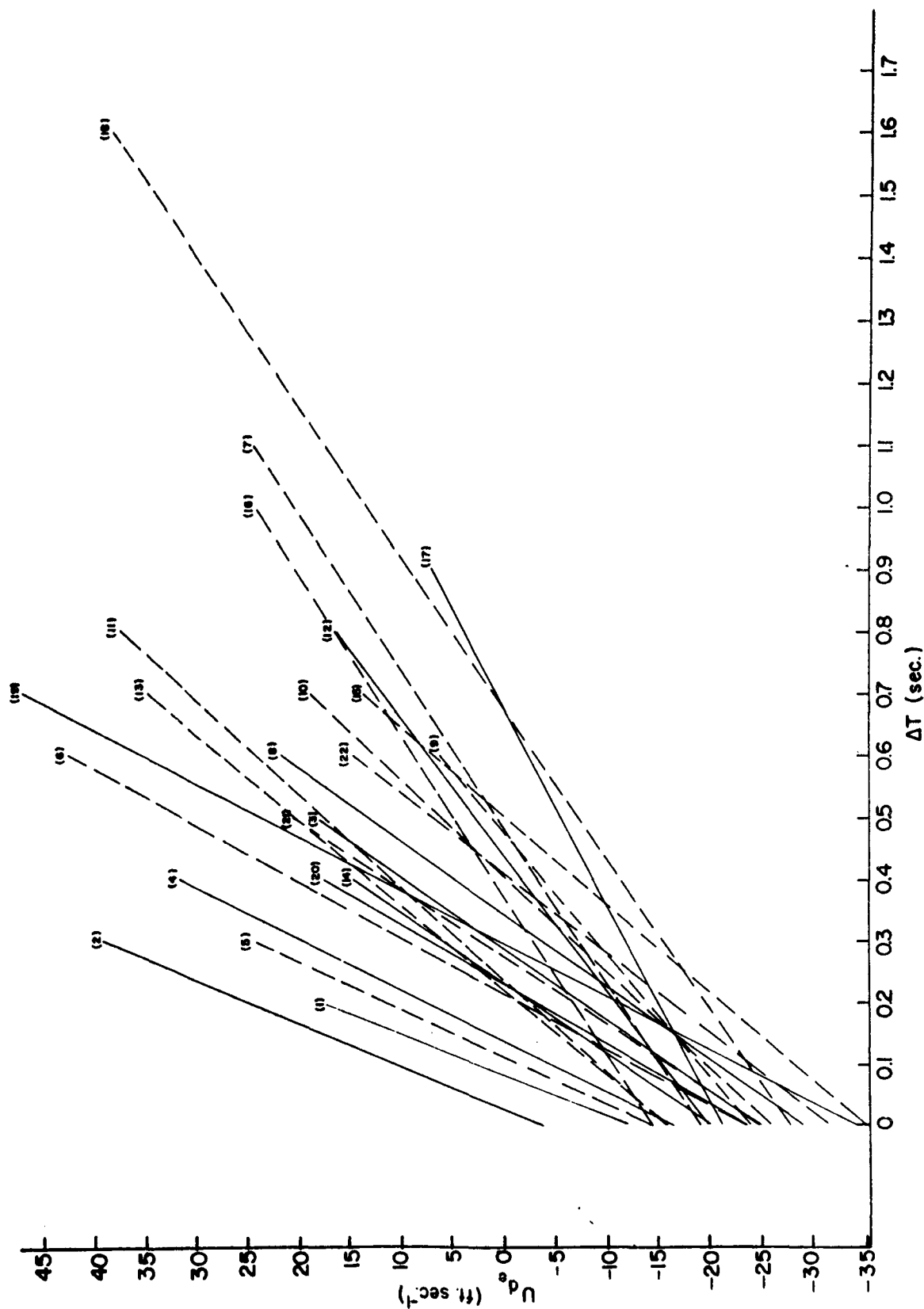


Figure 23.- Graph of the maximum time rate of change in derived gust velocities for each 1962 T-33 penetration analyzed. Dashed lines indicate use of negative slope for comparative purposes (for example #5 true slope is from +14.4 ft. sec.⁻¹ to -23.9 ft. sec.⁻¹). The number at the top end of each line is a code number assigned to each penetration and corresponds to the code numbers used in table 2.

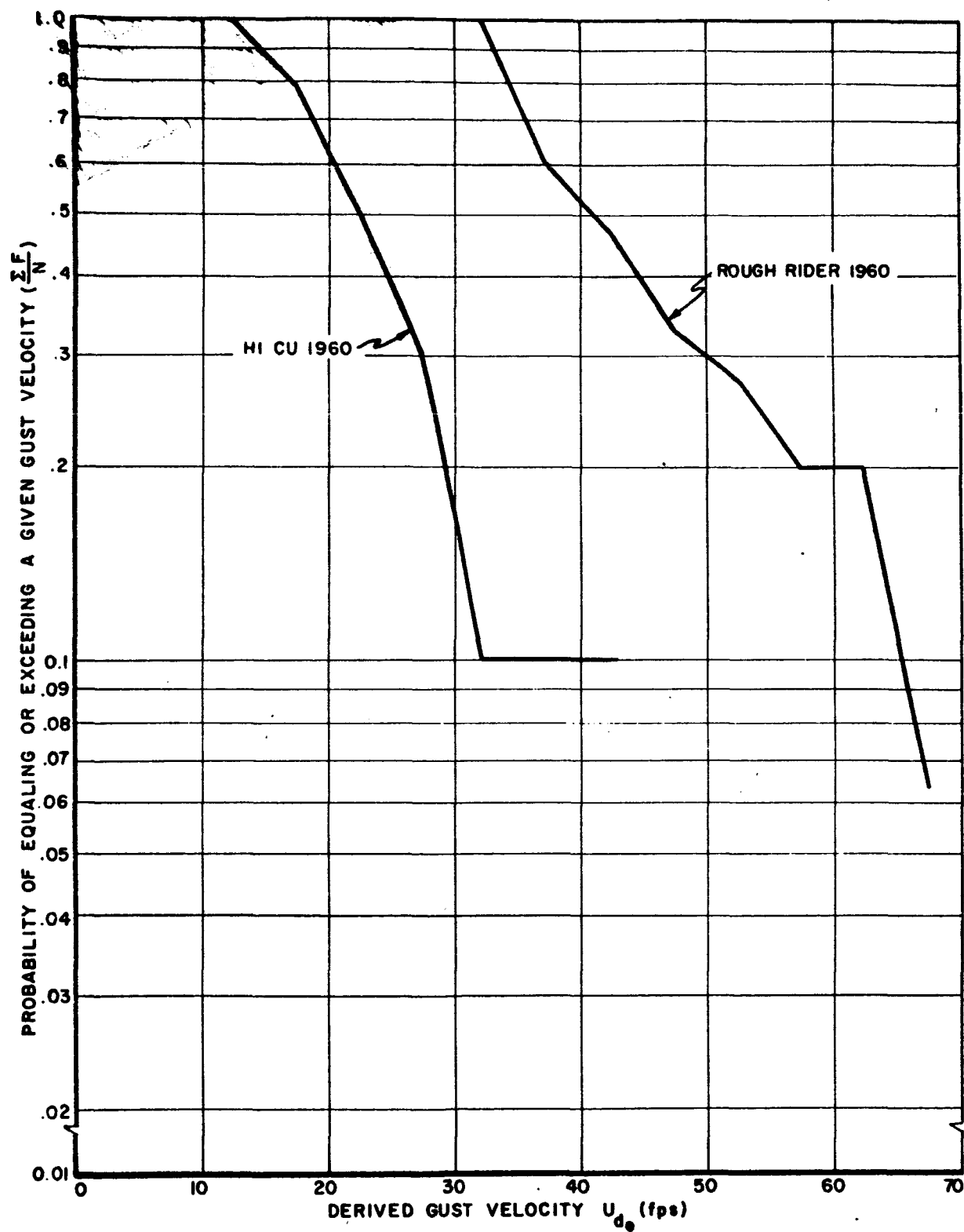


Figure 24.— Mean probabilities of equaling or exceeding a given absolute value of derived gust velocity from data collected in Projects Hi Cu and Rough Rider 1960 (after Roys [12]).

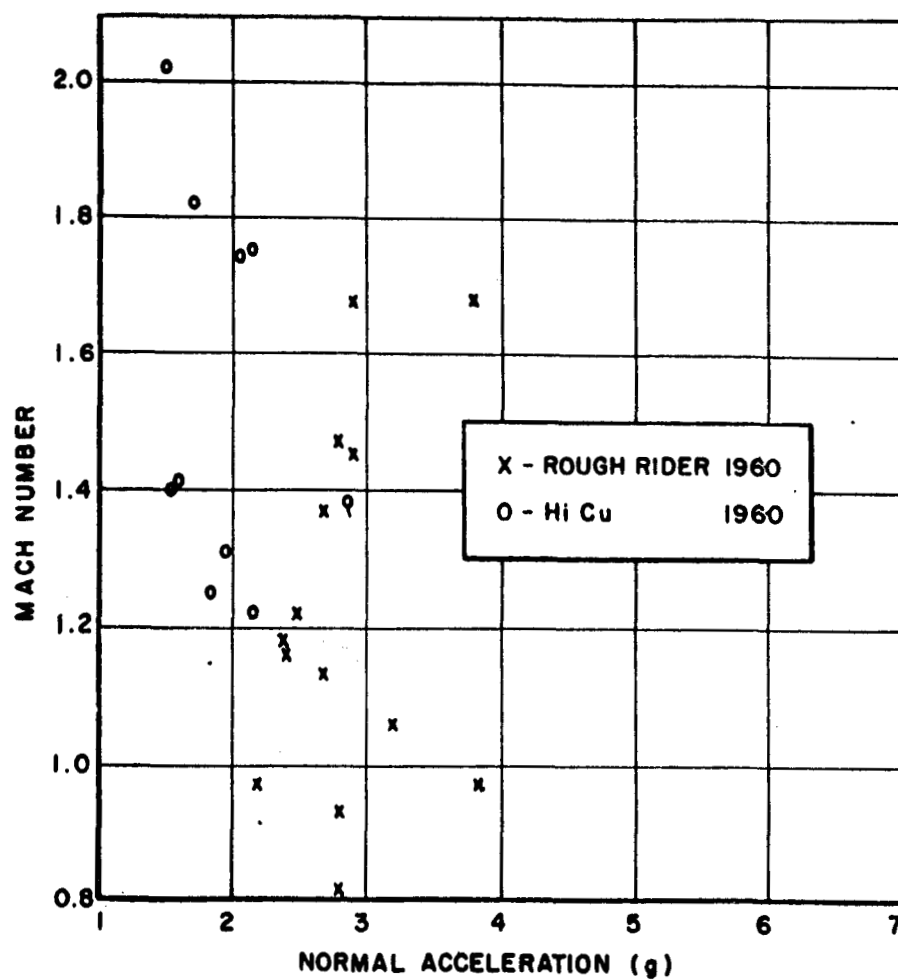


Figure 25.- Comparison of maximum absolute value of the normal accelerations experienced on each thunderstorm penetration of the F-106A at various Mach numbers for flights in Projects Hi Cu and Rough Rider 1960 (after Roys [12]).

N64-27400

ATTACHMENT IV

"ON VECTORING AIRCRAFT THROUGH THUNDERSTORMS "

C. F. Van Thullenar

ON VECTORING AIRCRAFT THROUGH THUNDERSTORMS

1. INTRODUCTION

The National Severe Storms Project (NSSP) has been involved in successfully vectoring military aircraft through thunderstorms within a radius of 150 n. mi. of Oklahoma City, Oklahoma, from 1960 through 1963. Most of these penetrations have been at altitudes in excess of 25,000 ft. Our experiences and equipment improvements during these years are reviewed and recommendations derived from these experiences stated.

Aircraft used in the project were furnished by the Air Force, Aeronautical Systems Division, Wright-Patterson AFB, Ohio (ASD). That organization also supplied pilot and maintenance crews. The National Aeronautics and Space Administration (NASA) instrumented one aircraft in each of the two years, 1960 and 1961. Instrumentation of other aircraft, and of all aircraft used in 1962 and 1963, was the responsibility of ASD. Data reduction was, or is being, performed by these two agencies during all four years and by Douglas Aircraft Co. in 1961.

During 1960 the Air Force furnished a T-33 to NASA for turbulence measuring instrumentation. The Air Force also participated in the project with an F-102 and F-106. These latter two aircraft had nonmeteorological objectives. In 1961 the Air Force furnished NASA with an F-106 for turbulence instrumentation, and also provided a T-33 as a lead aircraft, and a B-66

instrumented by Douglas Aircraft Co. for turbulence measurements. In 1962 the Aeronautical Systems Division supplied and instrumented an F-100 and a T-33. By this time emphasis on the collection of data was changing to include other parameters than turbulence. Such parameters as drop-size photography, equivalent liquid water content, infra-red measurement of the temperature of water drops and electric field, as well as turbulence, were included. 1963 was a repeat of 1962 with some improvements in instrumentation, but only the F-100 was instrumented.

The Federal Aviation Agency assigned a controller to the project since its beginning. All aircraft were ground-based-radar controlled. During 1960 an FPS-10 radar was used for control with additional information fed to the controller from a Weather Bureau's WSR-57. Beginning in 1961 control of the aircraft was from the WSR-57 site. During 1961 and 1962 control of penetration aircraft was from Oklahoma City, but in 1963 NSSP had its own WSR-57 and an MPS-4 height finder at Norman, Oklahoma. Since 1961 an MPX-7 radar was used to follow the aircraft.

Air-to-ground and ground-to-air communications were tape or wire recorded. Crews were debriefed at the conclusion of each mission.

2. VECTORING OF PENETRATION AIRCRAFT

A. 1960

During 1960, our first year of data collection, control of aircraft was from a site remote from the Weather Bureau's

WSR-57, using an FPS-10. Coordination was attempted by a "hot line" telephone from the controller to the WSR-57. It was felt necessary to use the WSR-57 because it had a great deal more flexibility, through echo attenuation capability, as well as antenna elevation control. This permitted an evaluation of storm intensity and stage of growth. Aircraft flight paths could thus be planned to sample various levels of storm intensities and gradients of intensities. However, since there was no flight following capability, other than skin paint of the aircraft, this method was considered unsatisfactory for comparing turbulence against radar return signals.

B. 1961

Prior to the beginning of the severe storm season of 1961 the Weather Bureau's WSR-57 at Oklahoma City was flight tested by FAA. During this season the controller was located at the site of the WSR-57 using an OA-175 scope. In addition to weather, an MPX-7 beacon-transmitter-receiver for aircraft following and a GPA-30 video mapper providing display of high altitude airways were added to the controller's scope. The weather display on the controller's scope was the same as on the main console of the WSR-57. On the control scope there was then displayed,

1. Weather from the WSR-57 radar,
2. Aircraft having transponders,
3. Aircraft without transponders but within the beam of the WSR-57, and
4. The high altitude airways from east of Tulsa, Oklahoma

to Amarillo, Texas, and from Wichita, Kansas, to Dallas, Texas.

Attenuation of the echoes on the controller's scope was accomplished by weather personnel from the main console. Only the single linear receiver of the '57 was used. Automatic step attenuation of echoes was added but left at a constant setting during penetrations (figs. 2 and 20 of Unit I).

C. 1962

Basic equipment for 1962 was the same as for 1961 but scope photography was considerably improved. Also two linear receivers were used on the WSR-57 so that the controller could use one independent of the main console scope. Also the controller was supplied with attenuation controls independent of the main console. This enabled the main console to be programmed for step attenuation during penetrations, thereby making possible a better evaluation of the directed flight path of the aircraft (fig. 1). This was a decided improvement over 1961. The only control common to both the main console scope and the controller's scope was the antenna elevation which was held constant during the penetration with the center of the beam programmed to the elevation of the penetration.

D. 1963

By 1963 NSSP had obtained a WSR-57 for its use and located it at Research Park of the University of Oklahoma at Norman. A height finder (MPS-4) was also added. Other equipment remained the same and the control of aircraft was then from Norman

instead of Oklahoma City. However, only one linear receiver was available and procedures were similar to 1961. More improvements in photography were made and, with this additional experience, step attenuations of the radar signal were more or less routine before and after each penetration and in between each run of the penetration (fig. 2).

A nonintegrating experimental contour circuit was built by Weather Bureau technicians and used on the logarithmic receiver of the WSR-57 during penetrations. Since it was experimental, it was not used for control purposes. It was used by the responsible meteorologist on a separate scope close to the height finder. This contouring circuit holds much promise and will be further improved. It permits the entire cloud at any particular elevation to be completely analyzed at each sweep of the antenna (fig. 3).

3. SUMMARY

The Weather Bureau embarked on this program with a great deal of confidence but little experience in actual control of penetration aircraft. The confidence was due to the known capability of the WSR-57 radar. The cooperative nature of the project provided the experts in the aircraft and control fields. The project was one of starting simply and improving each year. It should be clearly understood that in this project, with the possible exception of 1960, penetration aircraft could be fairly accurately vectored into any preselected portion of the

thunderstorm. The direction and particular path of each run on a penetration day were generally determined by the meteorologist and ASD's representative. These decisions could always be altered by the controller. However, even such alterations, whenever possible, were in consultation with the meteorologist. The team handling penetrations always consisted of a meteorologist, a representative of ASD and the controller.

Damage to aircraft due to turbulence, water erosion and/or hail did occur but never caused complete disabling of the aircraft or more than a few days down time for repairs. There were several instances when aircraft instrumentation was damaged to the extent where a lead aircraft was required to bring back to base the damaged plane.

4. CONCLUSIONS

In arriving at any conclusions concerning the vectoring of aircraft through thunderstorms it should be emphasized that experiences to date involved only jet trainer or fighter-type aircraft. However, with these experiences and the fortunate circumstance of having available an excellent basic radar for correlating turbulence and echo return, it is not too difficult to extend this knowledge to other types of aircraft.

From our four seasons of turbulence data gathering in thunderstorms,

- 1) It is not at all unreasonable to assume that severe

turbulence ($U_{de} = 35-50$ fps) can be encountered at some point in any storm.

2) In a growing thunderstorm or a large thunderstorm at the mature stage, extreme turbulence ($U_{de} > 50$ fps) should be expected to be present in some part of the storm.

3) It is not uncommon to encounter turbulence in the clear air near a thunderstorm or a line squall. Both positive and negative accelerations have been encountered.

4) Hail of some size is present in practically all thunderstorms.

5) Current-day airborne radar is not adequate for penetration of storms.

6) There is a danger in over-flying growing thunderstorms. It would not be uncommon to find the rate of vertical growth exceeding 5,000 ft. a minute.

7) Ignoring the question of passenger comfort, it should not be considered a normal operation for commercial type aircraft to fly through a thunderstorm.

8) In the event an emergency requires a commercial or executive type aircraft to fly through a thunderstorm, and that such flight cannot be accomplished at low elevations, it should be made only with the assistance of ground based radar. Such radar should have the following minimum capability.

- a. Antenna tilt to the elevation of penetration, and
- b. Step attenuation to determine storm intensity and to vector the aircraft through the edge of the storm, preferably outside the 12-db. level.

It is emphasized that penetrations of storms should not be made except in an emergency.

A final generalized comment may be of some value. Given a particular thunderstorm and the mean wind of the environment in which the storm is imbedded, maximum turbulence and the least chance for hail are to be expected on the upwind side of the center of the storm. The center of the storm is to be radar determined since the storms are generally asymmetrical. Minimum turbulence and the maximum chance of hail occur on the downwind side of the center of the storm. The chance of hail increases to the right of center on the downwind side.

Turbulence and hail are not the only elements of concern in thunderstorm flying. For the current and future supersonic aircraft, water erosion and water impact pressure may be of serious concern.

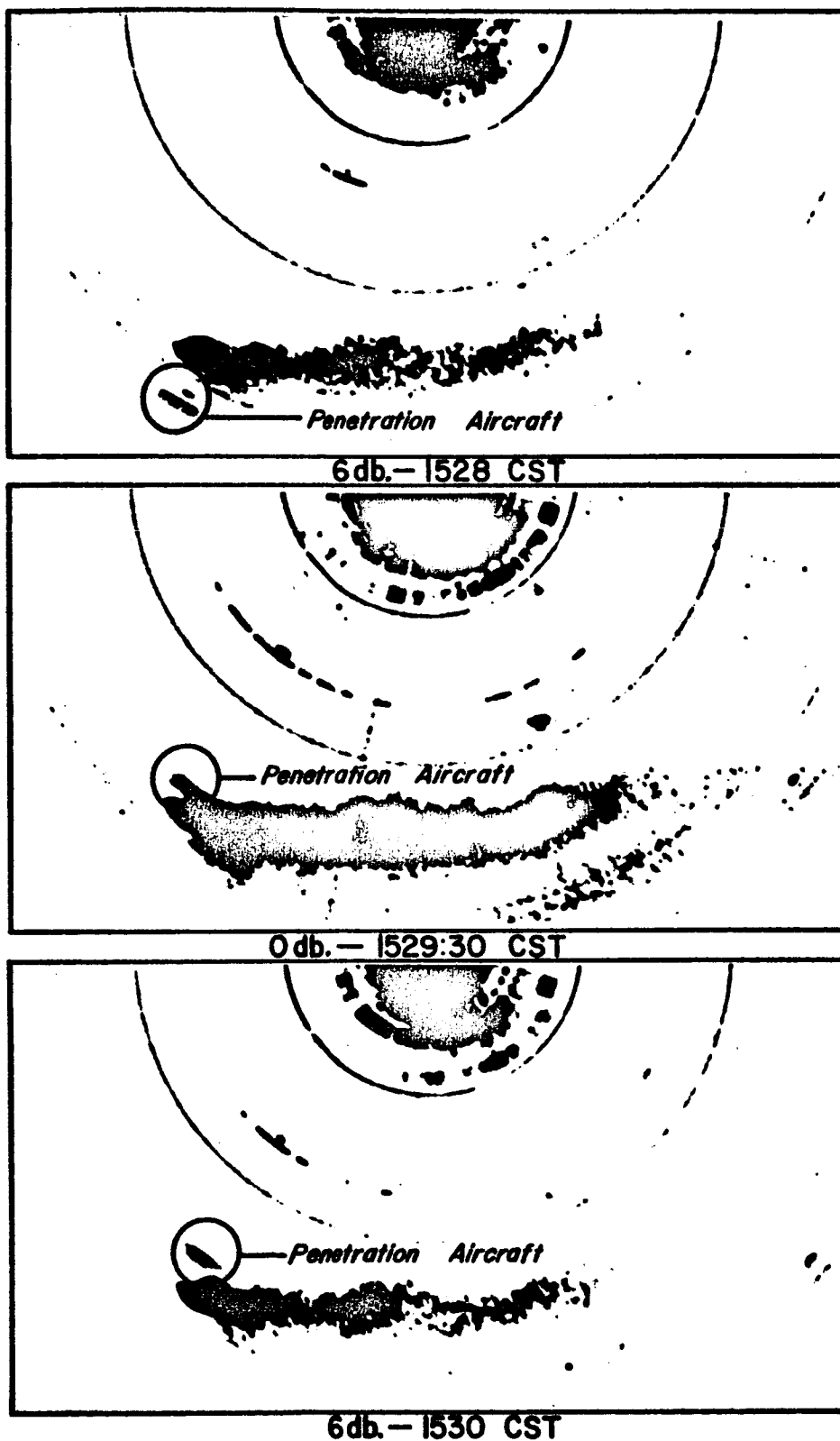
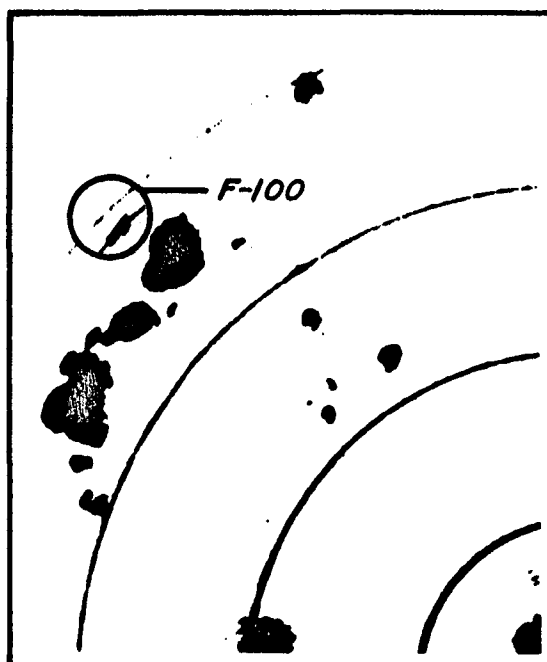
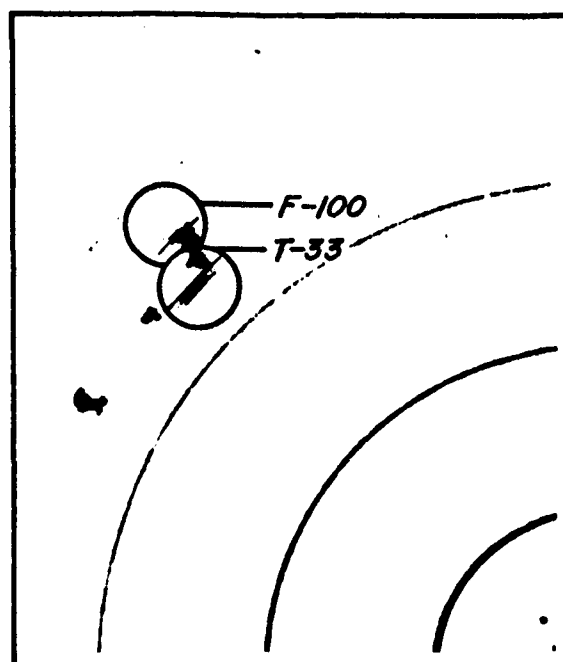


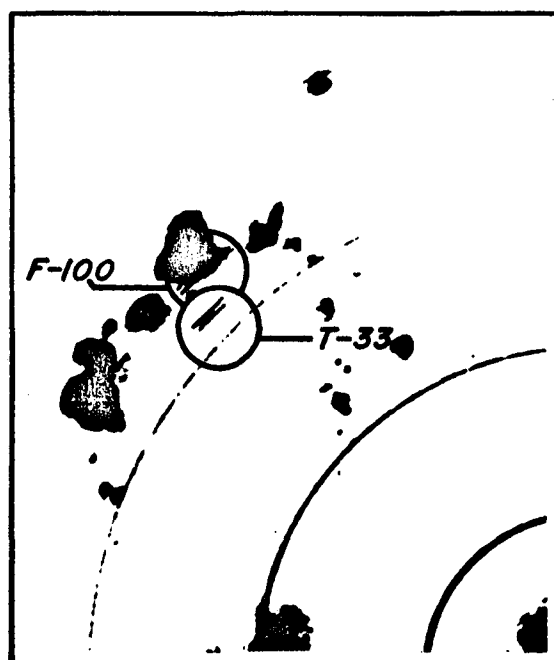
Figure 1.- (a) Aircraft (F-106) beginning penetration of a thunderstorm May 18, 1961. Note IFF pattern just back of "skin paint" echo and note also the long cirrus "blow off" to the east of main cell. (b) Penetration aircraft just emerging from northern portion of cell. (c) Penetration aircraft now clear of thunderstorm. 20-mi. range markers shown.



12 db. — 1703:30 CST



27 db. 1704:00 CST



12db. 1704:45 CST

Figure 2.— Case of step attenuation being used during penetration May 20, 1962. (a) F-100 approaching west side of storm; the T-33 is inside of cell shown with 12 db. attenuation. (b) Step attenuation of 27 db. shows centers of hard core. The T-33 has passed through the centers while the F-100 is approaching the hard core. (c) Attenuation returned to 12 db. The T-33 is out of cell and the F-100 is just leaving southeast portion of echo.

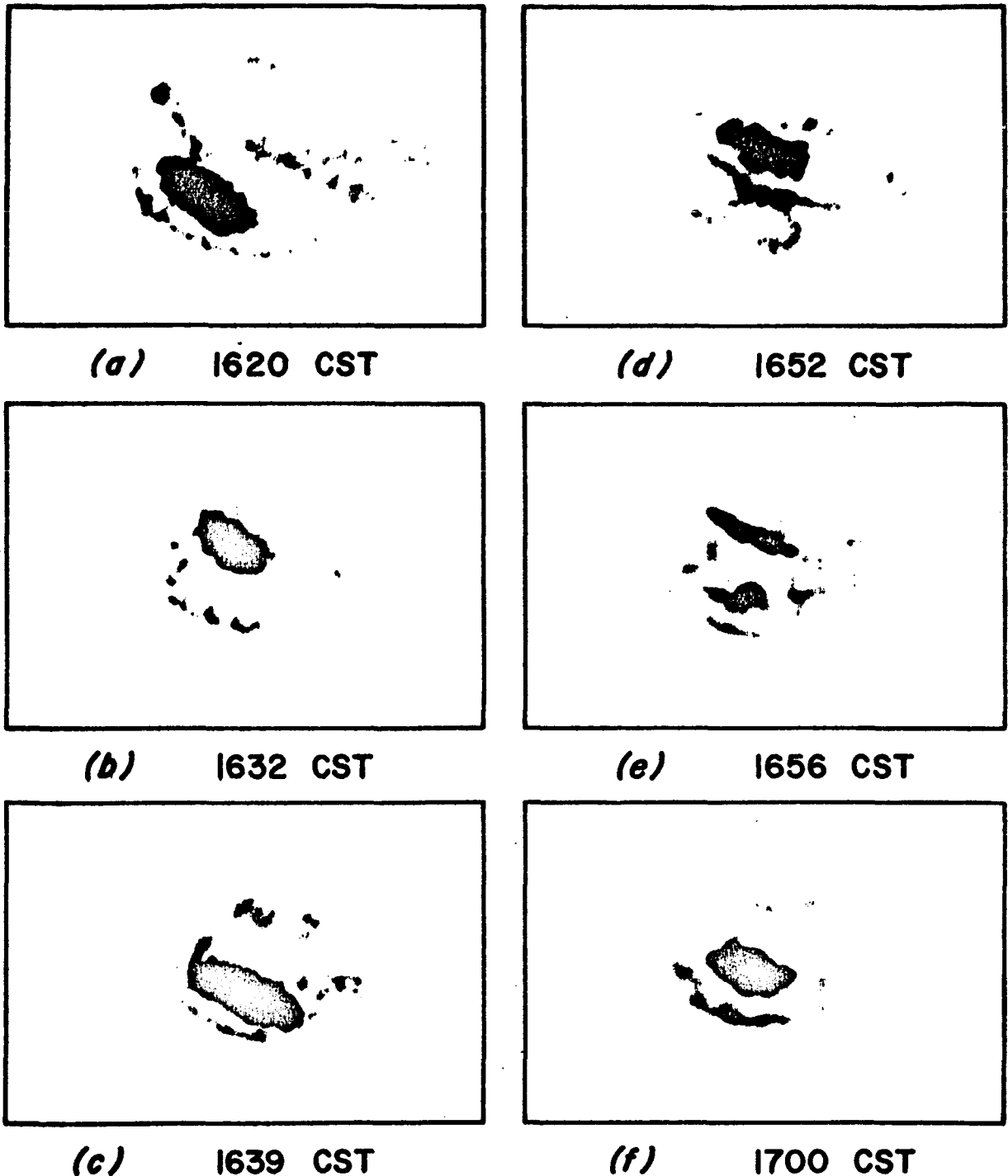
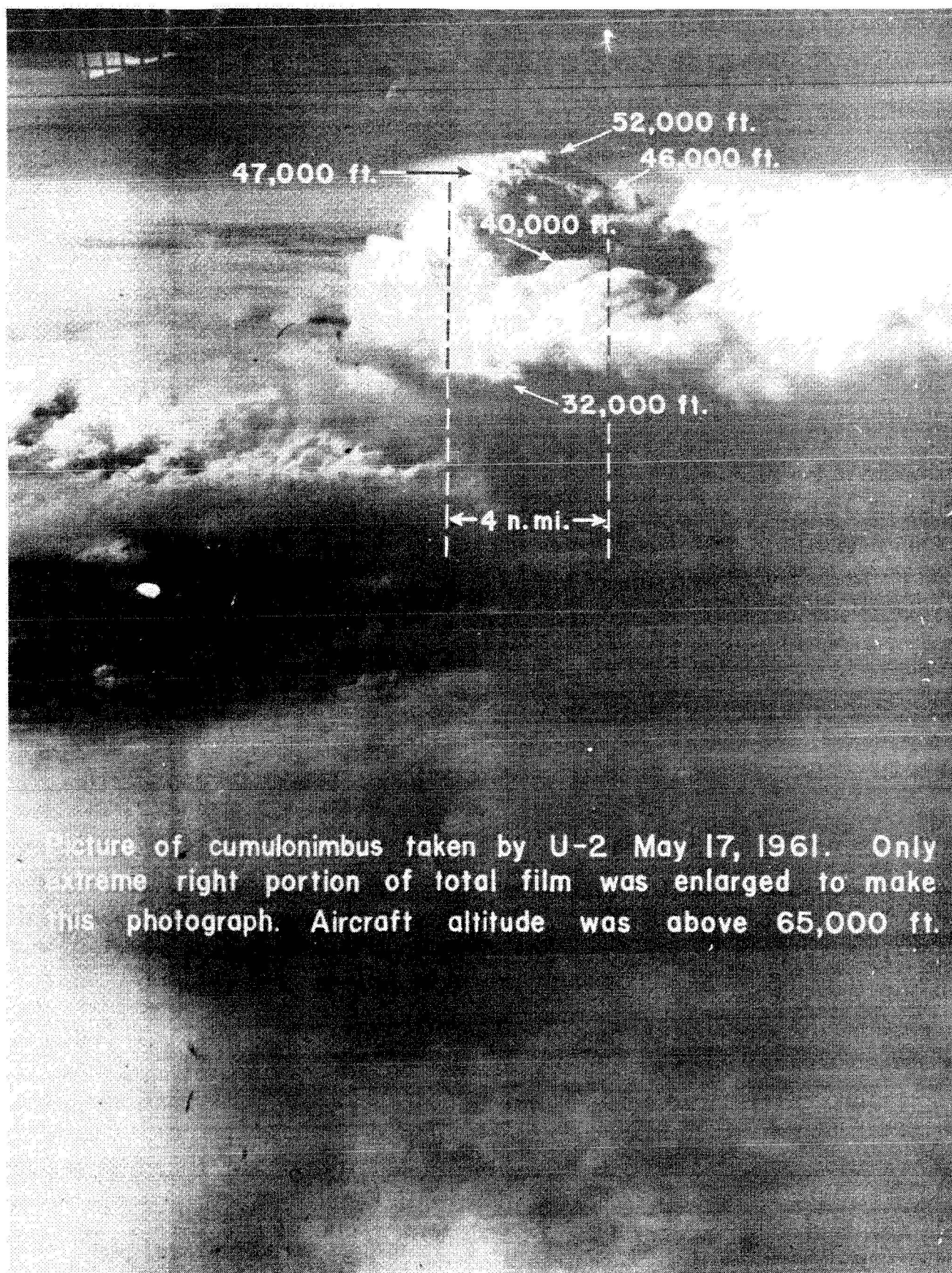


Figure 3.- Time series of echo growth patterns shown on radar scope using WRL's log contour circuitry. The approximate db. attenuation levels are the same for all of the illustrations but are marked in (a) only. (a) Hard core in southwestern portion of cell, 20-mi. range markers shown; (b) hard core has migrated into northwestern portion of cell; (c) first hard core dissipating and regeneration of hard core in southern portion of cell; (d) second hard core migrates to northern portion of cell; (e) new hard core seen in southern portion of cell while one in northern portion still strong; (f) northern hard core dissipates and southern one begins to move northward in cell. The two repetitive processes span a time interval less than a total of 45 minutes.

ATTACHMENT V

U-2 PHOTOGRAPH OF CUMULONIMBUS

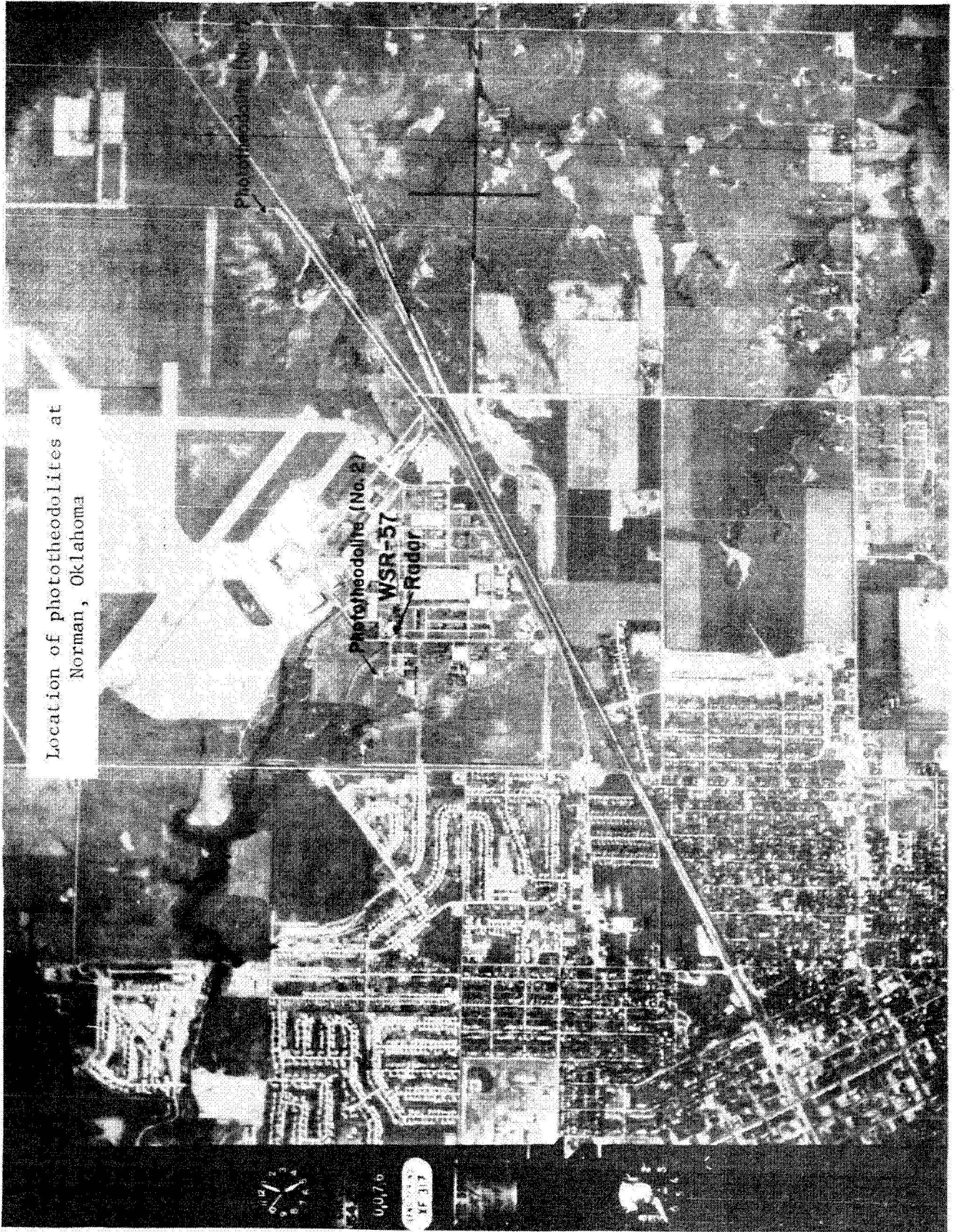


Picture of cumulonimbus taken by U-2 May 17, 1961. Only extreme right portion of total film was enlarged to make this photograph. Aircraft altitude was above 65,000 ft.

ATTACHMENT VI. a

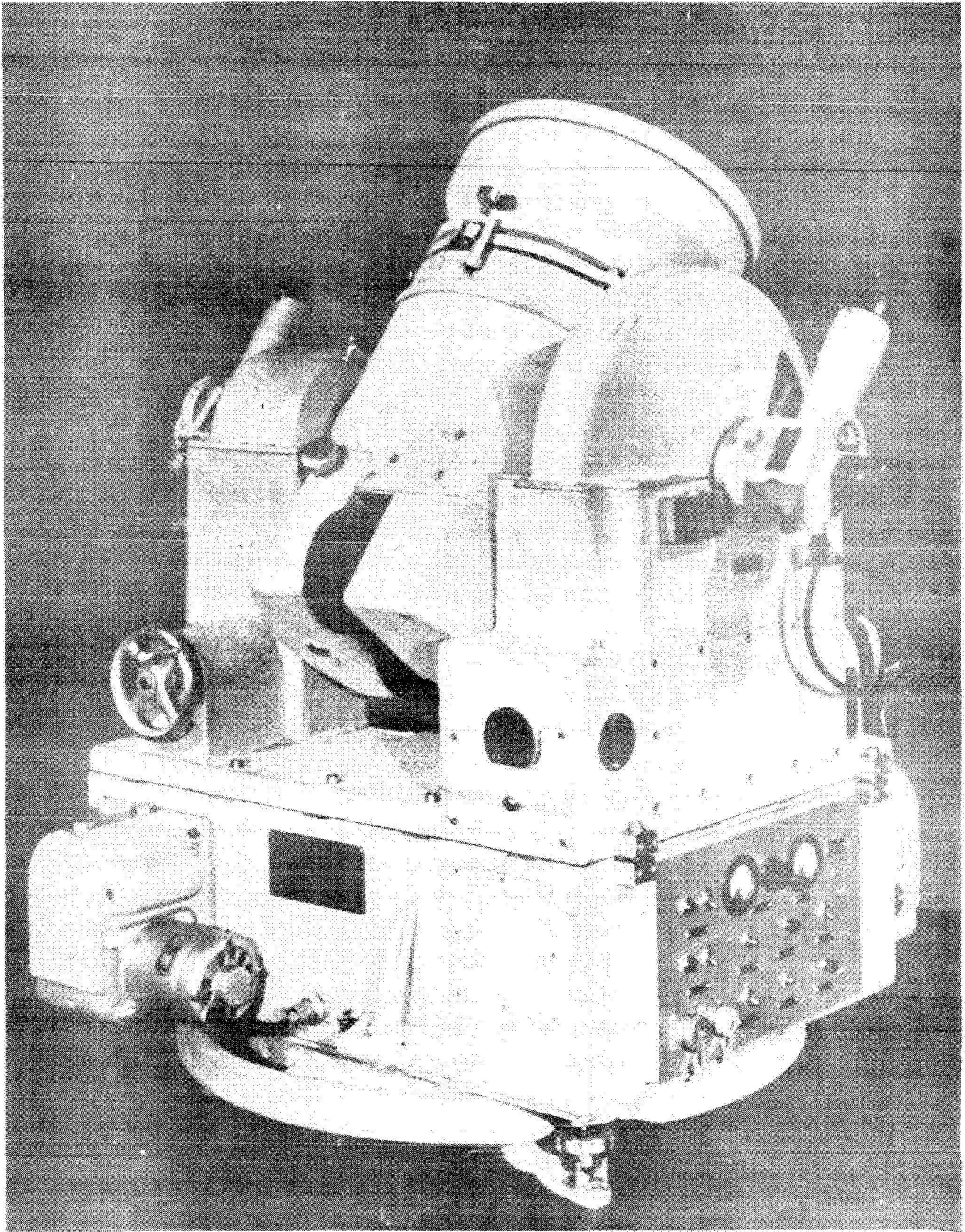
AERIAL PHOTO OF LOCATION OF PHOTOTHEODOLITES

Location of phototheodolites at
Norman, Oklahoma



ATTACHMENT VI.b

PHOTO OF PHOTOTHEODOLITE



Phototheodolite

N64-27401

Cat-21

ATTACHMENT VII

"VERTICAL VELOCITY AS EXPRESSED BY THE HORIZONTAL
EQUATION OF MOTION"

D. T. Williams

VERTICAL VELOCITY AS EXPRESSED BY
THE HORIZONTAL EQUATION OF MOTION

By

Dansy T. Williams
National Severe Storms Project
U. S. Weather Bureau
Kansas City, Missouri

Revised Copy, January 24, 1962

The horizontal equation of motion is expanded and manipulated to show vertical motion in terms of the features of horizontal flow. These features are: the horizontal wind field itself and its ageostrophicity, acceleration, divergence, vorticity, deformation, and vertical shear. Certain features of the flow can sometimes be used qualitatively to determine the direction of vertical motion.

AUT AOE

1. INTRODUCTION

Vertical velocity can be expressed by the horizontal equation of motion as a function of the horizontal wind and certain of its time and space derivatives. Although such an expression is not suitable for actual computation of vertical velocity, it does isolate certain features of the horizontal flow that contribute to vertical motion. Knowledge of these features can provide a better understanding of the mechanics of vertical motion, and occasionally, when a feature is outstanding, some diagnosis of the vertical motion can be made.

It is the purpose of this paper to solve the horizontal equation of motion for the vertical velocity and to point out the manner in which the components of the derived equation contribute to it.

2. EXPANSION OF THE EQUATION OF HORIZONTAL MOTION

The vector equation for horizontal flow, neglecting friction, curvature, and change in coriolis parameter terms, is:

$$\frac{d\mathbf{V}}{dt} = f(\mathbf{V}_2 - \mathbf{V}_{2g}) \times \mathbf{k} \quad (1)$$

where f is the coriolis parameter, \mathbf{V}_2 is the real wind, and \mathbf{V}_{2g} is the geostrophic wind.

Equation (1) can also be written as:

$$\begin{cases} \frac{du}{dt} \mathbf{i} = f(v - v_g) \mathbf{j} \times \mathbf{k} \\ \frac{dv}{dt} \mathbf{j} = f(u - u_g) \mathbf{i} \times \mathbf{k} \end{cases} \quad (2)$$

where u is component wind along the x-axis and v is the component wind along the y-axis.

Expanding the total derivatives in equation (2) and adding the two equations yields:

$$\left(\frac{\partial u}{\partial t} \mathbf{i} + \frac{\partial v}{\partial t} \mathbf{j}\right) + u\left(\frac{\partial u}{\partial x} \mathbf{i} + \frac{\partial v}{\partial x} \mathbf{j}\right) + v\left(\frac{\partial u}{\partial y} \mathbf{i} + \frac{\partial v}{\partial y} \mathbf{j}\right) + w\left(\frac{\partial u}{\partial z} \mathbf{i} + \frac{\partial v}{\partial z} \mathbf{j}\right) = f \left[(u \mathbf{i} + v \mathbf{j}) - (u_g \mathbf{i} + v_g \mathbf{j}) \right] \times \mathbf{k} \quad (3)$$

Solving for w, the vertical velocity, yields:

$$w = - \frac{u\left(\frac{\partial u}{\partial x} \mathbf{i} + \frac{\partial v}{\partial x} \mathbf{j}\right) + v\left(\frac{\partial u}{\partial y} \mathbf{i} + \frac{\partial v}{\partial y} \mathbf{j}\right) + \left(\frac{\partial u}{\partial t} \mathbf{i} + \frac{\partial v}{\partial t} \mathbf{j}\right)}{\left(\frac{\partial u}{\partial z} \mathbf{i} + \frac{\partial v}{\partial z} \mathbf{j}\right)} - f \frac{\left[(u \mathbf{i} + v \mathbf{j}) - (u_g \mathbf{i} + v_g \mathbf{j}) \right]}{\left(\frac{\partial u}{\partial z} \mathbf{i} + \frac{\partial v}{\partial z} \mathbf{j}\right)} \quad (4)$$

It may be noted that the vertical velocity is a function of the following:

1. u and v, the x- and y- components of the horizontal wind.
2. $\frac{\partial u}{\partial x} \mathbf{i}$ and $\frac{\partial v}{\partial y} \mathbf{j}$, the x- and y- components of horizontal dilatation and contraction.
3. $\frac{\partial u}{\partial y} \mathbf{i}$ and $\frac{\partial v}{\partial x} \mathbf{j}$, the x- and y- components of horizontal shear.
4. $\frac{\partial u}{\partial t} \mathbf{i}$ and $\frac{\partial v}{\partial t} \mathbf{j}$, the x- and y- components of horizontal acceleration.
5. $(u \mathbf{i} + v \mathbf{j}) - (u_g \mathbf{i} + v_g \mathbf{j}) \times \mathbf{k}$, the x- and y- components of ageostrophicity.
6. f, the coriolis parameter.
7. $\frac{\partial u}{\partial z} \mathbf{i}$ and $\frac{\partial v}{\partial z} \mathbf{j}$, the x- and y- components of vertical shear.

The terms $u(\frac{\partial u}{\partial x}i + \frac{\partial v}{\partial x}j) + v(\frac{\partial u}{\partial y}i + \frac{\partial v}{\partial y}j)$ in the numerator of (4) can be expanded into the four kinematic properties of horizontal flow, as follows:

$$\begin{aligned} & u(\frac{\partial u}{\partial x}i + \frac{\partial v}{\partial x}j) + v(\frac{\partial u}{\partial y}i + \frac{\partial v}{\partial y}j) = \\ & u\frac{\partial u}{\partial x}i + (v\frac{\partial u}{\partial x}j - v\frac{\partial u}{\partial x}j) + v\frac{\partial v}{\partial y}j + u\frac{\partial v}{\partial x}j + (u\frac{\partial u}{\partial y}j - u\frac{\partial u}{\partial y}j) + v\frac{\partial u}{\partial y}i = \\ & v(\frac{\partial u}{\partial x} + \frac{\partial v}{\partial y})j + u(\frac{\partial v}{\partial x} - \frac{\partial u}{\partial y})j + (u\frac{\partial u}{\partial x}i - v\frac{\partial u}{\partial x}j) + (u\frac{\partial u}{\partial y}j + v\frac{\partial u}{\partial y}i) = \\ & vj(\frac{\partial u}{\partial x} + \frac{\partial v}{\partial y}) - ui(\frac{\partial v}{\partial x} - \frac{\partial u}{\partial y}) \times k + (ui - vj)\frac{\partial u}{\partial x} - (ui - vj)\frac{\partial u}{\partial y} \times k. \quad (5) \end{aligned}$$

Alternately,

$$\begin{aligned} & u(\frac{\partial u}{\partial x}i + \frac{\partial v}{\partial x}j) + v(\frac{\partial u}{\partial y}i + \frac{\partial v}{\partial y}j) = \\ & u\frac{\partial u}{\partial x}i + (u\frac{\partial v}{\partial y}i - u\frac{\partial v}{\partial y}i) + v\frac{\partial v}{\partial y}j + v\frac{\partial u}{\partial y}i + (v\frac{\partial v}{\partial x}i - v\frac{\partial v}{\partial x}i) + u\frac{\partial v}{\partial x}j = \\ & u(\frac{\partial u}{\partial x} + \frac{\partial v}{\partial y})i - v(\frac{\partial v}{\partial x} - \frac{\partial u}{\partial y})i + (v\frac{\partial v}{\partial y}j - u\frac{\partial v}{\partial y}i) + (u\frac{\partial v}{\partial x}j + v\frac{\partial v}{\partial x}i) = \\ & ui(\frac{\partial u}{\partial x} + \frac{\partial v}{\partial y}) - vj(\frac{\partial v}{\partial x} - \frac{\partial u}{\partial y}) \times k - (ui - vj)\frac{\partial v}{\partial y} - (ui - vj)\frac{\partial v}{\partial x} \times k. \quad (6) \end{aligned}$$

Adding the last members of equations (5) and (6) and dividing by 2 yields:

$$\begin{aligned} & u(\frac{\partial u}{\partial x}i + \frac{\partial v}{\partial x}j) + v(\frac{\partial u}{\partial y}i + \frac{\partial v}{\partial y}j) = \\ & 1/2 \left[(ui + vj)(\frac{\partial u}{\partial x} + \frac{\partial v}{\partial y}) - (ui + vj)(\frac{\partial v}{\partial x} - \frac{\partial u}{\partial y}) \times k \right. \\ & \left. + (ui - vj)(\frac{\partial u}{\partial x} - \frac{\partial v}{\partial y}) - (ui - vj)(\frac{\partial v}{\partial x} + \frac{\partial u}{\partial y}) \times k \right] \quad (7) \end{aligned}$$

The following relationships are defined:

$$(\frac{\partial u}{\partial x} + \frac{\partial v}{\partial y}) = \text{Div}_2 \mathbf{V}_2, \text{ Horizontal velocity divergence.} \quad (8)$$

$$(\frac{\partial v}{\partial x} - \frac{\partial u}{\partial y}) \times k = \text{Rot}_2 \mathbf{V}_2, \text{ Vertical component of relative vorticity.} \quad (9)$$

$$(\frac{\partial u}{\partial x} - \frac{\partial v}{\partial y}) = \text{Def}_2 \mathbf{V}_2, \text{ Horizontal stretching deformation.} \quad (10)$$

$$(\frac{\partial v}{\partial x} + \frac{\partial u}{\partial y}) \times k = \text{Def}'_2 \mathbf{V}_2, \text{ Vertical component of horizontal shearing deformation.} \quad (11)$$

Substituting in (7) yields:

$$u\left(\frac{\partial u}{\partial x}i + \frac{\partial v}{\partial x}j\right) + v\left(\frac{\partial u}{\partial y}i + \frac{\partial v}{\partial y}j\right) =$$

$$1/2 \left[\mathbf{V}_2 (\text{Div}_2 \mathbf{V}_2 - \text{Rot}_2 \mathbf{V}_2) + (ui - vj)(\text{Def}_2 \mathbf{V}_2 - \text{Def}'_2 \mathbf{V}_2) \right] \quad (12)$$

Values of $\text{Div}_2 \mathbf{V}_2$ and $\text{Rot}_2 \mathbf{V}_2$ are independent of the orientation of \underline{x} - and \underline{y} - areas; but $\text{Def}_2 \mathbf{V}_2$ and $\text{Def}'_2 \mathbf{V}_2$ are not. Now assume that $\underline{y}j = 0$, i.e., the \underline{x} - axis has been oriented along a streamline. Then:

$$u\left(\frac{\partial u}{\partial x}i + \frac{\partial v}{\partial x}j\right) + v\left(\frac{\partial u}{\partial y}i + \frac{\partial v}{\partial y}j\right) =$$

$$1/2 \mathbf{V}_2 (\text{Div}_2 \mathbf{V}_2 - \text{Rot}_2 \mathbf{V}_2 + \text{Def}_2 \mathbf{V}_2 - \text{Def}'_2 \mathbf{V}_2) \quad (13)$$

Substituting for (13) in (4) yields:

$$w = - \frac{\mathbf{V}_2 (\text{Div}_2 \mathbf{V}_2 - \text{Rot}_2 \mathbf{V}_2 + \text{Def}_2 \mathbf{V}_2 - \text{Def}'_2 \mathbf{V}_2)}{2 \frac{\partial \mathbf{V}_2}{\partial z}}$$

$$- \frac{\frac{\partial \mathbf{V}_2}{\partial t} + f(\mathbf{V}_2 - \mathbf{V}_{g2}) \times \mathbf{k}}{\frac{\partial \mathbf{V}_2}{\partial z}} \quad (14)$$

Equation (14) expresses \underline{w} , the vertical velocity in terms of various features of the horizontal flow. These features are:

1. \mathbf{V}_2 , the actual horizontal wind.
2. $\text{Div}_2 \mathbf{V}_2$, horizontal velocity divergence.
3. $\text{Rot}_2 \mathbf{V}_2$, vertical component of relative vorticity.
4. $\text{Def}_2 \mathbf{V}_2$, horizontal stretching deformation.
5. $\text{Def}'_2 \mathbf{V}_2$, vertical component of horizontal shearing deformation.

6. $\frac{\partial v_z}{\partial t}$, local acceleration of the horizontal wind.
7. $(v_z - v_{gz}) \times k$, ageostrophicity of the horizontal wind.
8. f , coriolis parameter.
9. $\frac{\partial v_z}{\partial z}$, vertical shear of the horizontal wind.

3. MAGNITUDE OF TERMS AND SIGN OF VERTICAL MOTION

The numerator terms in equation (14) are usually of the same order of magnitude (around 10^{-4}sec^{-1}) when synoptic scale data (upper air data with observations taken ever 12 hours) are used. Certain terms may be negligibly small or unusually large in individual cases, but it cannot be assumed routinely that any term will be sufficiently small to be neglected, or that any term will be sufficiently large to be the only one needing consideration. The difficulty in using the equation quantitatively arises from the fact that the error in measuring some of the terms may exceed the real algebraic sum of the terms, i. e., the errors may be greater than the vertical motion itself.

The sign, or direction, of vertical motion is determined by the signs of the numerator and denominator of the right member of the equation. The following combinations are possible:

1. Numerator positive, denominator positive --- motion downward.
2. Numerator negative, denominator positive --- motion upward.
3. Numerator positive, denominator negative --- motion upward.
4. Numerator negative, denominator negative --- motion downward.

4. VERTICAL SHEAR

Effect on Sign: Since $\partial V_z / \partial z$ is the only term in the denominator of the equation, the sign of w will be determined by it, when the numerator is held constant. For example with the numerator negative, w would be positive (upward) for $\partial V_z / \partial z > 0$ (net increase of u - and v - components with height). w would be negative (downward) for $\partial V_z / \partial z < 0$ (net decrease in u - and v - components with height). For a positive numerator the signs of w would be reversed.

Effect on Magnitude: It may be noted that the magnitude of w varies inversely as the magnitude of vertical shear, when the numerator in (14) is held constant. Small values of vertical shear occasion large values of w and vice versa. The equation fails when $\partial V_z / \partial z = 0$, since w would then be infinite (with numerator $\neq 0$) or indeterminate (with numerator = 0). This suggests that some vertical shear must always exist, and that when it appears negligibly small, the data and/or the manner in which the shear was computed might be questionable.

The Relation of Shear to Jet Structures: Since a jet, or band of maximum winds, is featured by a peak velocity at some level, positive shear exists from the core of the jet downward and negative shear exists from the core of the jet upward. This is true in low and intermediate level jets, as well as in the high level jet stream. With the numerator negative in equation (14), this would imply upward motion below the jet and downward motion above it. The reverse would be true for a positive numerator.

Jet structures, including jet maxima, are important in the forecasting of weather in that the vertical motion fields associated with them may rapidly modify the environmental air mass. Certain features of the jet -- speed, vorticity, divergence, etc. (numerator terms of equation 14) -- are used to estimate its dynamic modification of the air mass. However, unless vertical shear is also considered, the effect of the jet may be badly estimated. A jet maximum of modest speed, existing through a considerable depth, could occasion rather strong vertical velocities, since the vertical shear through an appreciable depth would be small. On the other hand, a strong jet, existing through a very shallow depth, could occasion only small vertical velocities, since the vertical shear would be great. The sense of these facts is used in forecasting: An unusually strong wind at the jet stream level is given more credence if strong winds also exist at other levels, e. g., 200, 300, and/or 500 mb.

Vertical Motion near the Tropopause: Winds above the tropopause are generally quite light compared with the jet speed winds that may be present at or immediately below the tropopause. Vertical shear in the vicinity of the tropopause is thus quite great, and one would expect vertical velocity in its vicinity to be quite small.

Relation to Turbulence: Past thinking has been that CAT (clear-air turbulence) is most pronounced in regions where the vertical and horizontal shears of the horizontal wind are greatest.

However, if it is postulated that turbulence may result from vertical motion, then the optimum region of CAT would be in regions where the vertical shear was very small. Such regions might be expected near the core level of any jet and on the side where the numerator terms of equation (14) would have sufficiently large values. The above reasoning is not restricted to CAT. The existence of small vertical shear in the stack of a thunderstorm might be one aspect of thunderstorm turbulence.

5. NUMERATOR TERMS

Consider the effect of individual numerator terms of (14) that will contribute to vertical velocity, when $\frac{\partial V_z}{\partial z} > 0$

Div V_z . Motion is upward for negative values (convergence) and downward for positive values (divergence).

Rot V_z . Motion is upward for positive values (cyclonic vorticity) and downward for negative values (anticyclonic vorticity).

Def V_z . Motion is upward for negative values (stretching normal to the flow and contraction along the flow) and downward for positive values (contraction normal to the flow and stretching along the flow).

Def V_z . Motion is upward for positive values (cyclonic shear along the flow and anticyclonic shear normal to the flow) and downward for negative values (cyclonic shear normal to the flow and anticyclonic shear along the flow).

$\text{Def}_2 \mathbf{V}_2$ and $-\text{Def}'_2 \mathbf{V}_2$. Motion is upward when the algebraic sum is negative. If the absolute values of $\text{Def}_2 \mathbf{V}_2$ and $\text{Def}'_2 \mathbf{V}_2$ are the same, then the axis of deformation would be along a line from $22\ 1/2^\circ$ to $202\ 1/2^\circ$ for westerly flow, $157\ 1/2^\circ$ to $337\ 1/2^\circ$ for southwesterly flow, and $112\ 1/2^\circ$ to $292\ 1/2^\circ$ for southerly flow. For southwesterly flow this indicates that features should be deformed along a general northwest to southeast line. The southeast tilt of 500 mb. troughs has long been one parameter in the forecasting of severe thunderstorms. Assuming such tilt to result from optimum deformation in a southwesterly flow, the conclusion is that such a tilt favors upward motion. Motion is downward when the algebraic sum is positive. In such case (for $\text{Def}_2 \mathbf{V}_2$ numerically equal to $\text{Def}'_2 \mathbf{V}_2$) the axis of deformation would be along a line from $112\ 1/2^\circ$ to $292\ 1/2^\circ$ for westerly flow, $67\ 1/2^\circ$ to $247\ 1/2^\circ$ for southwesterly flow, and $22\ 1/2^\circ$ to $202\ 1/2^\circ$ for southerly flow.

$d\mathbf{V}_2/dt$. Motion is upward for negative values (deceleration) and downward for positive values (acceleration).

$(\mathbf{V}_2 - \mathbf{V}_{g2}) \times \mathbf{k}$. Motion is upward for negative values (subgeostrophic winds) and downward for positive values (supergeostrophic winds).

In most instances the numerator terms will be interrelated. There will be a tendency for one term to be balanced by the other terms. Nevertheless, when one term is unusually large, it can be interpreted as a warning of significant vertical motion, and other techniques can then be applied to ascertain if the vertical motion

is actually present.

6. SUMMARY

The expansion of the horizontal equation of motion isolates features of the horizontal flow that are related to vertical motion. Although the equation cannot be used to obtain quantitative values of vertical motion, it can be used to diagnose such features as divergence, vorticity, deformation, acceleration, ageostrophicity, and vertical shear of the horizontal flow, with respect to vertical motion.

N64-27402
Cat-21

ATTACHMENT VIII

"A DYNAMIC-KINEMATIC METHOD FOR COMPUTING
VERTICAL MOTION"

D. T. Williams

A DYNAMIC-KINEMATIC METHOD FOR COMPUTING VERTICAL MOTION*

Dansy T. Williams
National Severe Storms Project
U. S. Weather Bureau
Kansas City, Missouri
February 11, 1963

27402

ABSTRACT

27402

A method is presented for computing vertical velocity from winds aloft and contour height data. The values computed are instantaneous but are means with respect to small horizontal areas and shallow layers. The method is based on solutions to the first two equations of motion. As a by-product, local accelerations of the horizontal wind are also obtained, and from these the rates of vorticity and divergence production may also be computed. Two examples are presented in which the method was applied. The examples indicate that there may be typical vertical motion, vorticity production, and divergence production fields associated with thunderstorms and tornadoes. The method can be machine programmed for operational use in short range forecast problems.

Author

1. INTRODUCTION

Some knowledge of vertical velocity is required in most forecast problems. Since vertical velocity is seldom measured directly, estimates must be obtained by indirect methods. These methods may be

*This paper is intended only for internal distribution within the National Severe Storms Project and the District Meteorological Office at Kansas City, Missouri.

thermodynamic, kinematic, or dynamic in their approach. Many methods have been devised, but most have deficiencies that limit their use on an operational basis.

It is the purpose of this paper to present a new method of computing vertical velocity, which shows some promise of being useful, particularly with respect to the sub-synoptic scale motions associated with thunderstorm systems. The method is kinematic and dynamic in its approach; i.e., it is based on both wind and pressure parameters. It yields values of vertical velocity that are instantaneous but which are averages for small horizontal areas and for layers of fairly small thickness. The only basic data required are horizontal winds and contour heights. All of the computations can be machine programmed.

The method has not yet been tested sufficiently to establish its worth. The hand computed examples to be given indicate that it has merit. However, further testing will be required to determine if the method is acceptable for use. The method is described at this stage in order that it may be programmed and tested. It is offered specifically to the Severe Local Storms Center and to the National Severe Storms Project.

2. BASIC EQUATIONS

The method is based on compatible solutions to the first two equations of motion. It is assumed that friction and curvature terms are negligibly small, so that:

$$\frac{du}{dt} = f(v-v_g) \quad \text{and} \quad \frac{dv}{dt} = -f(u-u_g) \quad (1)$$

where \underline{u} and \underline{v} are the west-to-east and the south-to-north components of

the wind and $\underline{du/dt}$ and $\underline{dv/dt}$ are total accelerations. The subscript, g , indicates the geostrophic wind, and \underline{f} is the coriolis parameter.

Expanding $\underline{du/dt}$ and $\underline{dv/dt}$ and solving for \underline{w} , the vertical velocity, yields

$$\begin{aligned} \underline{w} &= \frac{f (v - v_g) - u \frac{\partial u}{\partial x} - v \frac{\partial u}{\partial y} - \frac{\partial u}{\partial t}}{\frac{\partial u}{\partial z}} \quad \text{and} \\ \underline{w} &= \frac{-f (u - u_g) - u \frac{\partial v}{\partial x} - v \frac{\partial v}{\partial y} - \frac{\partial v}{\partial t}}{\frac{\partial v}{\partial z}} \end{aligned} \quad (2)$$

In each equation of (2) there are terms describing the ageostrophicity, the horizontal shear, the horizontal dilatation, the local horizontal acceleration, and the vertical shear. Theoretically, either equation can be solved for \underline{w} , and the values obtained would be the same. In practice, however, one would find values of \underline{w} differing as the result of errors in the measurement of the various terms.

From synoptic wind and contour height data one can compute all terms except $\underline{\partial u / \partial t}$ and $\underline{\partial v / \partial t}$, which are the local accelerations of the horizontal wind. Computations of these present a problem. The accelerations, given as finite increments between conventional soundings, even at 6-hourly intervals, are too gross to provide anything close to the instantaneous values required. Attempts to use such values were fruitless; the values of \underline{w} obtained were inconsistent.

Attempts were also made to use assumed values of $\underline{\partial u / \partial t}$ and $\underline{\partial v / \partial t}$, the assumed values being obtained as the displacements that would occur as characteristic features of the flow advanced. These attempts were also fruitless.

A further relationship to obtain values of $\underline{\partial u / \partial t}$ and $\underline{\partial v / \partial t}$ is required.

3. MEAN AREAL ACCELERATIONS

The equations in (2) involve 3 unknowns; i.e., \underline{w} , $\frac{\partial u}{\partial t}$, and $\frac{\partial v}{\partial t}$. A third relationship is required to permit a solution.

To simplify the notations, let $[f(v - v_g) - u \frac{\partial u}{\partial x} - v \frac{\partial u}{\partial y}]$ and $[-f(u - u_g) - u \frac{\partial v}{\partial x} - v \frac{\partial v}{\partial y}]$ equal respectively \underline{A} and \underline{B} , let $\frac{\partial u}{\partial t}$ and $\frac{\partial v}{\partial t}$ equal respectively \underline{u}' and \underline{v}' , and let $\frac{\partial u}{\partial z}$ and $\frac{\partial v}{\partial z}$ equal respectively \underline{u}^* and \underline{v}^* . Then

$$\underline{w} = \frac{\underline{A} - \underline{u}'}{\underline{u}^*} \quad \text{and} \quad \underline{w} = \frac{\underline{B} - \underline{v}'}{\underline{v}^*} \quad (3)$$

At any point the value of \underline{w} must be the same from either equation in (3), so that

$$\frac{\underline{A} - \underline{u}'}{\underline{u}^*} = \frac{\underline{B} - \underline{v}'}{\underline{v}^*} \quad (4)$$

The problem has now been reduced to one equation in two unknowns, specifically, \underline{u}' and \underline{v}' .

An assumption is now made that values of \underline{u}' and \underline{v}' at two adjacent points, \underline{P}_0 and \underline{P}_1 , are approximately equal. Then

$$\begin{aligned} \frac{\underline{A}_0 - \underline{u}'}{\underline{u}_0^*} &= \frac{\underline{B}_0 - \underline{v}'}{\underline{v}_0^*} & \text{and} \\ \frac{\underline{A}_1 - \underline{u}'}{\underline{u}_1^*} &= \frac{\underline{B}_1 - \underline{v}'}{\underline{v}_1^*} \end{aligned} \quad (5)$$

The equations in (5) can now be solved for \underline{u}' and \underline{v}' and their values substituted in either equation in (3) to obtain \underline{w} . This maneuver assures consistent values of \underline{w} ; they will be the same in both equations in (3).

The assumption made is obviously not true. It does not yield \underline{u}' , \underline{v}' , and \underline{w} at either \underline{P}_0 or \underline{P}_1 . Rather, it is an approximation of these values which must be interpreted as the mean between \underline{P}_0 and \underline{P}_1 .

To obtain a more effective mean for a particular point, consider the area surrounding a point, P_0 , as defined by a cross with equi-distant points on the arms, P_1 , P_2 , P_3 , and P_4 as shown in figure 1. Form equations such as (5) for each of the 5 points. Then compute individual values of \underline{u}' and \underline{v}' with respect to the central point and the points on each arm of the cross. The four values each of \underline{u}' and \underline{v}' can then be averaged, and these average values used as mean areal accelerations for the area defined by the cross. The average values may then be substituted in either equation of (3) to yield a value of \underline{w} , which is a mean for the area defined by the cross. The value is also a mean with respect to a layer whose thickness is defined by \underline{u}^* and \underline{v}^* . The mean value obtained is then assumed to be the approximate value for the central point of the cross.

The use of both \underline{u}' and \underline{v}' in (3) to obtain \underline{w} is not necessary, except as a check. Either can be used. The value of \underline{w} will be the same in either case.

In the event that either \underline{u}^* or \underline{v}^* is zero, only one component of the local acceleration can be obtained. For \underline{u}^* equal to zero, \underline{u}' equals \underline{A} and \underline{v}' is not determined. for \underline{v}^* equal to zero, \underline{v}' equals \underline{B} , and \underline{u}' is not determined. If both \underline{u}^* and \underline{v}^* should be equal to zero, no solution is possible. Fortunately, this condition is not likely to occur. There is virtually always some vertical shear in the horizontal wind.

The mean values of \underline{u}' and \underline{v}' are useful by-products of the computations. Used by themselves, they show regions in which significant accelerations are occurring. If added to the initial winds for short

time intervals (e.g., one to three hours), they yield prognoses of the horizontal flow. In this application the prognosticated wind fields can then be analyzed to show the expected change of divergence and vorticity with respect to time.

There are no restrictions on the application of the method. It can be applied to any layer which can be adequately described by the horizontal wind and contour height fields. Errors that may occur in the measurements are not accumulative; computations for one layer are completely independent of those for another layer. Suggested levels of application are: 850 mb. contour heights and winds with vertical shear obtained from winds between 3,000 and 7,000 ft.; 700 mb. contour heights and winds with vertical shear obtained from winds between 8,000 and 12,000 ft.; and 500 mb. contour heights and winds with vertical shear obtained from winds between 16,000 and 20,000 ft.

The capability of making prognostic contour height charts at small reiterative intervals exists at the National Meteorological Center. Looking further ahead, it would be theoretically possible to use these prognoses with wind prognoses as obtained above to obtain reiterative prognoses of both contour height and wind fields. Such prognoses would probably tend to "run away" if attempted for long periods of time. However, they might be useful for the short periods of concern to the severe storm forecaster and to the aviation forecast of winds aloft.

4. AN EXAMPLE FOR A CONSTANT PRESSURE CHART

The sectional 500 mb. chart for 1800C, May 3, 1961, shown in figure 2, was used to test the method. A 60 n. mi. grid of 110 points

was applied to the central-midwest area. The various parameters were plotted at individual observing stations, and from analyses of the parameters, values were determined at each grid point. The analyses were as follows:

a. Horizontal wind components. Wind direction and wind speed were decomposed into \underline{u} - and \underline{v} - components at each observing station, and analyses were made of each. These analyses are shown in figures 3 and 4. Values were read and tabulated at each grid point. Values of the four horizontal space derivatives were obtained as finite differences for each of the 72 interior grid points, using a measuring interval of 120 n. mi. The products of the space derivatives with the appropriate \underline{u} - and \underline{v} - components were also formed and tabulated.

b. Ageostrophic wind components. Contour heights were analyzed for each 50 ft. and the geostrophic wind direction and wind speed were computed at each observing station. The contour analysis and geostrophic winds are shown in figure 5. In the computation of geostrophic wind speed, the same measuring interval of 120 n. mi. was used. This is necessary to assure that the computed values are of uniform scale. The direction and speed of the geostrophic wind was then decomposed into its \underline{u}_g and \underline{v}_g components. The differences, $(\underline{u} - \underline{u}_g)$ and $\underline{v} - \underline{v}_g$ were then formed at each observing station and were then multiplied by \underline{f} . A constant value of 0.3 hr^{-1} was used for \underline{f} . There was some error involved in assuming this value to be constant. Values of $\underline{f}(\underline{u} - \underline{u}_g)$ and $\underline{f}(\underline{v} - \underline{v}_g)$ were then plotted for each observing station, and analyses

were made. From these analyses values were read and tabulation for each of the 72 interior grid points. The analyses are shown in figures 6 and 7.

c. Vertical shear. Winds at 5 and 6 km. were used to obtain \underline{u}^* and \underline{v}^* . The winds at both levels were decomposed into their \underline{u} and \underline{v} components and \underline{u}^* and \underline{v}^* were determined as the differences. The units of vertical shear were then converted to kt. (n. mi.)^{-1} . The values were then analyzed, and from the analyses values were read and tabulated at each of the 72 interior grid points. The analyses are shown in figures 8 and 9.

d. Local accelerations. From the tabulated values, \underline{A} and \underline{B} were formed for each of the 72 interior grid points. Values of \underline{A} , \underline{B} , \underline{u}^* , and \underline{v}^* were then used to form equations of type (4) at each of the 72 interior grid points. These were then solved in the manner previously described to yield \underline{u}' and \underline{v}' . In the case of the outer rows and columns of the 72 interior grid points, the averages could be made only with respect to 3 arms of a cross. Elsewhere, all 4 arms of the cross were used. Values of \underline{u}' and \underline{v}' were tabulated. Analyses of \underline{u}' and \underline{v}' are shown in figures 10 and 11.

e. Vertical velocity. Values of \underline{A} , \underline{B} , \underline{u}' , \underline{v}' , \underline{u}^* and \underline{v}^* were then substituted in equations (3) to yield \underline{w} . Both equations were solved for a consistency check. An analysis of \underline{w} is shown in figure 12.

f. Sample computation. The computation with respect to grid point 24 (vicinity of Liberal, Kansas) is shown in Table 1.

TABLE 1 --- Tabulations and computations to obtain u' , v' , and w at Grid Point 24, 500 mb., 1800C, May 3, 1961.

Grid Pt.	u kt.	v kt.	$(\Delta u)_x$	$(\Delta u)_y$	$(\Delta v)_x$	$(\Delta v)_y$
			\longleftrightarrow kt. (120 n. mi.) ⁻¹ \longrightarrow			
4	29	12				
13	32	15				
14	33	12	2	-12	- 7	0
15	34	8				
22	33	18				
23	38	14	8	-13	- 6	3
24	41	12	4	-17	- 6	0
25	42	8	1	-14	- 8	0
26	42	4				
33	45	12				
34	50	12	3	-10	- 4	0
35	48	8				
44	51	12				

Grid Pt.	$-u\partial u/\partial x$ kt.hr. ⁻¹	$-v\partial u/\partial y$ kt.hr. ⁻¹	$-u\partial v/\partial x$ kt.hr. ⁻¹	$-v\partial v/\partial y$ kt.hr. ⁻¹	$f(v - v_g)$ kt.hr. ⁻¹	$-f(u - u_g)$ kt.hr. ⁻¹
14	-0.6	1.2	1.9	0.0	1.0	-1.0
23	-2.5	1.5	1.9	-0.4	-0.5	0.5
24	-1.4	1.9	2.0	0.0	0.5	-0.5
25	-0.3	0.9	2.8	0.0	5.0	-2.5
34	-1.3	1.0	1.7	0.0	-0.5	-3.5

Grid Pt.	A kt.hr. ⁻¹	B kt.hr. ⁻¹	u^* kt.n.mi. ⁻¹	v^* kt.n.mi. ⁻¹	Equation kt.n.mi. ⁻¹
14	1.6	0.9	- 2	-18	9 u' - v' = 13.5
23	-1.5	2.0	- 5	-15	3 u' - v' = 6.5
24	1.0	1.5	- 4	-18	9 u' - 2 v' = 6.0
25	5.6	0.3	1	-22	22 u' + v' = 123.5
34	0.8	0.7	- 2	-20	10 u' - v' = -8.7

Paired Solutions	$-u'$ kt.hr. ⁻¹	$-v'$ kt.hr. ⁻¹
24-14	-2.33	-7.50
24-23	-6.33	-25.50
24-25	-4.77	-18.46
24-34	2.13	12.58
Ave.	-2.82	-9.72

$$\frac{A - u'}{u^*} = \frac{1.0 - 2.8}{-4} = \frac{1.8}{4} = 0.46 \text{ kt.}$$

$$\frac{B - v'}{v^*} = \frac{1.5 - 9.72}{-18} = \frac{8.22}{18} = 0.46 \text{ kt.}$$

$w = 23 \text{ cm. sec.}^{-1}$ at Grid Pt. 24

g. Interpretation of the vertical velocity fields. The 500mb. field of \underline{w} at 1800C, May 3, 1961, was compared with the RADU plots of thunderstorm activity for the same time. The plots are shown in figure 12. One may note that regions of upward motion had no echoes at all, while three of the regions of downward motion were featured by echoes.

The region of downward motion from Amarillo to Childress to Abilene, Texas, shows a fair fit to the areal outline of echoes. The axis of the stronger echoes lay parallel to, but slightly west of, the axis of maximum downward motion. A tornado was reported in one of these echoes 40 miles east of Lubbock, Texas, a short time earlier at 1735C. Another tornado was reported near Amarillo, Texas, at 1705C. Intensity of the stronger echo centers ranged up to very strong with echo tops up to 45,000 ft. However, an hour later maximum tops had diminished to 35,000 ft.

The region of downward motion near Fort Stockton, Texas, was featured by a single strong echo. The area of northeastern Oklahoma and eastern Kansas was featured by an extensive area of echoes, some of which corresponded to the center of downward motion in eastern Oklahoma.

The presence of downward motion in areas of thunderstorm activity needs an explanation. This could come about as follows:

(1) Actual motions within the cores of the thunderstorms might be upward, but with downward motions outside the cores. With the area surrounding the thunderstorms considerably larger than the cores themselves, there would be more of the area subject to downward motion than upward motion. The computed \underline{w} , which is for an area, would then show the motion to be downward on the average.

(2) The thunderstorms might have been in the dissipating stage with downward motions in excess of upward motions. One would then expect the average w to be downward. Such appears to have been the case for the storms in the Texas panhandle, since their maximum tops were diminishing with time.

(3) Vertical velocities at the 500 mb. level would probably be different from those at lower levels. It is planned to compute w also at 700 mb. and 850 mb.

Time changes in relative humidity at the 500 mb. level can be used as a crude measure of the direction of vertical motion, under the assumption that relative humidity decreases with downward motion and vice versa. Six stations within the grid made serial rawinsonde observations so that the changes in relative humidity could be ascertained for the approximate period 1600-1730. The average changes for the layer 550 to 450 mb. were as follows:

<u>Station</u>	<u>Change in Relative Humidity</u>	<u>Vertical Velocity</u>
Abilene	0%	-50 cm sec ⁻¹
Amarillo	-17%	-40 cm sec ⁻¹
Altus	3%	0 cm sec ⁻¹
Ardmore	- 2%	-10 cm sec ⁻¹
Fort Worth	- 7%	-50 cm sec ⁻¹
Oklahoma City	- 6%	-35 cm sec ⁻¹

The comparisons appear reasonable for all stations except Abilene. It is indicated that at least the direction of vertical velocity was correctly determined by the method.

The region of upward motion from Gage to Wichita Falls had no thunderstorm activity at 1800C. However, by 2100C, a major squall line had formed in this area.

It is tentatively indicated that regions of incipient or developing thunderstorm activity would be featured by mean upward motion, while areas of mature or dissipating thunderstorm activity would be featured by mean downward motion at 500 mb. However, such a premise needs to be tested with many cases, and such cases should include also the computations of vertical velocity at other levels.

h. Production of vorticity and divergence. The local changes in vorticity and divergence can be computed from the mean local accelerations. From the analyses of \underline{u}' and \underline{v}' in figures 10 and 11, one can form $(\partial v'/\partial x - \partial u'/\partial y)$ and $(\partial u'/\partial x + \partial v'/\partial y)$, and assume that these are equal respectively to $\partial/\partial t (\partial v/\partial x - \partial u/\partial y)$, the local change in vorticity, and $\partial/\partial t (\partial u/\partial x + \partial v/\partial y)$, the local change in divergence. This was done for the 42 interior grid points and the analyses of these values are shown in figures 13 and 14. Also shown in the figures are three tornadoes that occurred a short time after 1800C.

One may note in figure 13 that all the tornadoes occurred in regions where vorticity production was positive; i.e., vorticity was becoming more cyclonic. The tornado at 1930C just south of Altus, Oklahoma, was nicely contained in the maximum vorticity production area of $42 \times 10^{-2} \text{ hr.}^{-2}$. The tornado at 1950 C somewhat south of Gage, Oklahoma, was not in either maximum area, but it was still in a region where the production of vorticity was at the rate of about $25 \times 10^{-2} \text{ hr.}^{-2}$. The tornado at 1830C near Fort Stockton, Texas, was south of the area where computations could be made; however, vorticity production was a maximum immediately north of its occurrence with a value of $58 \times 10^{-2} \text{ hr.}^{-2}$. It is indicated that tornadoes occur in regions where substantial amounts of cyclonic vorticity are being produced at 500 mb. One would expect and hope that computations at lower levels would show similar results.

Finally, one would expect that favored location for tornadoes would be in regions where the net production of cyclonic vorticity through the column was greatest. Further testing is required to ascertain if such might be the case, and one would want, also, to ascertain to what height above 500 mb. the production of cyclonic vorticity might exist.

One may note in figure 14 that all the tornadoes occurred in regions of positive divergence. The tornado at 1950C somewhat south of Gage, Oklahoma, is nicely contained in the maximum divergence production area of $45 \times 10^{-2} \text{ hr.}^{-2}$. The other two tornadoes are less favorably located with respect to the maximum areas. It is indicated that tornadoes occur in regions where substantial amounts of positive divergence are being produced at the 500 mb. level. One would expect that there would be convergence production at lower levels and that the favored location for tornadoes would be in regions of the most intense divergence-convergence couples. Further testing is, of course, required to substantiate this.

Finally, the favored location of the tornadoes ought to be in regions having (1) the maximum vorticity production throughout the column, and (2) the most intense divergence-convergence couple throughout the column.

5. AN EXAMPLE FOR A COLUMN

The 0501C, May 4, 1961, sounding at Ardmore, Oklahoma, was anomalously warm and dry in the column from 940 to 550 mb. A plot of this sounding is shown in figure 15. In another study the mean vertical motion occurring at this point during a period of somewhat less than

an hour was computed by the adiabatic method. A plot of this vertical motion profile with height is shown in figure 16. The motion was found to be downward everywhere between 940 and 550 mb. with a maximum downward motion of about 65 cm sec^{-1} near 750 mb. Since this computation had already been made, it was decided to apply the dynamic-kinematic method to constant pressure levels with respect to Ardmore and check the two results for consistency. Computations were made at 850, 700 and 500 mb., and the vertical motion profile so obtained is also shown in figure 16. The profiles are in good agreement with respect to their shapes, but the latter method gave values that were substantially less. Nevertheless, the worth of the dynamic-kinematic method is considered good for the case. The adiabatic computation gave a time averaged value for the column, while the other computation gave an instantaneous areally averaged value. Since the anomalous warming and dessication were quite local, the large values of subsidence would likewise have been quite local, and the average value of \underline{w} for the area would have been less than the value of \underline{w} for the local column.

6. SUGGESTIONS FOR MACHINE PROGRAMMING

It is first required that data from fixed stations be put into the computer so that values at grid points may be obtained. Values that would need to be obtained in this manner are: \underline{u} , \underline{v} , $\underline{f}(\underline{v} - \underline{v}_g)$, $\underline{f}(\underline{u} - \underline{u}_g)$, \underline{u}^* , and \underline{v}^* .

Next the computer would be required to form the four horizontal space derivatives and the products, $\underline{u} \frac{\partial \underline{u}}{\partial x}$, $\underline{v} \frac{\partial \underline{u}}{\partial y}$, $\underline{u} \frac{\partial \underline{v}}{\partial x}$, and $\underline{v} \frac{\partial \underline{v}}{\partial y}$.

Next the computer would be required to form \underline{A} and \underline{B} .

Next the computer would need to form the equations at all interior grid points, as $(\underline{A} - \underline{u}')/\underline{u}^* = (\underline{B} - \underline{v}')/\underline{v}^*$.

Next the proper pairs of equations would need to be solved for \underline{u}' and \underline{v}^* and their averages obtained.

Finally, either $(\underline{A} - \underline{u}')/\underline{u}^*$ or $(\underline{B} - \underline{v}')/\underline{v}^*$ would need to be computed to yield the values of \underline{w} .

Values of \underline{u}' , \underline{v}' , and \underline{w} would then be printed out, preferably in the proper place on a base map, so that the values could be hand analyzed.

Values of vorticity and divergence at the initial time could be computed, if desired, from the horizontal space derivatives.

Values of vorticity production and divergence production could be computed from the grid values of \underline{u}' and \underline{v}' .

Values of initial vorticity and divergence could be added to their rates of change to yield short period prognoses of vorticity and divergence. However, this probably should not be attempted for a period greater than 2 hours.

7. FURTHER COMMENTS

It is felt that the best application of the dynamic-kinematic method is to obtain values of vertical velocity and values of vorticity and divergence production. Actual values of vorticity and divergence, as well as values of shearing and stretching deformation, the resultant deformation, and the axes of dilatation, could also be obtained. For best results, the computations should be made at several constant pressure levels.

In an earlier work the equations in (2) were manipulated to express \underline{w} in terms of divergence, vorticity, stretching deformation, and shearing deformation, as well as the ageostrophicity, the local acceleration, and the vertical shear. This somewhat lengthier expression could still be used to obtain \underline{w} ; however, it is not necessary. The simpler forms in (2) are just as good.

The method for computing vertical motion need not be restricted to thunderstorm forecasting. As indicated earlier, it may have an application to the short period forecasting of winds aloft. It can also be applied to jet structures, and it is expected that such an application would yield some typical vertical motion and acceleration fields with respect to jet maxima. Perhaps the models currently in use could be improved from this application. It also appears that the method could be applied to the problem of clear air turbulence. Application to high level charts might reveal isolated areas of vertical motion and/or accelerating horizontal motions that would lead to clear air turbulence. It is hoped that the application can be tested on these problems.

The author considers the contents of this paper somewhat sketchy and incomplete. It is presented in order that the work done so far may be made a matter of record and that a basis for machine testing may be outlined. For this reason, this paper is not intended for distribution to other than those in the local group who may be interested in applying the method within the framework given. It is hoped that a more definitive paper, containing verified examples, may be prepared at a later date.

No specific references have been quoted. When the paper is revised at a later date, appropriate references will be included.

LEGENDS FOR FIGURES

Figure 1 --- Points used in computing mean \underline{u}' , \underline{v}' , and \underline{w} at \underline{P}_0 .

Figure 2 --- Sectional 500 mb. chart for 1800C, May 3, 1961.

Contours (solid lines) are at 200 ft. intervals. Isotherms (dashed lines) are at 2C intervals. Winds are plotted with a barb equal to 10 kt. and a pennant equal to 50 kt. A contour trough is indicated by the heavy dashed line.

Figure 3 --- Analysis of the \underline{u} -component of the wind. Isotachs are drawn at 5 kt. intervals. The outline of the 110 point grid is superimposed.

Figure 4 --- Analysis of the \underline{v} -component of the wind. Isotachs are drawn at 5 kt. intervals. Numbers of the grid points have been omitted on this and succeeding figures.

Figure 5 --- Detailed contour analysis with contours at 50 ft. intervals. Geostrophic winds are plotted.

Figure 6 --- Analysis of $\underline{f}(\underline{u} - \underline{u}_g)$. Isopleths are drawn at 2 kt. hr.^{-1} intervals.

Figure 7 --- Analysis of $\underline{f}(\underline{v} - \underline{v}_g)$. Isopleths are drawn at 2 kt. hr.^{-1} intervals.

Figure 8 --- Analysis of \underline{u}^* . Isopleths are drawn at $10 \text{ kt. (n.mi.)}^{-1}$ intervals.

Figure 9 --- Analysis of \underline{v}^* . Isopleths are drawn at $10 \text{ kt. (n.mi.)}^{-1}$ intervals.

Figure 10 --- Analysis of \underline{u}' . Isopleths are drawn at 10 kt. hr.^{-1} intervals.

Figure 11 --- Analysis of \underline{v}' . Isopleths are drawn at 10 kt. hr.^{-1} intervals.

Figure 12 --- Analysis of w . Isotachs are drawn at 25 cm. sec.^{-1} intervals. Areas of radar echoes are enclosed by heavy lines, and individual echoes are shown as solid areas. The positions and times of two tornadoes near the time of the computations are indicated by tornado symbols. Grid point #24 is indicated by an "X".

Figure 13 --- Analysis of vorticity production. Isopleths are drawn at $10 \times 10^{-2} \text{ hr.}^{-2}$ intervals. The position and times of the tornadoes occurring after 1800C are indicated by tornado symbols.

Figure 14 --- Analysis of divergence production. Isopleths are drawn at $10 \times 10^{-2} \text{ hr.}^{-2}$ intervals. The positions and times of the tornadoes occurring after 1800C are indicated by tornado symbols.

Figure 15 --- Temperature and dew point plot of the 0501C, May 4, 1961, sounding at Ardmore, Oklahoma. The plot is from the surface to 500 mb. One may note the evidence of subsidence in the layer from 940 to 550 mb.

Figure 16 --- Vertical velocity profiles at Ardmore, Oklahoma, with respect to the 0501C, May 4, 1961, sounding. The profiles were computed for portions of the column between the surface and 500 mb. The values are in cm. sec.^{-1} . The solid profile was obtained by the adiabatic method. The dashed profile was obtained by the dynamic-kinematic method with computations at 850, 700, and 500 mb.

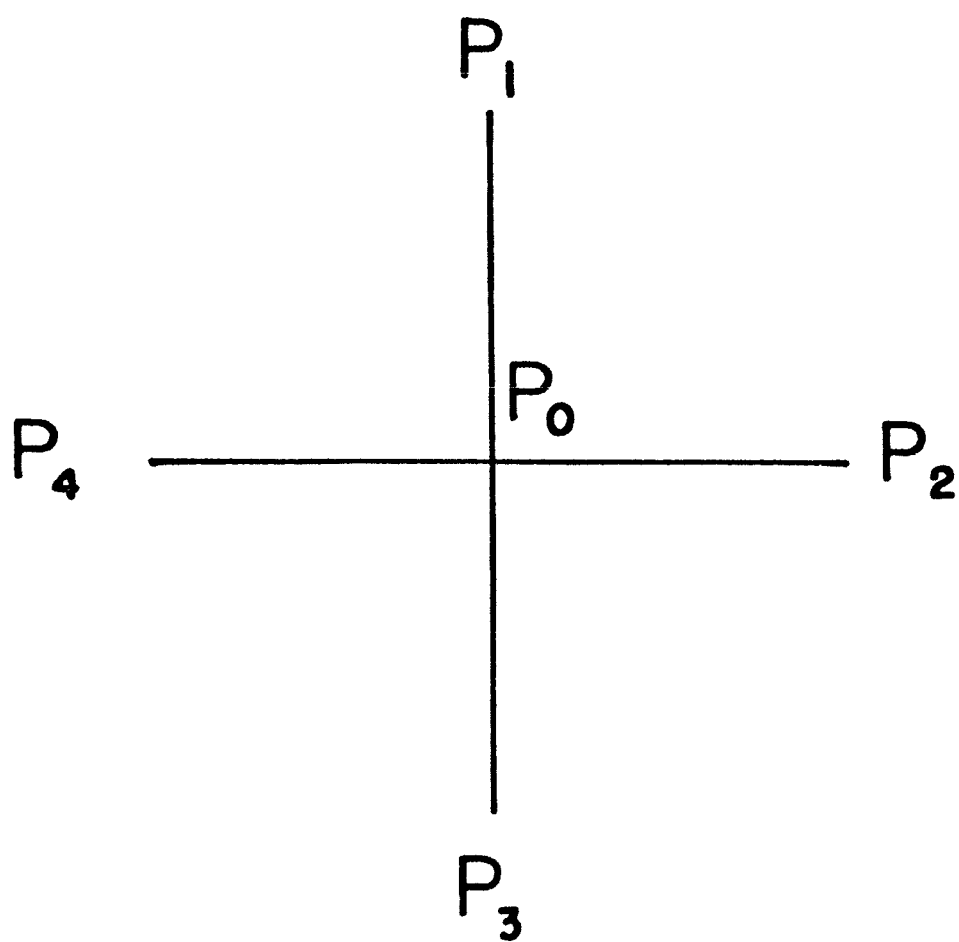


Figure 1

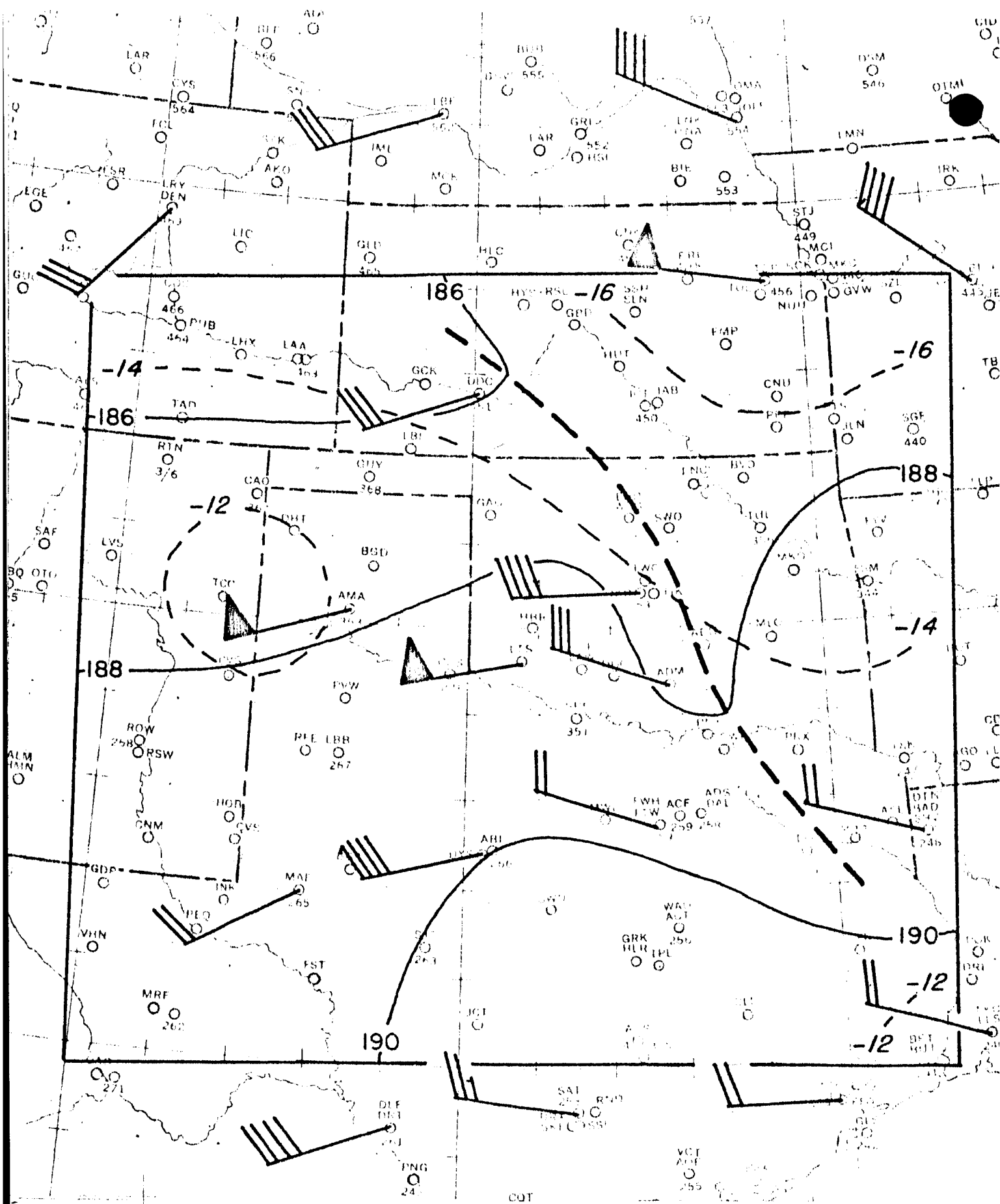


Figure 2

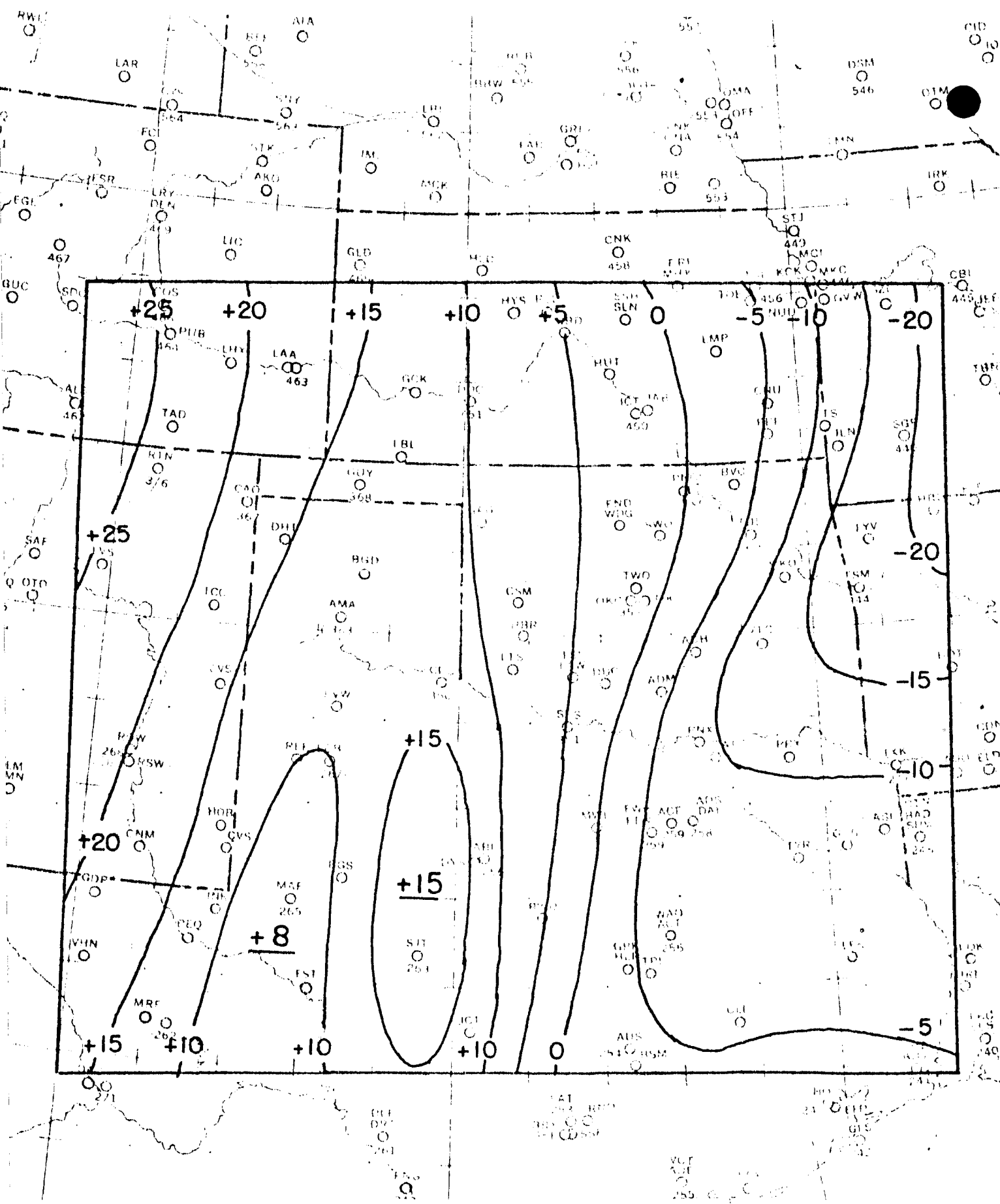


Figure 4

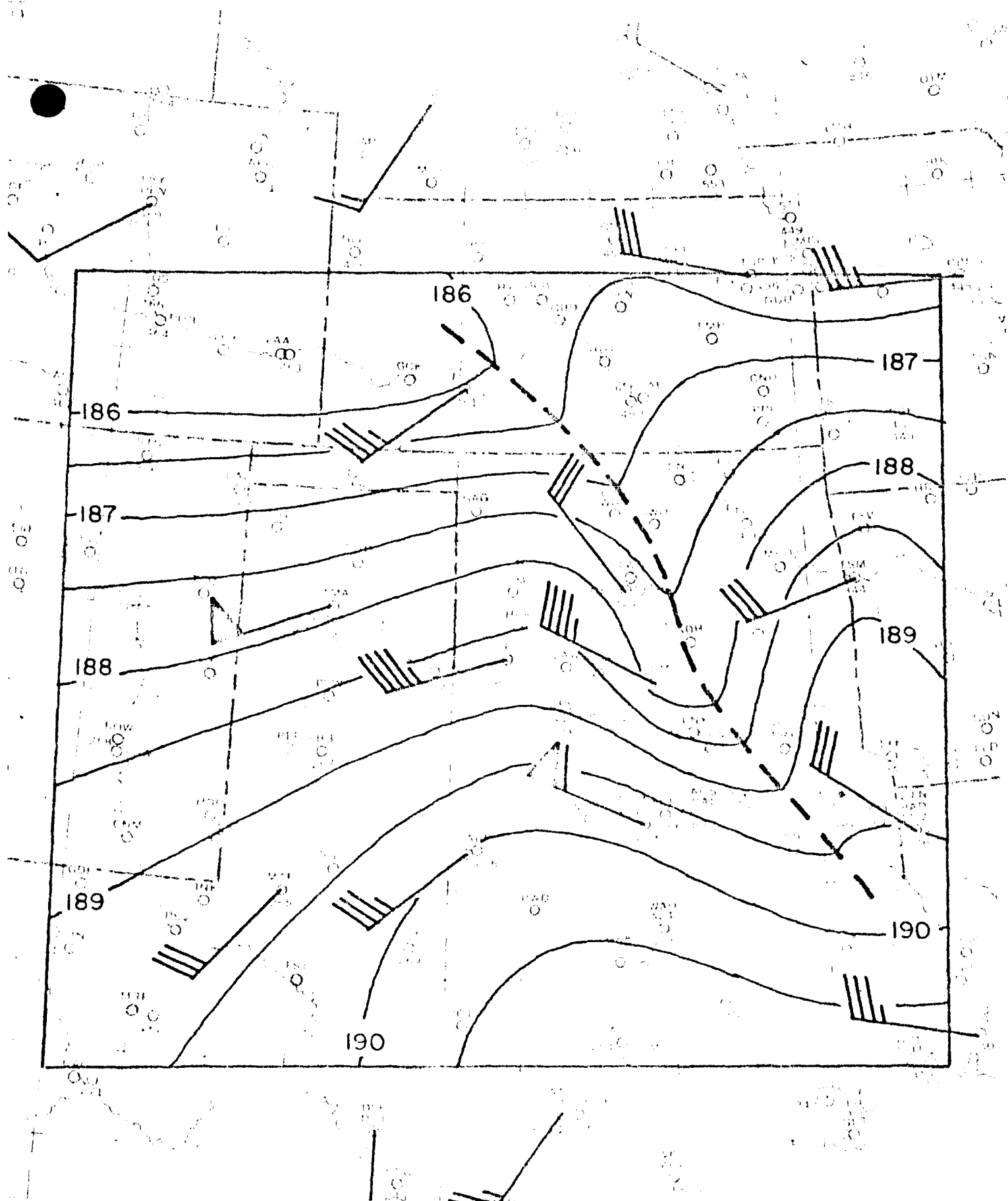


Figure 5

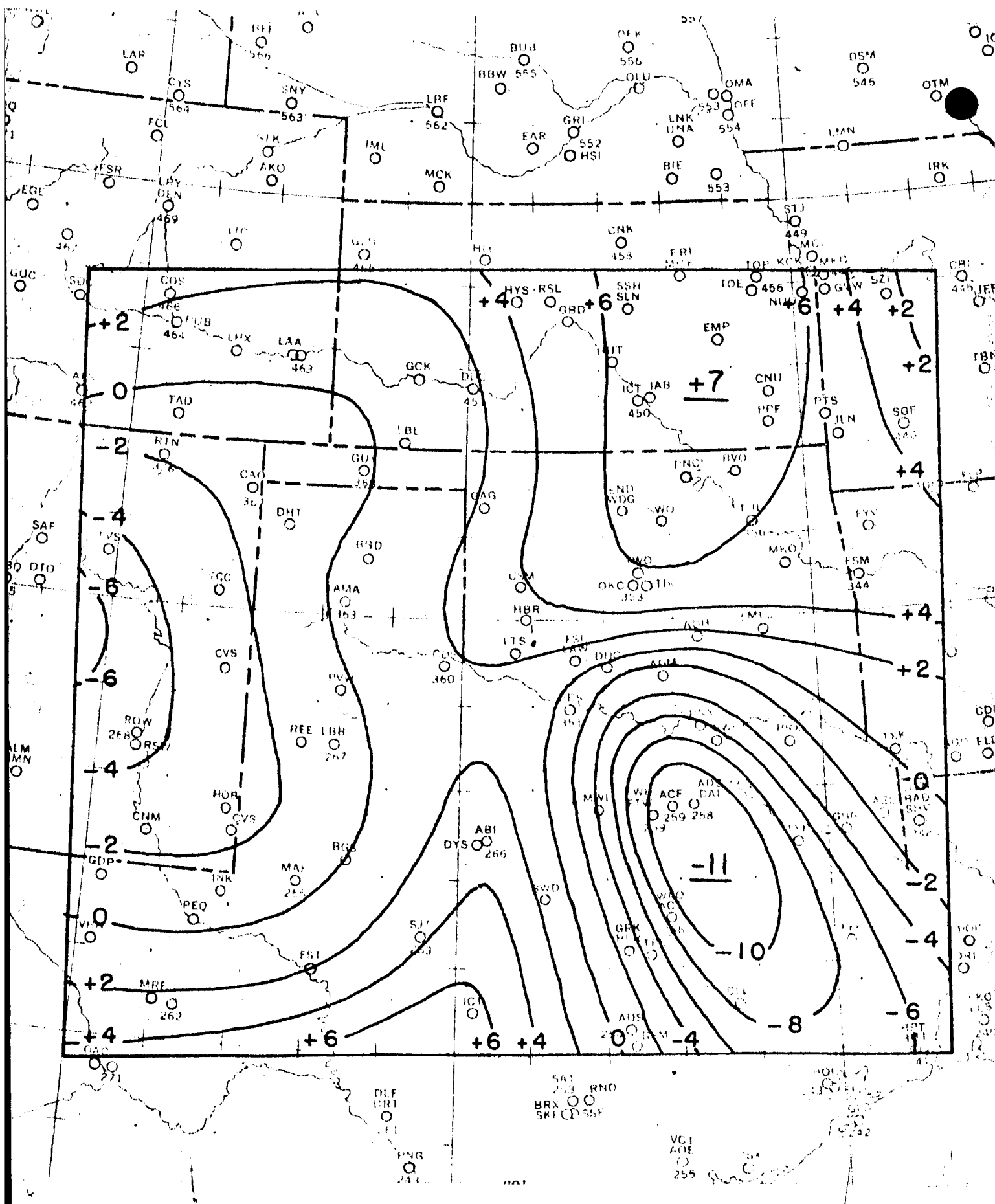


Figure 6

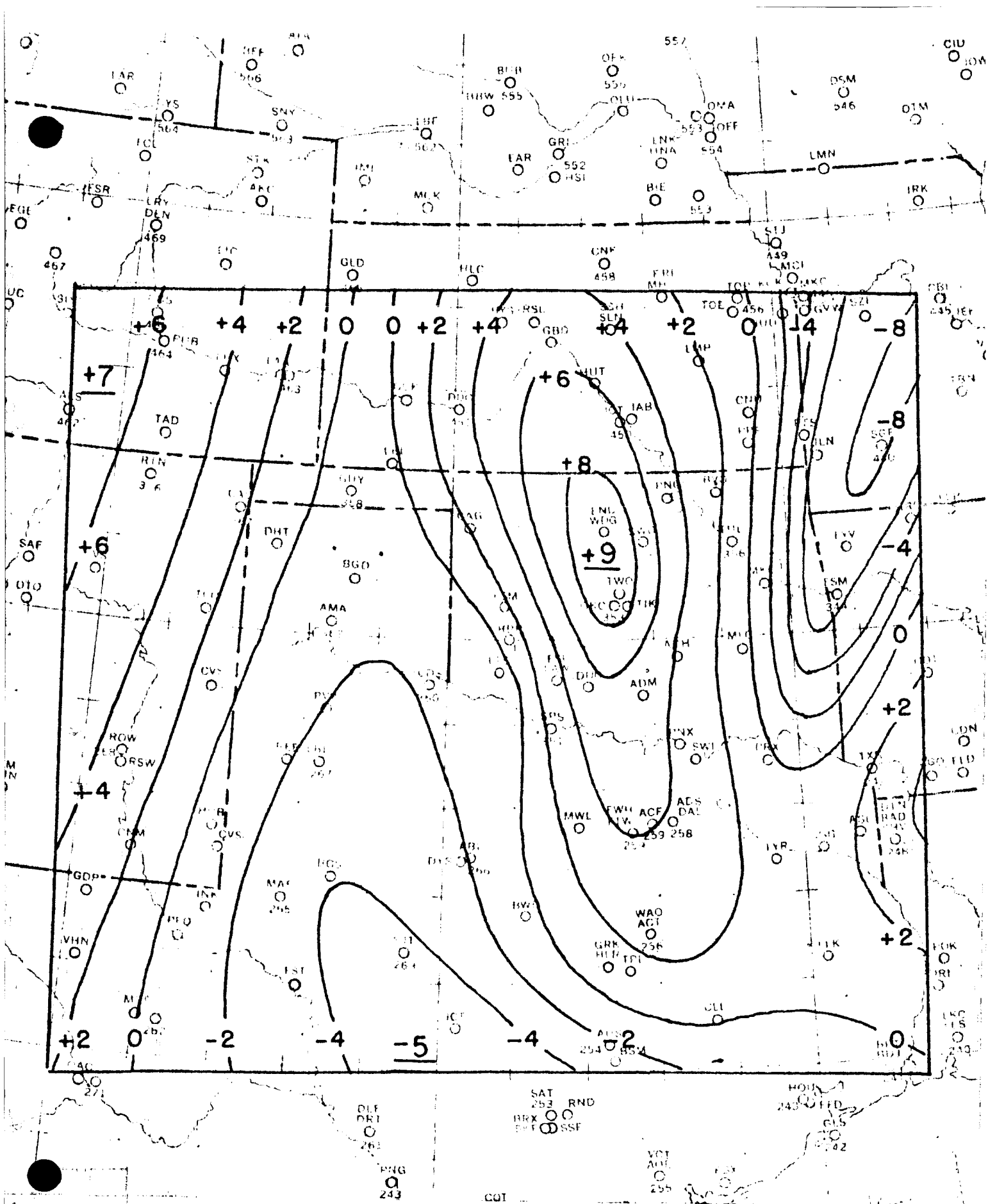


Figure 7

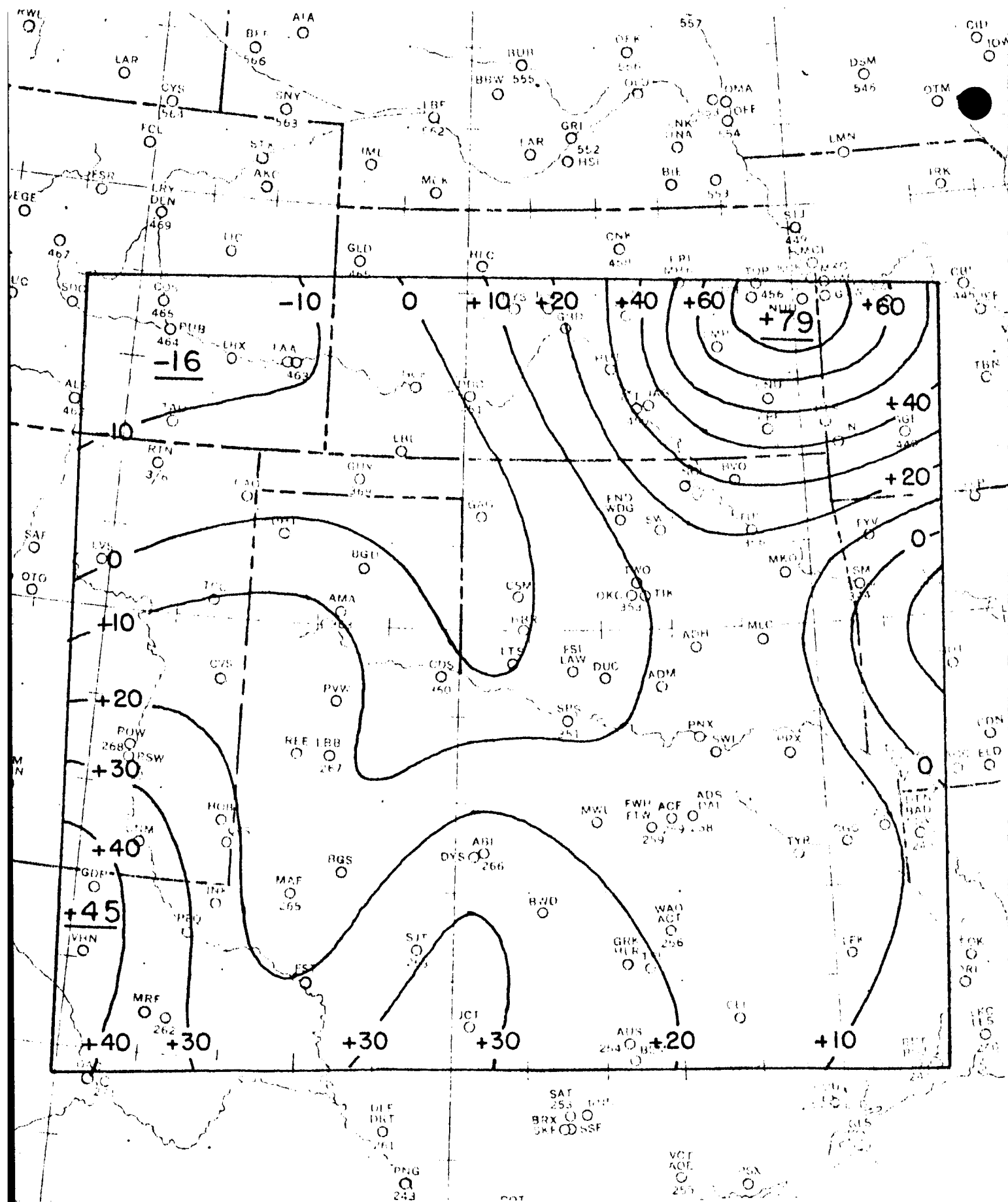


Figure 8

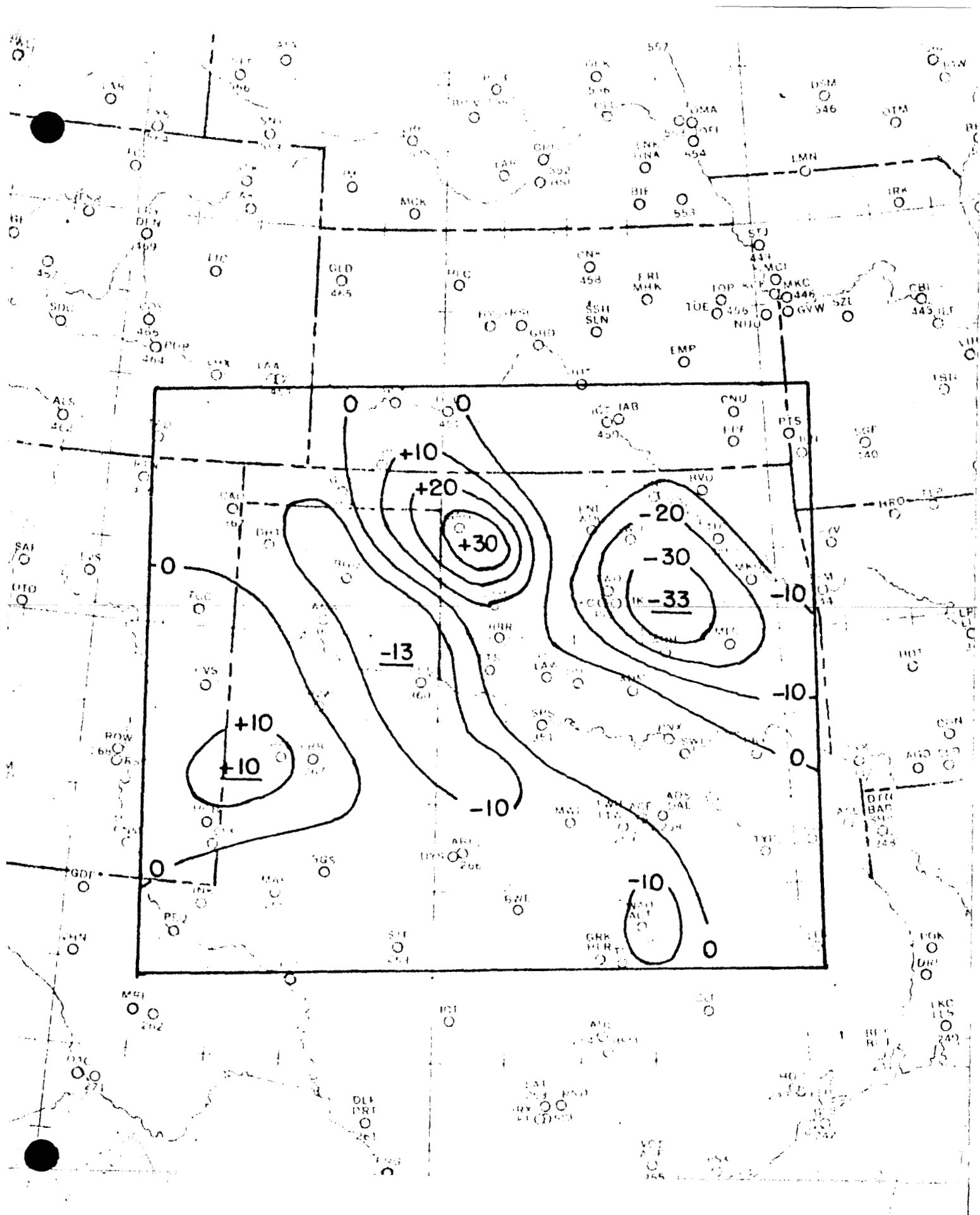


Figure 11

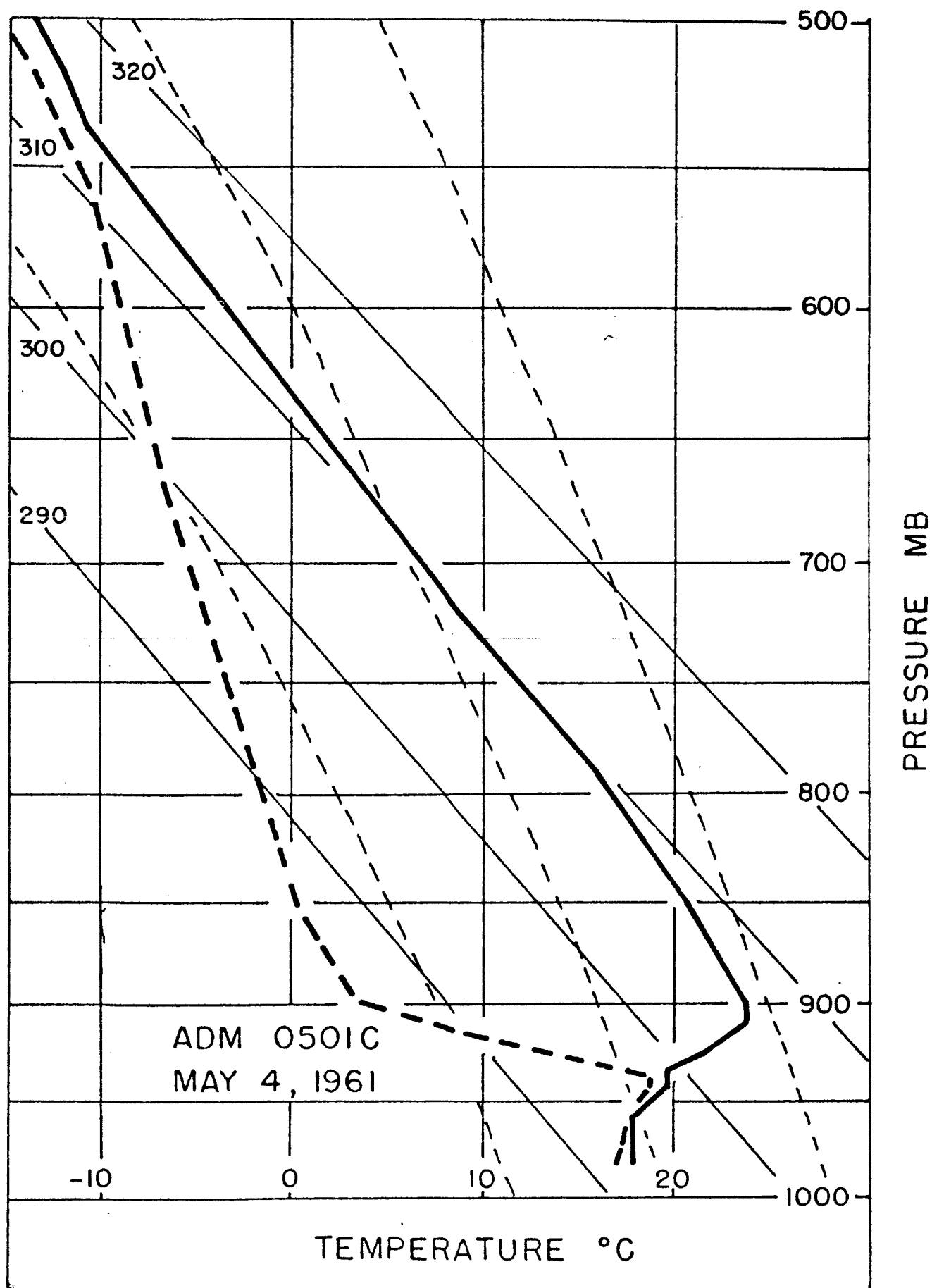


Figure 15

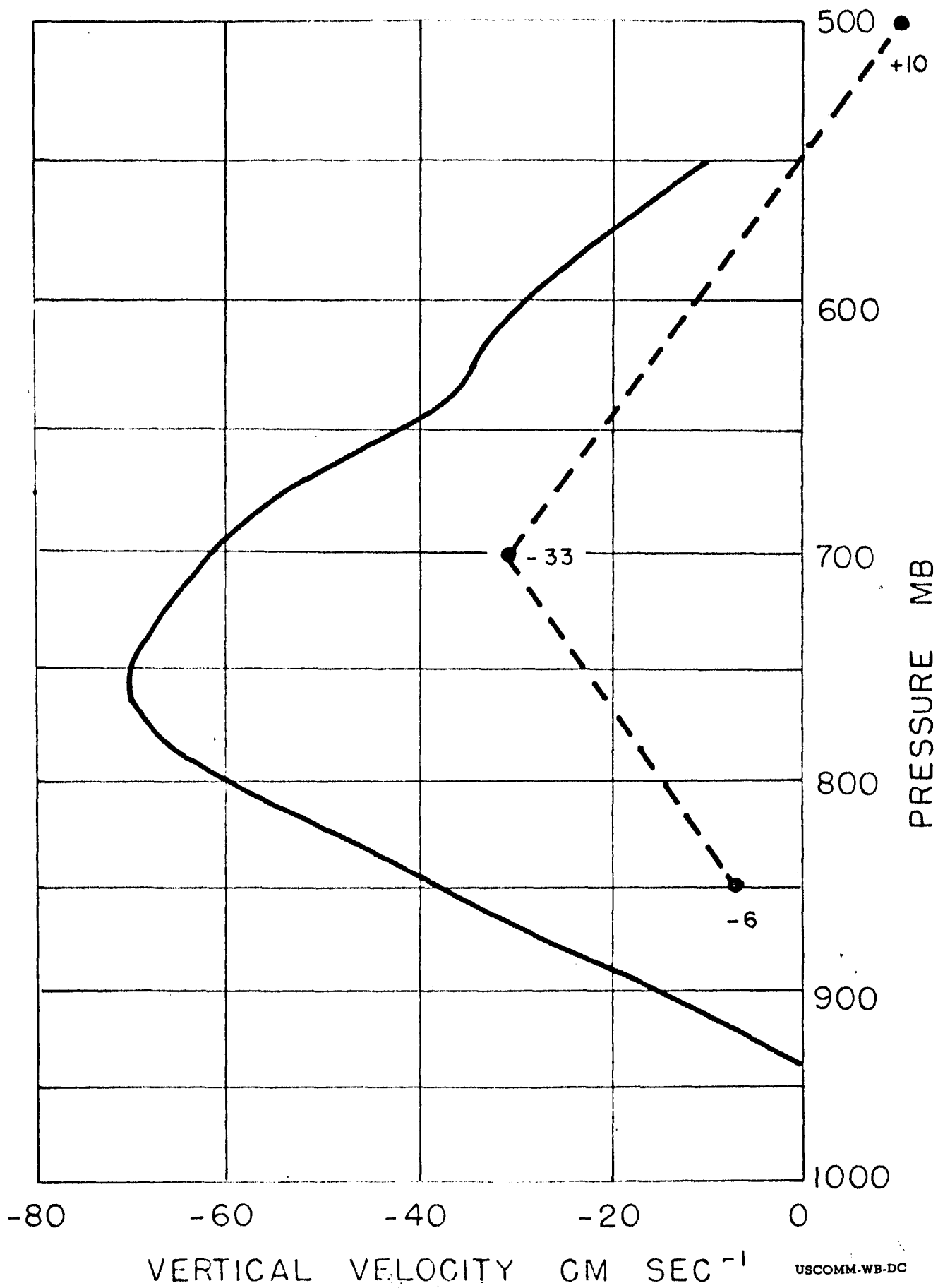


Figure 16